

JAERI-Data/Code

96-029



NEUTRON TRANSMISSION BENCHMARK PROBLEMS FOR  
IRON AND CONCRETE SHIELDS IN LOW, INTERMEDIATE AND  
HIGH ENERGY PROTON ACCELERATOR FACILITIES

September 1996

Yoshihiro NAKANE, Katsumi HAYASHI<sup>\*1</sup>, Yukio SAKAMOTO,  
Nobuaki YOSHIZAWA<sup>\*2</sup>, Noriaki NAKAO<sup>\*3</sup>, Syuichi BAN<sup>\*4</sup>,  
Hideo HIRAYAMA<sup>\*4</sup>, Yoshitomo UWAMINO<sup>\*5</sup>, Kazuo SHIN<sup>\*6</sup>  
and Takashi NAKAMURA<sup>\*7</sup>

日本原子力研究所  
Japan Atomic Energy Research Institute

本レポートは、日本原子力研究所が不定期に公刊している研究報告書です。  
入手の問合せは、日本原子力研究所研究情報部研究情報課（〒319-11 茨城県那珂郡東海村）あて、お申し越しください。なお、このほかに財団法人原子力弘済会資料センター（〒319-11 茨城県那珂郡東海村日本原子力研究所内）で複写による実費頒布をおこなっております。

This report is issued irregularly.

Inquiries about availability of the reports should be addressed to Research Information Division, Department of Intellectual Resources, Japan Atomic Energy Research Institute, Tokai-mura, Naka-gun, Ibaraki-ken, 319-11, Japan.

© Japan Atomic Energy Research Institute, 1996

編集兼発行 日本原子力研究所  
印 刷 いばらき印刷(株)

Neutron Transmission Benchmark Problems for Iron and Concrete Shields  
in Low, Intermediate and High Energy Proton Accelerator Facilities

Yoshihiro NAKANE, Katsumi HAYASHI<sup>\*1</sup>, Yukio SAKAMOTO, Nobuaki YOSHIZAWA<sup>\*2</sup>,  
Noriaki NAKAO<sup>\*3</sup>, Syuichi BAN<sup>\*4</sup>, Hideo HIRAYAMA<sup>\*4</sup>, Yoshitomo UWAMINO<sup>\*5</sup>,  
Kazuo SHIN<sup>\*6</sup> and Takashi NAKAMURA<sup>\*7</sup>

Department of Reactor Engineering  
Tokai Research Establishment  
Japan Atomic Energy Research Institute  
Tokai-mura, Naka-gun, Ibaraki-ken

(Received August 21, 1996)

Benchmark problems were prepared for evaluating the calculation codes and the nuclear data for accelerator shielding design by the Accelerator Shielding Working Group of the Research Committee on Reactor Physics in JAERI. Four benchmark problems: transmission of quasi-monoenergetic neutrons generated by 43 MeV and 68 MeV protons through iron and concrete shields at TIARA of JAERI, neutron fluxes in and around an iron beam stop irradiated by 500 MeV protons at KEK, reaction rate distributions inside a thick concrete shield irradiated by 6.2 GeV protons at LBL, and neutron and hadron fluxes inside an iron beam stop irradiated by 24 GeV protons at CERN are compiled in this document. Calculational configurations and neutron reaction cross section data up to 500 MeV are provided.

Keywords: Accelerator, Benchmark Problems, Transmission, Shielding, Neutron, Iron, Concrete

---

\*1 Hitachi Engineering Co. Ltd.

\*2 Mitsubishi Research Institute, INC.

\*3 University of Tokyo

\*4 National Laboratory for High Energy Physics

\*5 The Institute of Physical and Chemical Research

\*6 Kyoto University

\*7 Tohoku University

低、中間及び高エネルギー陽子加速器施設における鉄及びコンクリート遮蔽体の  
中性子透過に関するベンチマーク問題

日本原子力研究所東海研究所原子炉工学部

中根 佳弘・林 克己<sup>\*1</sup>・坂本 幸夫・義澤 宣明<sup>\*2</sup>

中尾 徳晶<sup>\*3</sup>・伴 秀一<sup>\*4</sup>・平山 英夫<sup>\*4</sup>・上妻 義明<sup>\*5</sup>

秦 和夫<sup>\*6</sup>・中村 尚司<sup>\*7</sup>

(1996年8月21日受理)

加速器施設遮蔽設計のための計算コード及び核データライブラリの評価を目的として、日本原子力研究所炉物理研究委員会の加速器遮蔽ワーキンググループにおいて、中性子の鉄及びコンクリート遮蔽体透過実験に基づいた4題のベンチマーク問題を作成した。このベンチマーク問題集には、原研高崎T I A R Aにおける43MeV及び68MeV陽子からの準単色中性子の鉄及びコンクリート遮蔽体透過、高エネルギー物理学研究所における500MeV陽子照射を受ける鉄ビームストップ内部および周囲での中性子束分布、L B Lにおける6.2GeV陽子照射を受けるコンクリート遮蔽体内部での反応率分布、C E R Nにおける24GeV陽子照射を受ける鉄ビームストップ内部での中性子束及びハドロン束分布に関する問題を収録した。併せて、解析を行う際の計算体系について提案し、500MeVまでの中性子反応断面積などの基本データについても収録した。

---

東海研究所：〒319-11 茨城県那珂郡東海村白方白根2-4

\*1 日立エンジニアリング(株)

\*2 (株)三菱総合研究所

\*3 東京大学

\*4 高エネルギー物理学研究所

\*5 理化学研究所

\*6 京都大学

\*7 東北大学

## Contents

Preface .....	1
1. Transmission of Quasi-Monoenergetic Neutrons Generated by 43 MeV and 68 MeV Protons Through Iron and Concrete Shields .....	2
2. Neutron Fluxes in and around Iron Beam Stop Irradiated by 500 MeV Protons .....	38
3. Reaction Rate Distributions inside Thick Concrete Shield Irradiated by 6.2 GeV Protons .....	59
4. Neutron and Hadron Fluxes inside Iron Beam Dump Irradiated by 24 GeV Protons ..	68
Postscript .....	80
Acknowledgements .....	80

## 目 次

緒 言 .....	1
1. 43MeV, 68MeV陽子により発生した準単色中性子の鉄及びコンクリート遮蔽体透過 .....	2
2. 500MeV陽子照射を受ける鉄ビームストップ内部及び周囲での中性子束分布 .....	38
3. 6.2GeV陽子照射を受ける厚いコンクリート遮蔽体内部での反応率分布 .....	59
4. 24GeV陽子照射を受ける鉄ビームダンプ内部での中性子束及びハドロン束分布 .....	68
後 記 .....	80
謝 辞 .....	80

## Preface

From the view point of shielding calculations for low, intermediate and high energy accelerators, experimental benchmark data are useful to evaluate calculation codes and the nuclear data used in the codes. Annotated references on neutron and photon productions from thick targets, shielding experiments and calculations of high energy particle transport have hitherto been collected<sup>1,2)</sup>. From these experiments, fifteen experiments for electron accelerators and ten experiments for proton accelerators have been selected and compiled<sup>3)</sup> for accelerator shielding benchmark calculations. The Accelerator Shielding Working Group of the Research Committee on Reactor Physics in JAERI have selected<sup>4,5)</sup> six kinds of benchmark problems on thick target neutron yields by protons, alphas and electrons, and shielding data of neutrons and photons generated by low and intermediate energy protons. Analyses of the benchmark experiments carried out<sup>6)</sup> by the Accelerator Shielding Working Group were presented and discussed at the Second Specialists' Meeting on Shielding Aspects of Accelerators, Targets and Irradiation Facilities, SATIF-2. In this meeting, it was decided that newly selected neutron transmission benchmark problems should be compiled for intercomparison of calculation codes for accelerator shielding. Four benchmark problems: transmission of quasi-monoenergetic neutrons generated by 43 MeV and 68 MeV protons through iron and concrete shields at TIARA of JAERI, neutron fluxes in and around an iron beam stop irradiated by 500 MeV protons at KEK, reaction rate distributions inside a thick concrete shield irradiated by 6.2 GeV protons at LBL, and neutron and hadron fluxes inside an iron beam stop irradiated by 24 GeV protons at CERN have therefore been prepared by the Working Group. In the present report, information including calculational configurations and reaction cross sections up to 500 MeV is compiled for benchmark analysis.

## References

1. Nakamura T. et al. : "Annotated References on Neutron and Photon Production from Thick Targets Bombarded by Charged Particles", Atomic Data and Nuclear Data Tables, 32, 471-501 (1985).
2. Hirayama H. et al. : "Annotated References of Shielding Experiment and Calculation of High Energy Particles", KEK report 90-18 (1990).
3. Hirayama H. et al. : "Accelerator Shielding Benchmark Problems", KEK report 92-17 (1993).
4. Hayashi H. et al. : "Accelerator Shielding Benchmark Analysis and future Items to be Solved", Proceedings of "First Specialists' Meeting on Shielding Aspects of Accelerators, Targets and Irradiation Facilities", OECD DOCUMENTS, OECD/NEA (1995).
5. Nakashima H. et al. : "Benchmark problems for intermediate and high energy accelerator shielding", JAERI-Data/Code 94-012 (1994).
6. Nakashima H. et al. : "Accelerator Shielding Benchmark Experiment Analyses", to be published as Proceedings of "Second Specialists' Meeting on Shielding Aspects of Accelerators, Targets and Irradiation Facilities", OECD DOCUMENTS, OECD/NEA in 1996.

1. Transmission of Quasi-Monoenergetic Neutrons Generated by 43 MeV and 68 MeV Protons Through Iron and Concrete Shields

(Summary)

- 1) Accelerator (Organization) : TIARA AVF Cyclotron (JAERI/Takasaki)
- 2) Projectile (Energy) : Proton (43 and 68 MeV)
- 3) Target (Thickness) : 99.9 % Enriched  $^7\text{Li}$  (3.6/5.2 mm for 43/68 MeV)
- 4) Shielding Material : Iron and Concrete
- 5) Geometry : Rectangular Slabs
- 6) Instruments : BC501A Liquid Scintillation Detector, Bonner Sphere Spectrometer,  $^{238}\text{U}$  and  $^{232}\text{Th}$  Fission Counters
- 7) Measured Quantities : Neutron Energy Spectra, Reaction Rates of Bonner Sphere Spectrometer,  $^{238}\text{U}$  and  $^{232}\text{Th}$  Fission Rates

### 1.1 Experimental Arrangement

Figure 1.1 shows a cross sectional view of the TIARA facility with the experimental arrangement. Quasi-monoenergetic source neutrons were generated by 43- and 68-MeV protons bombarding 3.6 mm thick and 5.2 mm thick  $^7\text{Li}$  targets, respectively. The protons penetrating the target with a 2-MeV energy loss were bent down toward the beam dump by a clearing magnet. The neutrons produced in the forward angle reached the experimental room through a 10.9 cm diameter and 225 cm long iron collimator embedded in the concrete wall. The intensity of source neutrons was monitored with a proton beam Faraday cup and two fission counters placed near the  $^7\text{Li}$ -target and the collimator. An iron test shield of 10 to 130 cm thickness was assembled<sup>1, 2)</sup> with 10 cm thick iron slabs of 120 cm x 120 cm rectangular surface on a movable stand. A concrete test shield of 25 to 200 cm thickness was also assembled<sup>3)</sup> with 120 x 120 x 25 cm slabs on the movable stand. An additional iron collimator shown in Fig. 1.2 was used for measurements of thinner test shields in order to depress the neutron leakage through the collimator wall and rotary shutter shown in Fig. 1.1. The additional collimator of 40 to 80 cm thickness was assembled with 120 x 120 x 10 cm slabs with a 10.9 cm diameter cylindrical hole on the movable stand. Thicknesses of the test shields and the additional collimator, peak flux of source neutrons per proton beam charge ( $\mu\text{C}$ ) are given in Table 1.1. Atom densities of the iron and concrete test shields and the additional collimator are given in Table 1.2.

### 1.2 Methods of Measurement and Instrument

To measure the neutron energy spectra, a 12.7 cm diameter x 12.7 cm long BC501A liquid scintillation detector was placed behind the test shields. The pulse height distributions of the detector were converted to neutron energy spectra by the FERDOU unfolding code<sup>4)</sup> and a measured response matrix<sup>5)</sup>.

A Bonner sphere spectrometer with four polyethylene moderators, shown in Fig. 1.3, was placed behind the test shields for measurements of energy dependent neutrons. The central part is a 5.08 cm diameter spherical proportional counter filled with 10 atm (at 22 °C)  $^3\text{He}$  gas. Reaction rates above  $\gamma$ -discrimination level were measured for five different moderator thicknesses. These five reaction rates were unfolded with the SAND-2 code<sup>6)</sup> and the response functions given by Uwamino et al<sup>7)</sup>. The response functions are shown in Fig. 1.4, and their values are given in Table 1.3.

To measure fission rates,  $^{238}\text{U}$  and  $^{232}\text{Th}$  fission counters (Centronic FC480/1000) with a 10.1 cm long x 3.81 cm diameter (active) were also placed behind the test shields. Absolute efficiencies of  $^{238}\text{U}$  and  $^{232}\text{Th}$  fission counters were  $(1.05 \pm 0.04) \times 10^3$  and  $(9.86 \pm 0.34) \times 10^2$  barn/cm<sup>2</sup>/counts, respectively, which were measured with a  $^{252}\text{Cf}$  neutron source.

### 1.3 Neutron Sources

Absolute fluxes of source neutrons in the monoenergetic peak, shown in Table 1.1, have been calibrated for proton beam charge ( $\mu\text{C}$ ) with a proton-recoil-counter-telescope(PRT) set at the position of 5.54 m from the Li target. The spectra of quasi-monoenergetic source neutrons were measured by the time of flight (TOF) method with the BC501A liquid scintillation detector. The detector was placed about 14 m away from the target. Measured source neutron energy spectra are shown in Fig. 1.5 and their normalized ones given in Tables 1.4 and 1.5.

### 1.4 Measured Results

Transmitted neutron energy spectra behind the iron test shields measured with the BC501A scintillation detector are shown in Figs. 1.6-1.14 and their values are given in Tables 1.6-1.14. Figures 1.6 and 1.11 show the spectra on the beam axis behind the iron test shields. Figures 1.7-1.10 and Figs. 1.12-1.14 show the spectra at the off beam positions. The error bars in the figures consist of errors of spectrum unfolding and counting statistics. Other errors in the source neutron flux are estimated to be less than 6.6%. Transmitted neutron energy spectra behind the concrete test shields measured with the BC501A scintillation detector are shown in Figs. 1.15-1.20, and their values are given in Tables 1.15-1.20.

The reaction rates of the Bonner sphere spectrometer behind the iron and concrete test shields are shown in Fig. 1.21 and Fig. 1.22, and their values are given in Tables 1.21-1.22 and Tables 1.23-1.24, respectively. Neutron spectra behind the iron and concrete test shields obtained from the reaction rates using the SAND-2 unfolding code and the response functions are shown in Figs. 1.23-1.24 and Figs. 1.25-1.26, and their values are given in Tables 1.25-1.26 and Tables 1.27-1.28, respectively. The experimental errors of the Bonner sphere spectrometer could not be estimated by the SAND-2 unfolding code.

The fission rates measured behind the iron and concrete test shields using fission counters are shown in Figs. 1.27-1.28 and 1.29-1.30, and their values are given in Tables 1.29-1.30 and Tables 1.31

-1.32, respectively. The uncertainties of the measured data shown in the figures include the counting statistics of the fission counters and neutron fluence monitors.

### 1.5 Model for Calculation

#### a. Source Condition

We propose to use the measured source neutron energy spectra by 43- and 68-MeV p-Li reactions given in Tables 1.4 and 1.5. The 43- and 68-MeV p-Li neutron beams impinge on the shielding assembly at its center. A neutron beam spreading is  $5.94 \times 10^4$  sr as shown in Fig. 1.31.

#### b. Calculation Geometry

We propose to use a three-dimensional(X,Y,Z) calculation model for the experimental arrangement shown in Fig. 1.31. However, it can be expressed with a two-dimensional(R-Z) model.

#### c. Material Descriptions

Atom densities of the test shields and the additional collimator are given in Table 1.2.

### 1.6 Fission cross sections

To calculate the fission rate, We propose to use fission cross sections of  $^{238}\text{U}$  and  $^{232}\text{Th}$  in JENDL-3<sup>8)</sup> in the neutron energy up to 20 MeV, and those measured by Lisowski et al.<sup>9)</sup> in the energy region between 20 and 400 MeV. The cross sections are shown in Fig. 1.32 and the group cross section data are given in Table 1.33.

### 1.7 Normalization Between Calculation and Measurement

Calculated values of the transmitted spectra and count rates are requested to be normalized by proton beam charge ( $\mu\text{C}$ ). Total source neutrons per proton beam charge can be calculated with the peak flux given in Table 1.1 and the energy spectrum given in Tables 1.4 and 1.5.

### References

- Nakashima H., Nakao N., Tanaka Sh., Nakamura T., Shin K., Tanaka Su., Meigo S., Nakane Y., Takada H., Sakamoto Y. and Baba M. : JAERI-Data/Code 96-005, "Experiments on Iron Shield Transmission of Quasi-monoenergetic Neutrons Generated by 43- and 68-MeV Protons via the  $^7\text{Li}(\text{p},\text{n})$  Reaction" (1996).
- Nakashima H., Nakao N., Tanaka Sh., Nakamura T., Shin K., Tanaka Su., Takada H., Meigo S., Nakane Y., Sakamoto Y. and Baba M. : "Transmission through Shields of Quasi-Monoenergetic

Neutrons Generated by 43- and 68-MeV Protons. Part-II ····· Iron Shielding Experiment and Analysis for Investigating Calculation Methods and Cross Section Data", to be published to Nucl. Sci. Eng. (Jan, 1997).

3. Nakao N., Nakashima H., Nakamura T., Tanaka Sh., Tanaka Su., Shin K., Baba M., Sakamoto Y. and Nakane Y. : "Transmission through Shields of Quasi-Monoenergetic Neutrons Generated by 43- and 68-MeV Protons. Part-I ····· Concrete Shielding Experiment and Calculation for Practical Application", to be published to Nucl. Sci. Eng. (Jan, 1997).
4. Shin K., Uwamino Y. and Hyodo T. : "Propagation of Errors from Response Functions to Unfolded Spectrum," Nucl. Technol., 53, 78 (1981).
5. Nakao N., Nakamura T., Baba M., Uwamino Y., Nakanishi N., Nakashima H. and Tanaka S. : "Measurements of Response Function of Organic Liquid Scintillator for Neutron Energy Range up to 135 MeV", Nucl. Instrum. Methods, A362, 454 (1995).
6. McElroy W. N., Berg S., Crockett T. and Hawkins R. G. : "A Computer Automated Iterative Methods for Neutron Flux Spectra Determination by Foil Activation", AFWL-TR-67-41, Air Force Weapons Laboratory, Kirtland Air Force Base, vol. 1-4 (1967).
7. Uwamino Y., Nakamura T. and Hara A.: "Two Type of Multi-Moderator Neutron Spectrometers: Gamma-Ray Insensitive Type and High-Efficiency Type", Nucl. Instrum. Methods in Phys. Res., A239, 299 (1985).
8. Shibata K. et al.: "Japanese Evaluated Nuclear Data Library, Version-3 -JENDL-3-", JAERI 1319 (1990).
9. Lisowski P. W. et al.: "Fission Cross Sections in the Intermediate Energy Region", Proc. Spec. Meet. on Neutron Cross Section Standards for the Energy Region above 20 MeV, Uppsala, Sweden, 21-23 May, 1991, p.177-186 (1991).

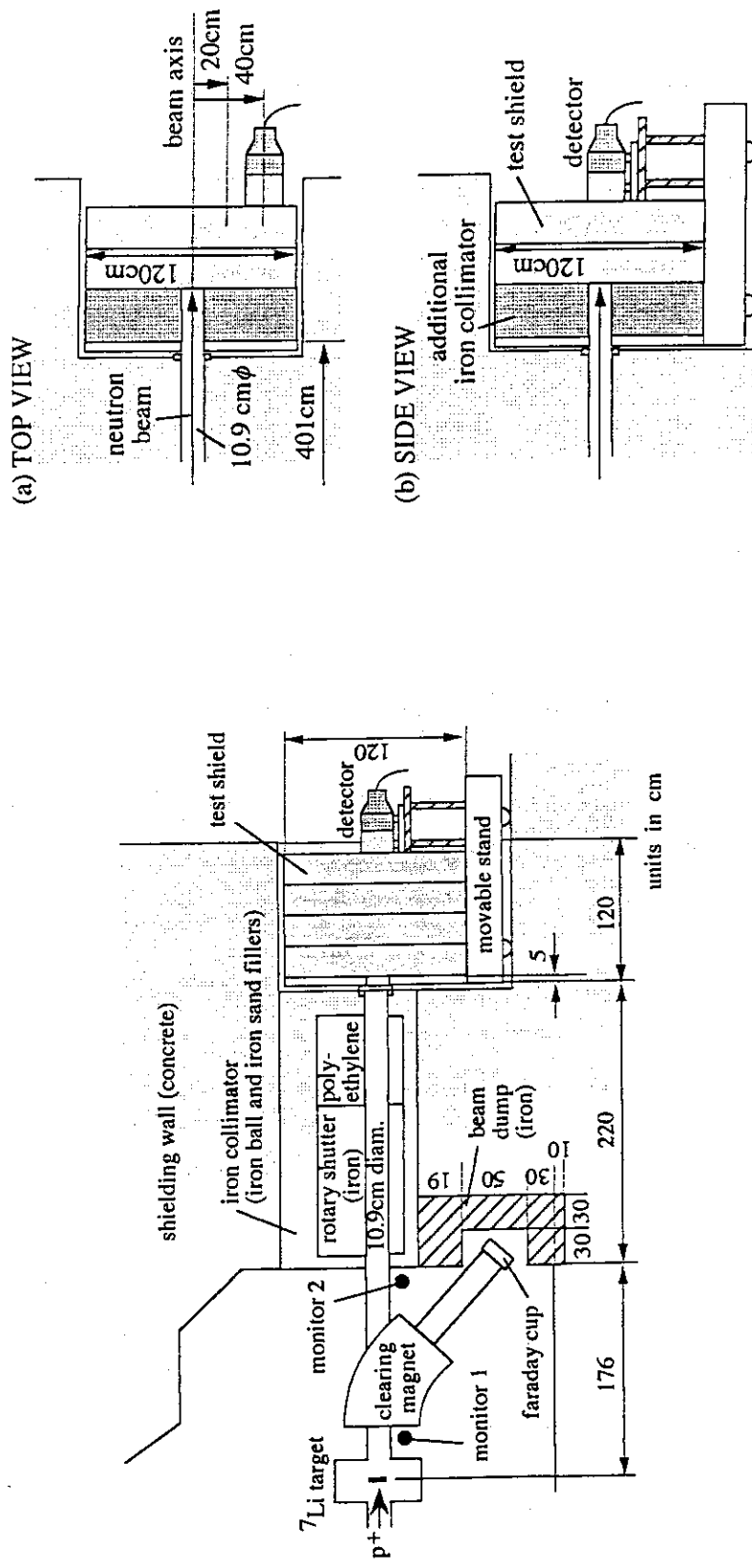


Fig.1.1 Cross sectional view of the TIARA facility with the experimental arrangement  
( Monitor1:  $^{238}\text{U}$ -Fission Counter  
Monitor2:  $^{232}\text{Th}$ -Fission Counter )

Fig.1.2 Top view and side view of the experimental arrangement for the iron and concrete shield with additional iron collimator

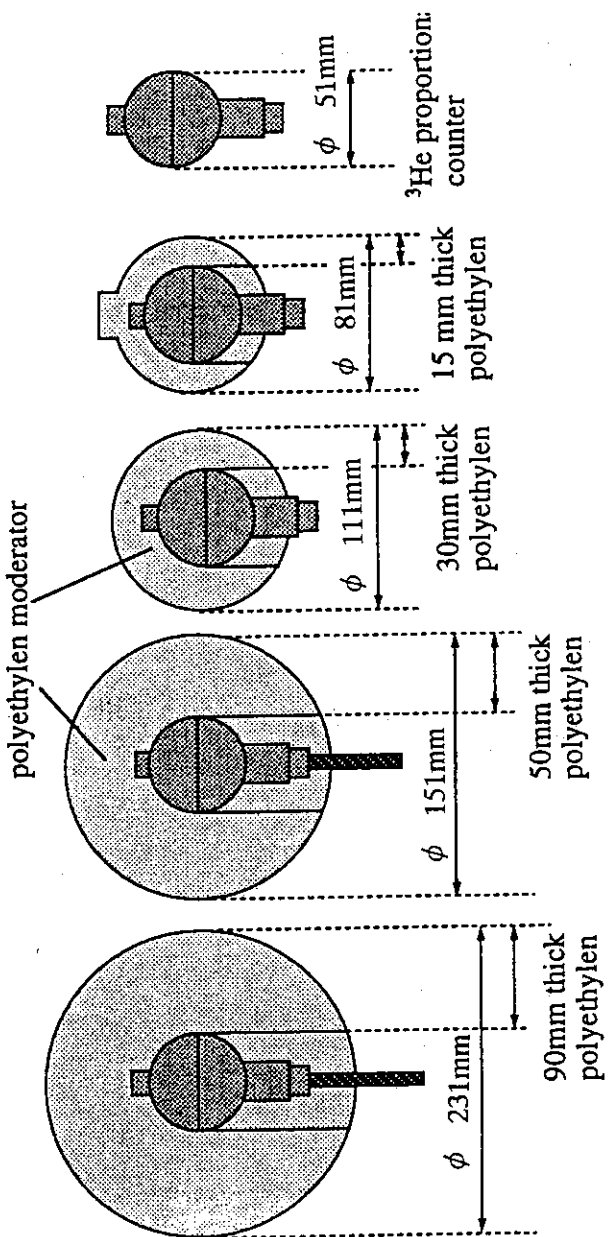


Fig.1.3 Bonner sphere spectrometer  
 Thermal neutron detector : 5.08-cm-diam. spherical proportional counter with 0.0508-cm-thickness  
 stainless steel wall made by LND inc. filled with 10 atm (at 22 °C)  $^3\text{He}$  gas  
 $^3\text{He}$  proportionality counter : density 0.928g/cm<sup>3</sup>

Table 1.1 Dimensions of the test shields, the additional collimator, the peak flux of source neutrons and the detector positions

Ep <sup>a</sup> (MeV)	Test Shield (cm)	Additional Collimator (cm)	Peak flux of source neutron (n sr <sup>-1</sup> μC <sup>-1</sup> )	Detector position (cm) (distance from beam axis) BC501A Bonner F.C. <sup>c</sup>
Iron Test Shield	0	0	3.15x10 <sup>3</sup>	0, 20
43	10	0	3.15x10 <sup>3</sup>	0, 20
	20	0	3.15x10 <sup>3</sup>	0, 20
	40	0	3.15x10 <sup>3</sup>	0, 20
	70	0	3.15x10 <sup>3</sup>	0, 20
	100	0	3.15x10 <sup>3</sup>	0, 20
	0	80	3.45x10 <sup>3</sup>	20, 40
	10	70	3.45x10 <sup>3</sup>	20, 40
	20	60	3.45x10 <sup>3</sup>	20, 40
	40	40	3.45x10 <sup>3</sup>	20, 40
68	0	0	4.00x10 <sup>3</sup>	0, 20
	20	0	4.00x10 <sup>3</sup>	0, 20
	40	0	4.00x10 <sup>3</sup>	0, 20
	70	0	4.00x10 <sup>3</sup>	0, 20
	100	0	4.00x10 <sup>3</sup>	0, 20
	130	0	4.00x10 <sup>3</sup>	0, 20
	0	80	4.77x10 <sup>3</sup>	20, 40
	20	60	4.77x10 <sup>3</sup>	20, 40
	40	40	4.77x10 <sup>3</sup>	20, 40
Concrete Test Shield	25	0	3.15x10 <sup>3</sup>	0, 20
43	50	0	3.15x10 <sup>3</sup>	0, 20
	100	0	3.15x10 <sup>3</sup>	0, 20
	150	0	3.15x10 <sup>3</sup>	0, 20
	25	40	3.45x10 <sup>3</sup>	0, 20, 40
	50	40	3.45x10 <sup>3</sup>	0, 20, 40
67	25	0	4.00x10 <sup>3</sup>	0, 20
	50	0	4.00x10 <sup>3</sup>	0, 20
	100	0	4.00x10 <sup>3</sup>	0, 20
	150	0	4.00x10 <sup>3</sup>	0, 20
	200	0	4.00x10 <sup>3</sup>	0, 20
	25	80	4.77x10 <sup>3</sup>	0, 20, 40
	50	80	4.77x10 <sup>3</sup>	0, 20, 40

<sup>a</sup> Proton energy

<sup>b</sup> Bonner sphere spectrometer

<sup>c</sup> <sup>238</sup>U and <sup>232</sup>Th fission counters  
The BC501A, Bonner sphere spectrometer, fission counters were used for measurements behind the test shields.

Table 1.2 Atom densities of the test shields and the iron collimator

Material	Density (g cm <sup>-3</sup> )	Atom	Atom Density (10 <sup>22</sup> cm <sup>-3</sup> )
Iron	7.87	Iron	8.487
Concrete	2.31	Hydrogen	1.498
		Oxygen	4.188
		Sodium	0.123
		Magnesium	0.062
		Aluminum	0.312
		Silicon	1.110
		Potassium	0.038
		Calcium	0.430
		Iron	0.141

Table 1.3 Calculated neutron response function of the Bonner sphere spectrometer

Energy boundary (MeV)	Neutron response (counts · cm <sup>-2</sup> )				
	Bare*	1. 5cm <sup>b</sup>	1. 5cm+Cd <sup>c</sup>	3 cm	5 cm
4. 00E+2 <sup>d</sup>	0. 0	7. 509E-3	1. 212E-1	6. 624E-2	2. 465E-1
3. 50E+2	0. 0	7. 603E-3	1. 204E-1	6. 710E-2	2. 492E-1
3. 00E+2	0. 0	8. 210E-3	1. 168E-1	7. 326E-2	2. 737E-1
2. 50E+2	0. 0	8. 831E-3	1. 131E-1	7. 866E-2	2. 934E-1
2. 00E+2	0. 0	9. 648E-3	1. 110E-1	8. 484E-2	3. 132E-1
1. 60E+2	0. 0	1. 110E-2	1. 090E-1	9. 654E-2	3. 529E-1
1. 20E+2	0. 0	1. 280E-2	1. 072E-1	1. 04E-1	3. 998E-1
1. 00E+2	0. 0	1. 425E-2	1. 072E-1	1. 226E-1	4. 425E-1
8. 00E+1	0. 0	1. 565E-2	1. 069E-1	1. 349E-1	4. 868E-1
6. 50E+1	0. 0	1. 702E-2	1. 049E-1	1. 468E-1	5. 296E-1
5. 50E+1	0. 0	1. 809E-2	1. 024E-1	1. 560E-1	5. 623E-1
4. 50E+1	0. 0	1. 957E-2	1. 018E-1	1. 690E-1	6. 106E-1
3. 50E+1	3. 089E-3	2. 312E-2	1. 185E-1	1. 995E-1	7. 198E-1
2. 75E+1	7. 928E-3	2. 808E-2	1. 154E-1	2. 409E-1	8. 649E-1
2. 25E+1	1. 133E-2	3. 749E-2	1. 284E-1	3. 165E-1	1. 115E+0
1. 75E+1	1. 730E-2	5. 766E-2	1. 396E-1	4. 246E-1	1. 438E+0
1. 35E+1	2. 313E-2	8. 420E-2	1. 263E-1	5. 348E-1	1. 758E+0
1. 00E+1	3. 072E-2	1. 239E-1	1. 541E-1	7. 926E-1	2. 498E+0
6. 70E+0	3. 902E-2	2. 010E-1	2. 399E-1	1. 273E+0	3. 721E+0
4. 49E+0	4. 692E-2	3. 001E-1	3. 509E-1	1. 830E+0	4. 882E+0
3. 01E+0	5. 285E-2	4. 456E-1	5. 126E-1	2. 587E+0	6. 317E+0
2. 02E+0	5. 474E-2	6. 413E-1	7. 286E-1	3. 482E+0	7. 721E+0
1. 35E+0	3. 315E-2	8. 836E-1	9. 762E-1	4. 420E+0	8. 785E+0
9. 07E-1	1. 558E-2	1. 276E+0	1. 387E+0	5. 539E+0	9. 560E+0
1. 50E-2	1. 616E-1	5. 194E+0	5. 175E+0	9. 251E+0	7. 861E+0
3. 35E-3	4. 011E-1	6. 778E+0	6. 808E+0	9. 768E+0	5. 165E+0
4. 54E-4	1. 572E+0	9. 425E+0	8. 548E+0	1. 066E+1	1. 740E+0
2. 26E-5	4. 537E+0	1. 208E+1	1. 171E+1	1. 040E+1	5. 536E+0
5. 04E-6	9. 596E+0	1. 275E+1	1. 239E+1	9. 083E+0	4. 437E+0
1. 12E-6	1. 759E+1	1. 143E+1	7. 941E+0	6. 992E+0	3. 254E+0
4. 14E-7	1. 881E+1	4. 797E+0	1. 300E+2	2. 607E+0	1. 190E+0

\* Response function of <sup>3</sup>He counter (10 atm)

<sup>b</sup> Thickness of polyethylene moderator of the Bonner sphere spectrometer  
<sup>c</sup> 1.5-cm thick polyethylene moderator covered with Cd(1mm thick) thermal neutron absorber

<sup>d</sup> Read as 4.00 x 10<sup>-2</sup>

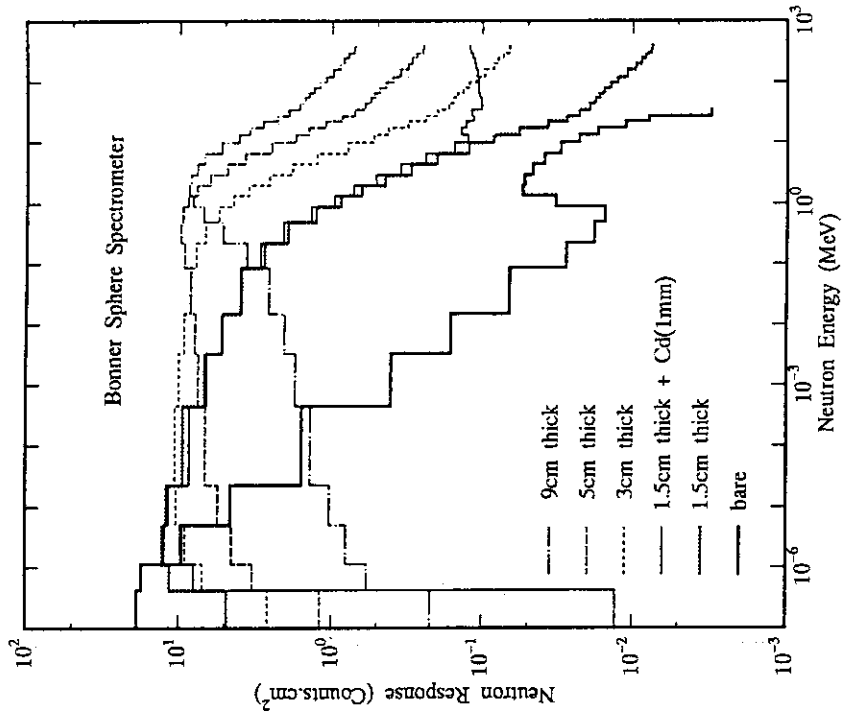


Fig.1.4

Neutron responses of the Bonner sphere spectrometer for each moderator thickness; bare, 1.5, 1.5(Cd), 3, 5 and 9 cm. The almost responses were calculated by Uwamino et al. from adjoint calculations using the ANISN code except for the 1.5-cm thick moderator. The response for the detector with 1.5-cm thick moderator was estimated by Ishikawa et al.

Table 1.4 Energy spectrum of 43-MeV  $p - {}^7\text{Li}$  source neutrons. The flux at peak region (37.5–43.0 MeV) is normalized to unity. The absolute peak flux for each experiment can be obtained from Table 1.1.

Energy (MeV)	Flux	Error	Energy (MeV)	Flux	Error
<7. 0E+0	4. 60E-2 <sup>a</sup>		2. 6E+1	4. 03E-2	1. 83E-3
			2. 7E+1	4. 29E-2	2. 18E-3
7. 0E+0	4. 60E-2	2. 42E-3	2. 8E+1	3. 27E-2	1. 53E-3
8. 0E+0	4. 38E-2	2. 39E-3	2. 9E+1	3. 58E-2	1. 72E-3
9. 0E+0	4. 41E-2	2. 49E-3	3. 0E+1	2. 99E-2	1. 70E-3
1. 0E+1	4. 54E-2	2. 36E-3	3. 1E+1	2. 64E-2	1. 74E-3
1. 1E+1	4. 48E-2	2. 32E-3	3. 2E+1	2. 09E-2	1. 12E-3
1. 2E+1	4. 37E-2	2. 11E-3	3. 3E+1	2. 10E-2	1. 54E-3
1. 3E+1	4. 68E-2	2. 28E-3	3. 4E+1	1. 25E-2	1. 17E-3
1. 4E+1	4. 71E-2	2. 85E-3	3. 5E+1	1. 24E-2	1. 15E-3
1. 5E+1	5. 34E-2	2. 92E-3	3. 6E+1	1. 03E-2	7. 33E-4
1. 6E+1	5. 31E-2	2. 81E-3	3. 7E+1	6. 19E-3	7. 80E-4
1. 7E+1	4. 63E-2	1. 76E-3	3. 8E+1	7. 08E-3	8. 18E-4
1. 8E+1	5. 19E-2	1. 82E-3	3. 9E+1	1. 28E-1	3. 41E-3
1. 9E+1	4. 94E-2	2. 32E-3	4. 0E+1	3. 88E-1	5. 81E-3
2. 0E+1	4. 82E-2	2. 19E-3	4. 1E+1	3. 88E-1	4. 73E-3
2. 1E+1	4. 83E-2	2. 39E-3	4. 2E+1	8. 59E-2	2. 65E-3
2. 2E+1	4. 70E-2	2. 31E-3	4. 3E+1	3. 74E-3	5. 46E-4
2. 3E+1	4. 76E-2	2. 58E-3	4. 4E+1	3. 87E-4	1. 73E-4
2. 4E+1	4. 53E-2	2. 15E-3	4. 5E+1	7. 53E-5	7. 53E-5
2. 5E+1	4. 20E-2	2. 26E-3	4. 6E+1	1. 47E-4	1. 04E-4

\* Read as  $7.0 \times 10^0$

<sup>a</sup> Neutron spectrum below 7 MeV is assumed to be constant.

Table 1.5 Energy spectrum of 68-MeV  $p - {}^7\text{Li}$  source neutrons. The flux at peak region (61.0–69.0 MeV) is normalized to unity. The absolute peak flux for each experiment can be obtained from Table 1.1.

Energy (MeV)	Flux	Error	Energy (MeV)	Flux	Error	Energy (MeV)	Flux	Error
<7. 0E+0	2. 45E-2 <sup>b</sup>		<7. 0E+0	2. 45E-2 <sup>b</sup>		3. 9E+1	3. 36E-2	1. 91E-03
						4. 0E+1	3. 48E-2	1. 41E-03
7. 0E+0	4. 60E-2	2. 42E-3	7. 0E+0	2. 45E-2	1. 53E-3	4. 1E+1	3. 45E-2	1. 35E-03
8. 0E+0	4. 38E-2	2. 39E-3	8. 0E+0	2. 43E-2	1. 55E-3	4. 2E+1	3. 44E-2	1. 31E-03
9. 0E+0	4. 41E-2	2. 49E-3	9. 0E+0	2. 43E-2	1. 55E-3	4. 3E+1	3. 01E-2	1. 71E-03
1. 0E+1	4. 54E-2	2. 36E-3	1. 0E+1	2. 56E-2	1. 59E-3	4. 4E+1	3. 29E-2	1. 27E-03
1. 1E+1	4. 48E-2	2. 32E-3	1. 1E+1	2. 38E-2	1. 52E-3	4. 5E+1	3. 06E-2	1. 56E-03
1. 2E+1	4. 37E-2	2. 11E-3	1. 2E+1	2. 29E-2	1. 51E-3	4. 6E+1	3. 4E-2	1. 57E-03
1. 3E+1	4. 68E-2	2. 28E-3	1. 3E+1	2. 85E-2	1. 73E-3	4. 7E+1	3. 05E-2	1. 18E-03
1. 4E+1	4. 71E-2	2. 85E-3	1. 4E+1	2. 60E-2	1. 63E-3	4. 8E+1	3. 07E-2	1. 63E-03
1. 5E+1	5. 34E-2	2. 92E-3	1. 5E+1	3. 08E-2	1. 78E-3	4. 9E+1	2. 91E-2	1. 20E-03
1. 6E+1	5. 31E-2	2. 81E-3	1. 6E+1	2. 89E-2	1. 71E-3	5. 0E+1	2. 71E-2	1. 50E-03
1. 7E+1	4. 63E-2	1. 76E-3	1. 7E+1	2. 78E-2	1. 69E-3	5. 1E+1	2. 97E-2	1. 56E-03
1. 8E+1	5. 19E-2	1. 82E-3	1. 8E+1	3. 14E-2	1. 54E-3	5. 2E+1	2. 56E-2	1. 44E-03
1. 9E+1	4. 94E-2	2. 32E-3	1. 9E+1	3. 10E-2	1. 91E-3	5. 3E+1	2. 67E-2	1. 46E-03
2. 0E+1	4. 82E-2	2. 19E-3	2. 0E+1	3. 33E-2	1. 97E-3	5. 4E+1	2. 30E-2	9. 97E-04
2. 1E+1	4. 83E-2	2. 39E-3	2. 1E+1	3. 30E-2	1. 98E-3	5. 5E+1	2. 14E-2	1. 29E-03
2. 2E+1	4. 70E-2	2. 31E-3	2. 2E+1	3. 34E-2	1. 93E-3	5. 6E+1	2. 05E-2	1. 02E-03
2. 3E+1	4. 76E-2	2. 58E-3	2. 3E+1	3. 34E-2	1. 77E-3	5. 7E+1	1. 61E-2	1. 01E-03
2. 4E+1	4. 53E-2	2. 15E-3	2. 4E+1	3. 79E-2	2. 01E-3	5. 8E+1	1. 22E-2	1. 33E-03
2. 5E+1	4. 20E-2	2. 26E-3	2. 5E+1	3. 76E-2	1. 94E-3	5. 9E+1	1. 46E-2	1. 44E-03
2. 6E+1	4. 17E+0	2. 26E-3	2. 6E+1	3. 70E-2	1. 95E-3	6. 0E+1	7. 50E-3	1. 01E-03
2. 7E+1	3. 47E-2	1. 89E-3	2. 7E+1	3. 47E-2	1. 89E-3	6. 1E+1	9. 05E-3	1. 09E-03
2. 8E+1	3. 74E-2	1. 92E-3	2. 8E+1	3. 74E-2	1. 92E-3	6. 2E+1	7. 72E-3	1. 15E-04
2. 9E+1	4. 02E-2	2. 09E-3	2. 9E+1	4. 02E-2	2. 09E-3	6. 3E+1	3. 40E-2	2. 04E-03

\* Read as  $7.0 \times 10^0$

<sup>a</sup> Neutron spectrum below 7 MeV is assumed to be constant.

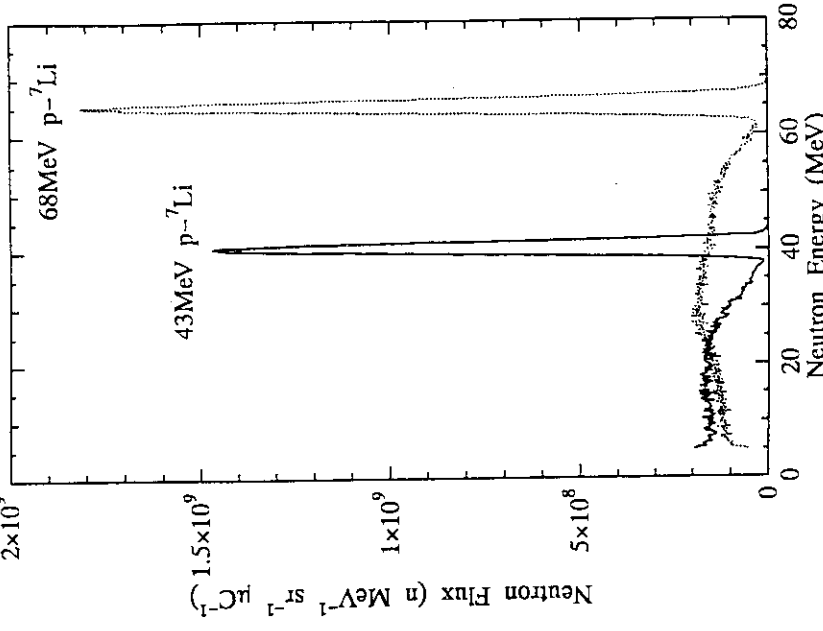


Table 1.5 Energy spectrum of 68-MeV  $p - {}^7\text{Li}$  source neutrons. The flux at peak region (61.0–69.0 MeV) is normalized to unity. The absolute peak flux for each experiment can be obtained from Table 1.1.

Fig.1.5 Source neutron spectra generated via the  $\text{Li}(\text{p},\text{n})$  reaction by 43- and 68-MeV protons. The Spectra were measured by the time-of-flight methods with the BC50A scintillation counter and normalized by the measurements using the recoil-proton counter telescope.

\* Read as  $7.0 \times 10^0$

<sup>b</sup> Neutron spectrum below 7 MeV is assumed to be constant.

Table 1.6 Neutron spectra behind 10, 20, 40, 70 and 100cm thick iron measured by the BC501A detector for 43-MeV p-Li neutrons

Energy (MeV)	Flux • Error (%)	Flux	Error (%)	Flux	Error (%)	Flux	Error (%)	Flux	Error (%)
thick	10cm	20cm	40cm	70cm	100cm				
4. 6E+1	4. 695E+3	11. 1	1. 115E+3	16. 6	6. 705E+1	12. 5	8. 704E-2	95. 4	2. 330E-2
4. 4E+1	4. 252E+4	6. 4	3. 220E+3	23. 0	1. 942E+2	15. 8	3. 359E-2	20. 6	2. 332E-2
4. 3E+1	1. 252E+4	2. 6	7. 499E+3	18. 4	1. 622E+0	14. 3	4. 162E-2	85. 4	4. 232E-2
4. 2E+1	2. 758E+4	2. 5	1. 127E+4	10. 0	5. 926E+2	3. 4	2. 788E-0	12. 2	6. 126E-2
4. 1E+1	4. 193E+4	2. 5	1. 430E+3	33. 2	4. 591E+2	5. 3	5. 009E+0	7. 0	7. 272E-2
4. 0E+1	4. 114E+4	3. 7	1. 007E+4	5. 4	4. 594E+2	6. 3	4. 954E+0	7. 1	6. 116E-2
3. 9E+1	2. 513E+4	4. 1	5. 012E+3	8. 7	8. 991E+1	4. 7	4. 194E+0	15. 0	4. 342E-2
3. 8E+1	9. 753E+3	2. 8	1. 430E+3	37. 6	2. 836E+1	18. 1	2. 526E+0	21. 1	2. 672E-2
3. 7E+1	3. 267E+3	1. 6	6. 438E+2	39. 8	1. 053E+1	2. 5	1. 052E+0	11. 4	1. 597E-2
3. 6E+1	2. 097E+3	1. 6	7. 633E+2	34. 5	2. 073E+1	25. 1	2. 052E+0	1. 4	2. 36. 1
3. 5E+1	2. 275E+3	10. 6	8. 491E+2	36. 0	2. 562E+1	15. 9	5. 042E-1	35. 2	1. 158E-2
3. 4E+1	2. 613E+3	7. 2	8. 753E+2	26. 5	3. 105E+1	10. 5	4. 668E-1	33. 0	1. 104E-2
3. 3E+1	2. 951E+3	8. 8	8. 917E+2	17. 7	8. 7	5. 141E+1	30. 1	1. 187E-2	50. 7
3. 2E+1	3. 261E+3	10. 8	9. 053E+2	12. 4	3. 842E+1	8. 2	5. 474E+1	25. 8	1. 270E-2
3. 1E+1	3. 504E+3	10. 1	9. 148E+2	9. 8	4. 055E+1	7. 5	5. 823E+1	20. 9	1. 315E-2
3. 0E+1	3. 661E+3	6. 8	9. 240E+2	8. 8	4. 183E+1	6. 9	6. 305E-1	13. 0	1. 311E-2
2. 9E+1	3. 779E+3	3. 9	9. 416E+2	9. 7	4. 234E+1	7. 2	6. 684E-1	7. 6	1. 257E-2
2. 8E+1	3. 945E+3	4. 6	9. 734E+2	12. 6	4. 157E+1	9. 1	6. 571E-1	8. 6	1. 16E-2
2. 7E+1	4. 190E+3	8. 6	1. 014E+3	12. 5	4. 157E+1	12. 4	5. 881E-1	18. 5	1. 043E-2
2. 6E+1	4. 418E+3	13. 8	1. 044E+3	19. 9	4. 080E+1	15. 7	4. 998E-1	36. 4	9. 328E-3
2. 5E+1	4. 476E+3	16. 5	1. 046E+3	21. 5	4. 001E+1	17. 4	4. 403E-1	50. 1	8. 538E-3
2. 4E+1	4. 303E+3	15. 9	1. 011E+3	20. 8	3. 912E+1	16. 6	4. 234E-1	48. 1	8. 081E-3
2. 3E+1	3. 988E+3	12. 5	9. 449E+2	17. 4	3. 807E+1	13. 3	4. 320E-1	34. 6	7. 676E-3
2. 2E+1	3. 660E+3	7. 6	8. 609E+2	11. 0	3. 685E+1	1. 9	4. 520E-1	18. 7	7. 372E-3
2. 1E+1	3. 368E+3	2. 1	7. 706E+2	2. 7	3. 559E+1	1. 8	4. 869E-1	5. 1	6. 840E-3
2. 0E+1	3. 087E+3	7. 1	6. 860E+2	10. 3	3. 418E+1	6. 3	5. 436E-1	11. 8	6. 300E-3
1. 9E+1	2. 816E+3	15. 3	6. 189E+2	19. 2	3. 227E+1	11. 1	6. 000E-1	21. 0	5. 889E-3
1. 8E+1	2. 616E+3	17. 9	5. 765E+2	20. 1	2. 941E+1	7. 7	5. 947E-1	23. 2	5. 617E-3
1. 7E+1	2. 524E+3	9. 8	5. 505E+2	12. 0	2. 568E+1	7. 3	4. 845E-1	15. 5	5. 432E-3
1. 6E+1	2. 456E+3	4. 1	5. 192E+2	3. 4	2. 183E+1	2. 2	3. 261E-1	10. 1	5. 353E-3
1. 5E+1	2. 281E+3	9. 6	4. 663E+2	4. 8	1. 882E+1	3. 8	2. 441E-1	26. 8	5. 409E-3
1. 4E+1	1. 993E+3	3. 4	3. 969E+2	2. 6	1. 639E+1	1. 9	2. 837E-1	12. 1	5. 522E-3
1. 3E+1	1. 725E+3	9. 6	3. 283E+2	14. 9	1. 538E+1	9. 7	3. 569E-1	13. 7	5. 578E-3
1. 2E+1	1. 537E+3	16. 7	2. 701E+2	27. 1	1. 466E+1	15. 7	3. 697E-1	20. 5	5. 545E-3
1. 1E+1	1. 346E+3	16. 2	2. 213E+2	32. 3	1. 204E+1	17. 5	3. 227E-1	20. 1	5. 410E-3
5. 0E+0	1. 118E+3	13. 0	1. 797E+2	31. 5	1. 089E+1	16. 7	2. 761E-1	15. 9	5. 148E-3
9. 0E+0	9. 082E+2	11. 5	1. 520E+2	17. 9	1. 639E+1	9. 8	2. 693E-1	12. 1	5. 486E-3
8. 0E+0	7. 898E+2	6. 3	1. 508E+2	27. 5	6. 529E+0	20. 2	2. 359E-1	15. 6	4. 955E-3
7. 0E+0	7. 640E+2	45. 4	1. 496E+2	56. 3	5. 532E+0	53. 6	6. 468E-2	23. 7	6. 492E-3
6. 0E+0	5. 555E+2	15. 7	9. 150E+1	23. 3	6. 221E+0	36. 5	7. 569E-3	10. 7	5. 669E-3

<sup>a</sup> unit: n cm<sup>-2</sup> Lethergy<sup>-1</sup> μ C<sup>-1</sup>  
<sup>b</sup> Read as 4. 6 × 10<sup>-1</sup>

Fig. 1.6 Neutron spectra behind various thicknesses of iron measured by the BC501A detector on the beam axis for 43-MeV p-Li neutrons

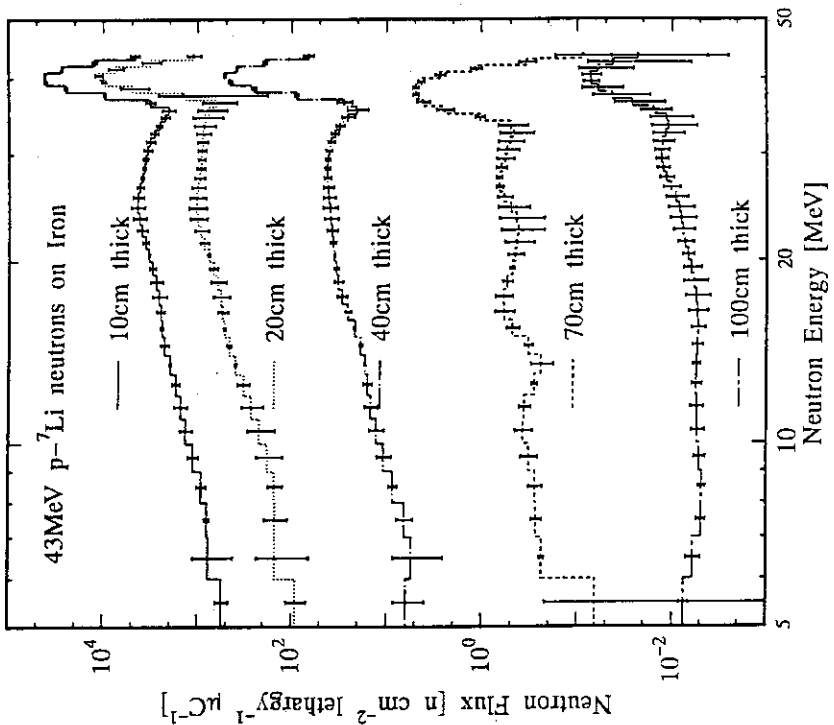


Fig. 1.6 Neutron spectra behind various thicknesses of iron measured by the BC501A detector on the beam axis for 43-MeV p-Li neutrons

Table 1.7 Neutron spectra behind 0cm thick iron measured by the BC501A detector for 43-MeV p-Li neutrons

Energy (MeV)	Flux *	Error (%)	Flux	Error (%)
20cm off axis	20cm off axis	40cm off axis	40cm off axis	
4.8E+1	1.112E+0	41.6	1.467E-1	25.1
4.6E+1	1.957E+0	44.5	2.764E-1	22.3
4.4E+1	5.473E+0	31.2	6.266E-1	17.0
4.3E+1	1.761E+1	11.3	1.245E+0	14.3
4.2E+1	4.183E+1	8.2	2.114E+0	11.8
4.1E+1	6.240E+1	8.5	3.168E+0	11.5
4.0E+1	6.127E+1	6.2	4.118E+0	8.2
3.9E+1	4.950E+1	9.9	3.993E+0	8.5
3.8E+1	3.995E+1	17.7	2.635E+0	24.0
3.7E+1	2.677E+1	24.7	1.360E+0	39.6
3.6E+1	1.396E+1	13.0	9.061E-1	14.1
3.5E+1	9.106E+0	21.5	9.192E-1	18.9
3.4E+1	9.402E+0	22.4	1.016E+0	18.0
3.3E+1	1.070E+1	17.1	1.086E+0	14.7
3.2E+1	1.176E+1	14.3	1.123E+0	13.2
3.1E+1	1.252E+1	11.5	1.140E+0	11.3
3.0E+1	1.307E+1	7.4	1.150E+0	7.5
2.9E+1	1.343E+1	4.3	1.172E+0	4.5
2.8E+1	1.354E+1	4.8	1.217E+0	4.8
2.7E+1	1.341E+1	9.7	1.289E+0	8.9
2.6E+1	1.316E+1	16.5	1.367E+0	14.1
2.5E+1	1.297E+1	20.3	1.426E+0	16.5
2.4E+1	1.280E+1	14.0	1.458E+0	11.0
2.3E+1	1.258E+1	8.0	1.447E+0	6.3
2.2E+1	1.258E+1	12.7	1.335E+0	10.1
2.1E+1	1.227E+1	2.4	1.420E+0	2.0
2.0E+1	1.203E+1	6.3	1.378E+0	5.0
1.9E+1	1.194E+1	12.7	1.331E+0	11.2
1.8E+1	1.178E+1	14.1	1.306E+0	6.1
1.7E+1	1.131E+1	8.1	1.285E+0	4.2
1.6E+1	1.090E+1	3.7	1.301E+0	2.8
1.5E+1	1.009E+1	7.7	1.288E+0	5.4
1.4E+1	1.009E+1	2.6	1.265E+0	1.9
1.3E+1	1.033E+1	5.7	1.265E+0	4.2
1.2E+1	1.052E+1	8.6	1.285E+0	6.3
1.1E+1	1.049E+1	7.4	1.309E+0	5.3
1.0E+1	1.049E+1	5.0	1.339E+0	3.5
9.0E+0	1.086E+1	3.6	1.416E+0	2.5
8.0E+0	1.134E+1	1.4	1.560E+0	9.9
7.0E+0	1.072E+1	17.1	1.617E+0	10.1
6.0E+0	7.637E+0	39.0	1.258E+0	21.1
5.0E+0				

\* unit:  $n \text{ cm}^{-2} \text{ Lethargy}^{-1} \mu \text{C}^{-1}$   
Read as  $4.8 \times 10^5$

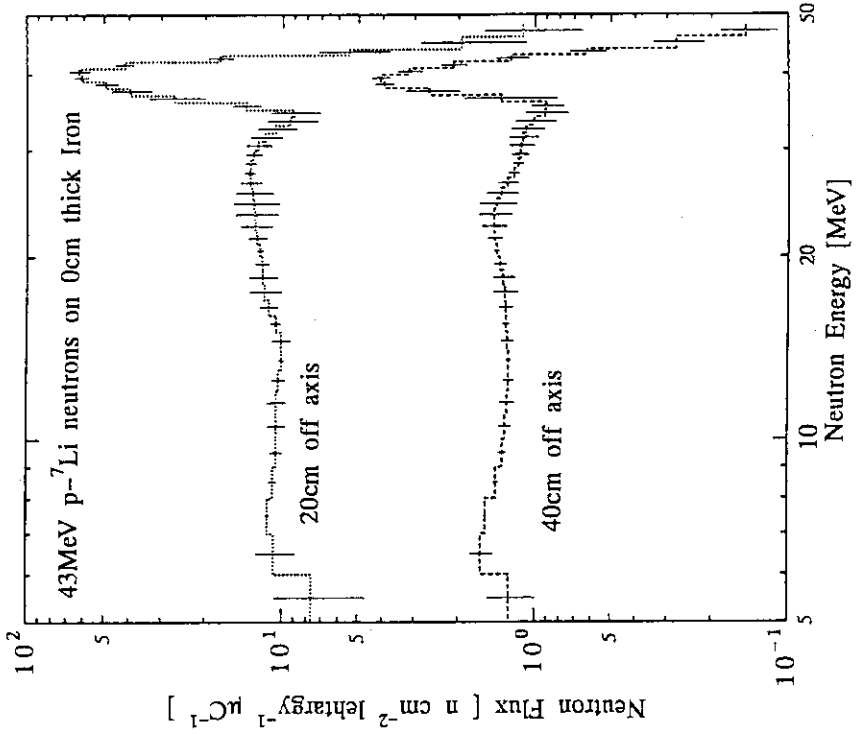


Fig.1.7 Neutron spectra behind 0cm thick iron measured by the BC501A detector on 20- and 40-cm off axis for 43-MeV p-Li neutrons

Table 1.8 Neutron spectra behind 10cm thick iron measured by the BC501A detector for 43-MeV p-Li neutrons

Energy (MeV)	Flux *	Error (%)	Flux	Error	Flux	Error (%)
beam axis			20cm off axis		40cm off axis	
4.4E+1	4.695E+3	11.1	2.396E+1	30.9	2.635E+0	22.9
4.3E+1	1.252E+4	6.4	7.559E+1	10.1	6.868E+0	12.0
4.2E+1	2.758E+4	2.6	1.920E+2	7.3	1.373E+1	9.2
4.1E+1	4.193E+4	2.5	2.657E+2	7.5	1.856E+1	10.3
4.0E+1	4.114E+4	3.1	2.657E+2	7.5	1.809E+1	8.4
3.9E+1	2.513E+4	4.1	1.903E+2	10.7	1.515E+1	11.5
3.8E+1	9.753E+3	2.8	1.714E+2	14.6	1.172E+1	23.4
3.7E+1	3.267E+3	1.6	1.388E+2	18.2	7.727E+0	32.2
3.6E+1	2.097E+3	16.7	1.388E+2	18.2	4.999E+0	13.1
3.5E+1	2.275E+3	10.6	5.030E+1	13.8	4.456E+0	16.9
3.4E+1	2.613E+3	7.2	4.817E+1	15.9	5.002E+0	16.2
3.3E+1	2.951E+3	8.8	5.272E+1	12.7	5.704E+0	2.4
3.2E+1	3.261E+3	10.8	5.719E+1	10.8	6.258E+0	10.5
3.1E+1	3.504E+3	10.1	6.105E+1	8.0	6.583E+0	8.6
3.0E+1	3.61E+3	6.8	6.430E+1	5.6	6.706E+0	5.7
2.9E+1	3.779E+3	3.9	6.659E+1	3.2	6.770E+0	3.4
2.8E+1	3.945E+3	4.4	6.755E+1	3.5	6.952E+0	3.7
2.7E+1	4.190E+3	8.6	6.730E+1	7.2	7.304E+0	7.1
2.6E+1	4.418E+3	13.8	6.648E+1	12.8	7.686E+0	11.1
2.5E+1	4.476E+3	16.5	6.569E+1	15.0	7.899E+0	13.1
2.4E+1	4.303E+3	15.9	6.494E+1	14.0	7.862E+0	12.2
2.3E+1	3.988E+3	12.5	6.395E+1	10.4	7.630E+0	9.2
2.2E+1	3.660E+3	7.6	6.274E+1	10.0	7.285E+0	11.6
2.1E+1	3.368E+3	2.1	6.171E+1	1.8	6.854E+0	1.8
2.0E+1	3.087E+3	7.1	6.117E+1	4.6	6.336E+0	4.7
1.9E+1	2.816E+3	15.3	6.081E+1	9.3	5.866E+0	10.1
1.8E+1	2.616E+3	17.9	5.974E+1	10.4	5.625E+0	11.6
1.7E+1	2.424E+3	9.8	5.734E+1	6.0	5.712E+0	6.3
1.6E+1	2.456E+3	4.1	5.421E+1	6.0	5.894E+0	4.4
1.5E+1	2.281E+3	9.6	5.221E+1	5.5	5.828E+0	5.3
1.4E+1	1.933E+3	3.4	5.256E+1	1.8	5.494E+0	1.9
1.3E+1	1.755E+3	9.6	5.420E+1	4.0	5.223E+0	4.4
1.2E+1	1.533E+3	16.7	5.469E+1	6.2	5.222E+0	6.9
1.1E+1	1.316E+3	16.2	5.355E+1	5.4	5.405E+0	5.7
1.0E+1	1.118E+3	13.0	5.277E+1	3.7	5.652E+0	3.7
9.0E+0	9.082E+2	11.5	5.392E+1	2.7	5.974E+0	2.6
8.0E+0	7.898E+2	6.3	5.626E+1	1.1	6.629E+0	1.0
7.0E+0	7.640E+2	45.4	5.406E+1	12.6	7.377E+0	9.8
6.0E+0	5.555E+2	15.7	3.922E+1	28.3	6.299E+0	18.6
5.0E+0						

\* unit:  $n \text{ cm}^{-2} \text{ Lethargy}^{-1} \mu \text{ C}^{-1}$

Read as  $4.4 \times 10^4$

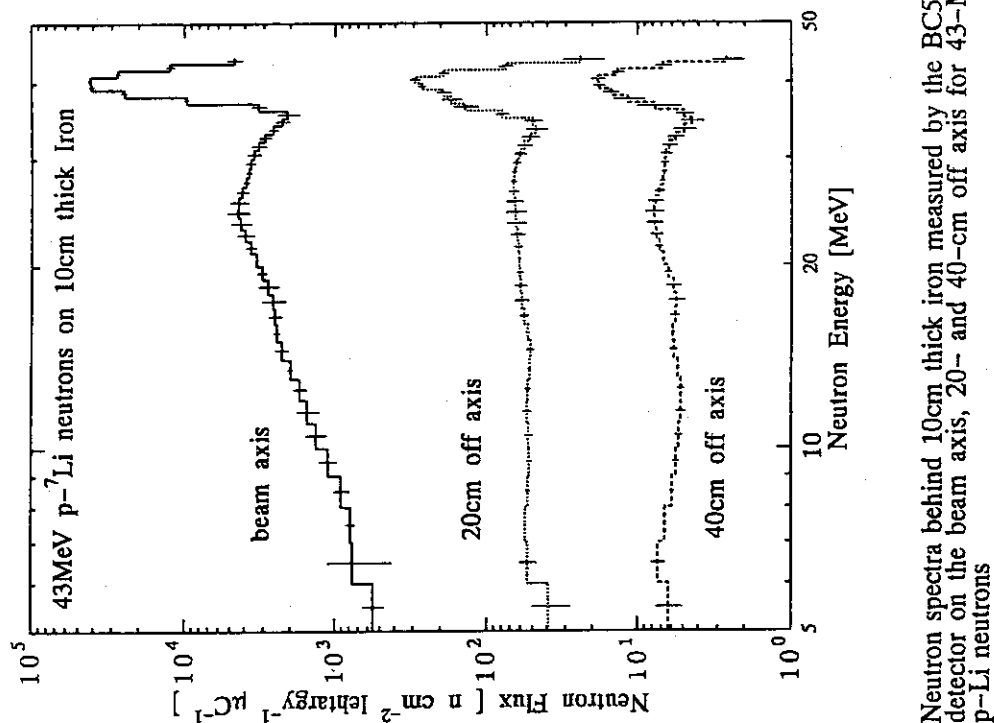


Fig.1.8 Neutron spectra behind 10cm thick iron measured by the BC501A p-Li neutrons  
detector on the beam axis, 20- and 40-cm off axis for 43-MeV

Table 1.9 Neutron spectra behind 20cm thick iron measured by the BC501A detector for 43-MeV p-Li neutrons.

Energy (MeV)	Flux * [ $\text{n cm}^{-2} \text{Lethergy}^{-1} \mu\text{C}^{-1}$ ]	Error (%)	Flux beam axis 20cm off axis	Error (%)	Flux 40cm off axis	Error (%)
4.4E+1 <sup>b</sup>	1.115E+3	16.6	2.763E+1	8.4	2.366E+0	23.9
4.3E+1	3.220E+3	23.0	7.307E+1	5.7	5.772E+0	25.2
4.2E+1	7.499E+3	18.4	1.519E+2	3.9	1.170E+1	29.1
4.1E+1	1.127E+4	10.0	2.250E+2	4.0	1.650E+1	15.9
4.0E+1	1.007E+4	5.4	2.416E+2	3.7	1.689E+1	13.5
3.9E+1	5.012E+3	33.2	2.052E+2	4.1	1.366E+1	20.3
3.8E+1	1.430E+3	87.6	1.487E+2	11.7	8.946E+0	32.4
3.7E+1	6.438E+2	39.8	9.034E+1	16.0	5.399E+0	58.3
3.6E+1	7.633E+2	34.5	5.127E+1	6.2	4.161E+0	19.7
3.5E+1	8.491E+2	36.0	3.940E+1	12.2	4.108E+0	20.6
3.4E+1	8.753E+2	26.5	4.079E+1	12.4	4.204E+0	22.0
3.3E+1	8.917E+2	17.7	4.410E+1	10.3	4.195E+0	18.2
3.2E+1	9.053E+2	12.4	4.627E+1	9.3	4.135E+0	16.0
3.1E+1	9.148E+2	19.9	4.713E+1	8.6	4.116E+0	13.4
3.0E+1	9.240E+2	8.8	4.707E+1	5.4	4.173E+0	8.8
2.9E+1	9.416E+2	9.7	4.662E+1	3.2	4.246E+0	5.5
2.8E+1	9.734E+2	12.6	4.630E+1	3.6	4.236E+0	6.6
2.7E+1	1.014E+3	16.5	4.630E+1	7.3	4.122E+0	12.8
2.6E+1	1.044E+3	19.9	4.666E+1	12.2	4.001E+0	21.3
2.5E+1	1.046E+3	21.5	4.642E+1	14.9	3.914E+0	25.6
2.4E+1	1.011E+3	20.8	4.527E+1	14.1	4.034E+0	23.2
2.3E+1	9.449E+2	17.4	4.316E+1	10.9	4.094E+0	16.9
2.2E+1	8.609E+2	11.0	4.064E+1	6.5	4.103E+0	9.8
2.0E+1	7.806E+2	2.7	3.828E+1	2.9	4.108E+0	3.2
1.9E+1	6.189E+2	19.2	3.446E+1	11.5	4.264E+0	13.9
1.8E+1	5.765E+2	20.1	3.298E+1	13.1	4.234E+0	15.7
1.7E+1	5.192E+2	3.4	3.192E+1	3.2	3.507E+0	4.2
1.6E+1	5.192E+2	3.4	3.192E+1	3.2	3.507E+0	4.2
1.5E+1	4.663E+2	4.8	3.040E+1	6.7	3.222E+0	9.2
1.4E+1	3.969E+2	2.6	2.987E+1	2.2	3.235E+0	3.3
1.3E+1	3.283E+2	14.9	2.964E+1	5.2	3.406E+0	6.5
1.2E+1	2.701E+2	27.1	2.932E+1	8.1	3.495E+0	10.0
1.1E+1	2.213E+2	32.3	2.847E+1	7.2	3.423E+0	8.6
1.0E+1	1.797E+2	31.5	2.753E+1	5.0	3.324E+0	5.9
9.0E+0	1.520E+2	17.9	2.750E+1	3.7	3.378E+0	4.4
8.0E+0	1.508E+2	27.5	2.871E+1	1.4	3.451E+0	1.8
7.0E+0	1.496E+2	56.3	2.900E+1	16.6	2.960E+0	23.6
6.0E+0	9.150E+1	23.3	2.271E+1	34.4	1.755E+0	65.2
5.0E+0						

\* unit:  $n \text{ cm}^{-2} \text{ Lethergy}^{-1} \mu\text{C}^{-1}$

<sup>b</sup> Read as  $4.4 \times 10^3$

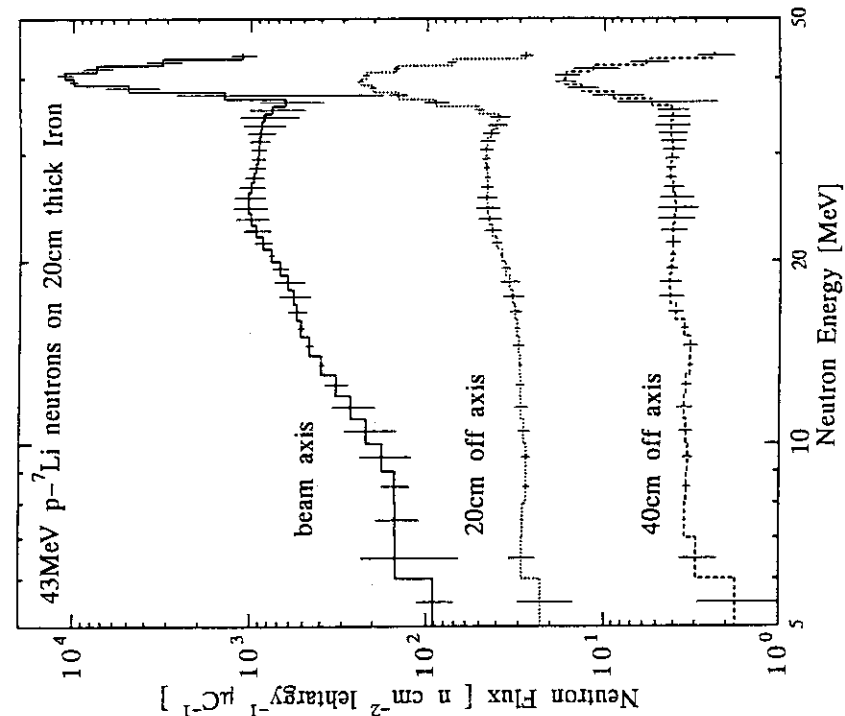


Fig.1.9 Neutron spectra behind 20cm thick iron measured by the BC501A detector on the beam axis, 20- and 40-cm off axis for 43-MeV p-Li neutrons

Table 1.10 Neutron spectra behind 40cm thick iron measured by the BC501A detector for 43-MeV p-Li neutrons

Energy (MeV)	Flux *	Error (%)	Flux	Error (%)	Flux	Error (%)
beam axis	20cm off axis		40cm off axis			
4.4E+1	6.705E+1	12.5	6.384E+0	15.8	9.880E-1	21.1
4.3E+1	1.942E+2	5.8	1.805E+1	10.0	2.025E+0	12.2
4.2E+1	3.922E+2	2.6	3.981E+1	6.6	3.880E+0	10.6
4.1E+1	5.260E+2	3.4	6.4	5.927E+0	10.8	
4.0E+1	4.591E+2	5.3	6.408E+1	6.0	6.529E+0	6.7
3.9E+1	2.541E+2	6.3	4.998E+1	7.4	4.882E+0	12.1
3.8E+1	8.991E+1	4.7	3.292E+1	22.5	2.611E+0	30.0
3.7E+1	2.836E+1	18.1	1.996E+1	30.9	1.568E+0	48.5
3.6E+1	2.073E+1	2.5	1.254E+1	11.1	1.467E+0	14.8
3.5E+1	2.562E+1	15.9	1.017E+1	20.1	1.539E+0	14.1
3.4E+1	3.105E+1	10.5	1.013E+1	20.9	1.519E+0	15.1
3.3E+1	3.532E+1	8.7	1.052E+1	17.3	1.552E+0	13.3
3.2E+1	3.842E+1	8.2	1.082E+1	15.6	1.440E+0	12.7
3.1E+1	4.055E+1	7.5	1.093E+1	13.3	1.366E+0	11.5
3.0E+1	4.183E+1	6.9	1.088E+1	9.0	1.294E+0	8.1
2.9E+1	4.234E+1	7.2	1.066E+1	5.6	1.243E+0	5.1
2.8E+1	4.217E+1	9.1	1.036E+1	6.3	1.206E+0	5.8
2.7E+1	4.155E+1	12.4	1.052E+1	12.7	1.174E+0	10.9
2.6E+1	4.080E+1	15.7	9.899E+0	21.9	1.145E+0	20.4
2.5E+1	4.000E+1	17.4	9.555E+0	27.5	1.118E+0	25.4
2.4E+1	3.912E+1	16.6	9.052E+0	26.8	1.093E+0	24.0
2.3E+1	3.807E+1	13.3	8.405E+0	21.2	1.063E+0	18.1
2.2E+1	3.685E+1	7.9	7.717E+0	13.0	1.019E+0	10.8
2.1E+1	3.559E+1	1.8	7.102E+0	4.1	9.532E-1	3.5
2.0E+1	3.418E+1	6.3	6.583E+0	11.6	8.708E-1	9.5
1.9E+1	3.227E+1	11.1	6.141E+0	24.5	7.861E-1	20.7
1.8E+1	2.941E+1	11.7	5.820E+0	28.3	7.220E-1	24.8
1.7E+1	2.568E+1	7.3	5.646E+0	15.8	6.938E-1	14.4
1.6E+1	2.183E+1	2.2	5.491E+0	7.1	6.917E-1	6.3
1.5E+1	1.882E+1	3.8	5.228E+0	14.9	6.907E-1	12.1
1.4E+1	1.699E+1	1.9	4.944E+0	5.1	6.809E-1	4.1
1.3E+1	1.587E+1	9.7	4.742E+0	12.4	6.726E-1	9.4
1.2E+1	1.465E+1	15.7	4.485E+0	20.2	6.706E-1	14.6
1.1E+1	1.284E+1	17.5	4.084E+0	19.0	6.622E-1	12.6
1.0E+1	1.069E+1	16.7	3.817E+0	13.7	6.439E-1	8.7
9.0E+0	8.595E+0	9.8	3.884E+0	10.0	6.454E-1	6.5
8.0E+0	6.529E+0	20.2	4.218E+0	3.8	6.952E-1	2.5
7.0E+0	5.532E+0	53.6	4.562E+0	40.1	7.319E-1	26.9
6.0E+0	6.227E+0	36.5	3.857E+0	77.0	5.873E-1	54.5
5.0E+0						

\* unit:  $n \text{ cm}^{-2} \text{ Lethargy}^{-1} \mu\text{C}^{-1}$

<sup>b</sup> Read as  $4.4 \times 10^1$

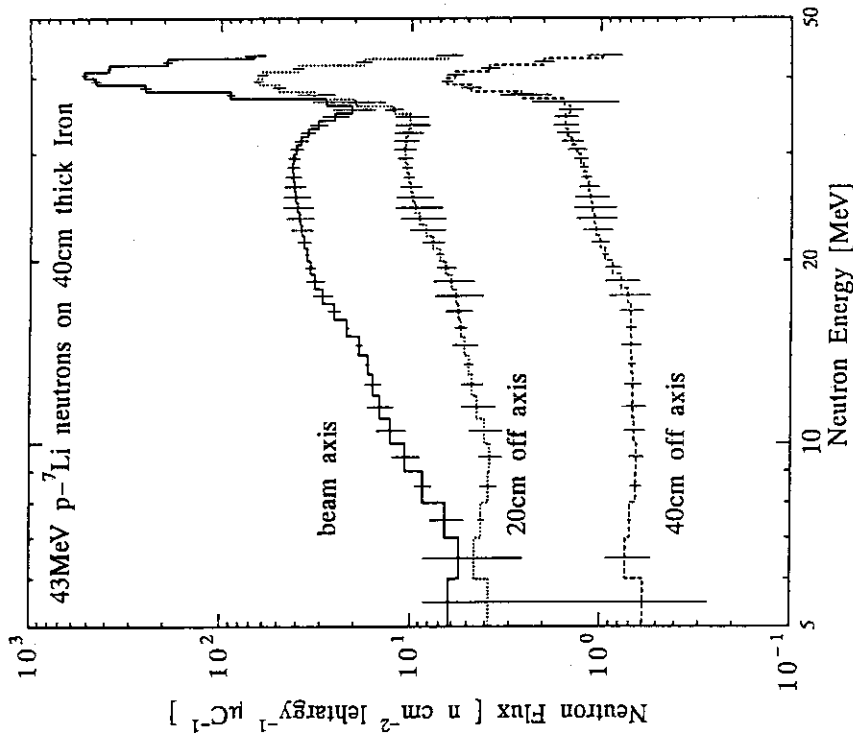


Fig.1.10 Neutron spectra behind 40cm thick iron measured by the BC501A detector on the beam axis, 20- and 40-cm off axis for 43-MeV p-Li neutrons

Table 1.11 Neutron spectra behind 20, 40, 70, 100 and 130cm thick iron measured by the BC501A detector for 68-MeV p-Li neutrons

Energy (MeV)	Flux *	Error (%)	Flux	Error (%)						
thick	20cm	40cm	70cm	100cm	130cm					
7.8E+1	1.749E+4	5.3	1.317E+3	8.6	3.045E+1	12.7	8.076E-1	17.7	5.212E-2	33.4
6.6E+1	1.935E+4	5.3	3.23E+3	4.9	6.989E+1	12.9	2.074E-1	17.8	1.167E-2	19.6
6.4E+1	9.488E+4	5.0	1.069E+2	6.7	4.456E+1	12.9	2.575E+0	10.9	7.148E-2	41.9
6.2E+1	1.322E+4	5.1	2.624E+2	3.0	4.313E+1	21.1	1.217E+0	12.5	6.278E-2	44.9
5.8E+1	3.507E+3	4.2	1.533E+2	29.3	4.691E+0	29.2	2.211E-0	59.6	5.186E-3	155.0
5.6E+1	5.566E+3	4.2	1.534E+2	6.6	4.014E+0	20.5	2.154E-0	28.8	7.440E-2	88.0
5.4E+1	1.421E+3	4.1	1.534E+2	7.6	8.521E+0	6.9	3.732E-0	1.1	1.033E-2	24.6
5.2E+1	2.953E+3	3.9	1.534E+2	5.6	9.587E+0	6.9	3.992E-0	7.9	1.160E-2	26.3
5.0E+1	4.020E+3	4.0	3.219E+2	6.0	9.459E+0	8.1	3.760E-0	1.3	1.232E-2	26.3
4.8E+1	4.115E+3	4.0	3.219E+2	7.0	9.459E+0	8.5	3.760E-0	1.3	1.232E-2	27.5
4.6E+1	4.335E+3	4.0	3.219E+2	7.4	6.723E+0	11.0	2.416E-0	5.6	1.623E-2	22.8
4.4E+1	4.483E+3	4.0	3.219E+2	8.0	6.325E+0	11.6	2.309E-0	16.8	1.745E-2	22.0
4.2E+1	4.632E+3	4.0	3.219E+2	8.6	6.284E+0	12.5	2.178E-0	17.7	1.728E-2	22.5
4.0E+1	4.782E+3	4.0	3.219E+2	9.2	6.227E+0	13.5	2.143E-0	19.3	1.655E-2	22.6
3.8E+1	4.932E+3	4.0	3.219E+2	9.8	6.152E+0	14.0	2.107E-0	20.8	1.577E-2	23.0
3.6E+1	5.088E+3	4.0	3.219E+2	10.4	6.087E+0	14.4	2.049E-0	21.5	1.505E-2	24.0
3.4E+1	5.242E+3	4.0	3.219E+2	11.0	6.021E+0	15.0	2.012E-0	22.4	1.432E-2	24.9
3.2E+1	5.397E+3	4.0	3.219E+2	11.6	5.955E+0	15.6	1.975E-0	22.7	1.360E-2	25.6
3.0E+1	5.552E+3	4.0	3.219E+2	12.2	5.889E+0	16.0	1.938E-0	23.1	1.289E-2	26.0
2.8E+1	5.707E+3	4.0	3.219E+2	12.8	5.823E+0	16.5	1.891E-0	23.7	1.227E-2	26.6
2.6E+1	5.862E+3	4.0	3.219E+2	13.4	5.757E+0	17.0	1.844E-0	24.3	1.165E-2	27.1
2.4E+1	6.017E+3	4.0	3.219E+2	14.0	5.691E+0	17.5	1.797E-0	24.9	1.103E-2	27.9
2.2E+1	6.172E+3	4.0	3.219E+2	14.6	5.625E+0	18.0	1.750E-0	25.5	1.041E-2	28.5
2.0E+1	6.327E+3	4.0	3.219E+2	15.2	5.559E+0	18.5	1.703E-0	26.1	9.789E-3	29.1
1.8E+1	6.482E+3	4.0	3.219E+2	15.8	5.493E+0	19.0	1.656E-0	26.7	9.132E-3	29.7
1.6E+1	6.637E+3	4.0	3.219E+2	16.4	5.427E+0	19.5	1.609E-0	27.3	8.475E-3	30.3
1.4E+1	6.792E+3	4.0	3.219E+2	17.0	5.361E+0	20.0	1.562E-0	27.9	7.818E-3	30.9
1.2E+1	6.947E+3	4.0	3.219E+2	17.6	5.295E+0	20.5	1.515E-0	28.5	7.161E-3	31.5
1.0E+1	7.102E+3	4.0	3.219E+2	18.2	5.239E+0	21.0	1.468E-0	29.1	6.504E-3	32.1
8.0E+0	7.257E+3	4.0	3.219E+2	18.8	5.173E+0	21.5	1.421E-0	29.7	5.847E-3	32.7
6.0E+0	7.412E+3	4.0	3.219E+2	19.4	5.107E+0	22.0	1.374E-0	30.3	5.200E-3	33.3
4.0E+0	7.557E+3	4.0	3.219E+2	20.0	5.031E+0	22.5	1.327E-0	30.9	4.553E-3	33.9
2.0E+0	7.692E+3	4.0	3.219E+2	20.6	4.955E+0	23.0	1.280E-0	31.5	3.906E-3	34.5
0.0E+0	7.827E+3	4.0	3.219E+2	21.2	4.879E+0	23.5	1.233E-0	32.1	3.259E-3	35.1

Read as  $7.0 \times 10^{-1}$  unit:  $\text{cm}^{-2} \text{Lethargy}^{-1} \mu\text{C}^{-1}$

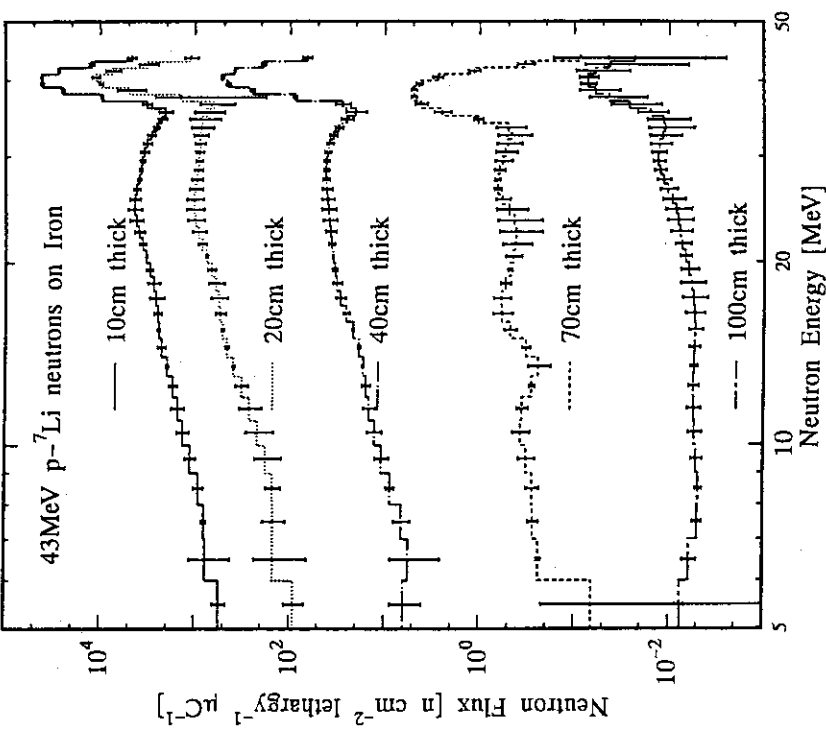


Fig.1.11

Neutron spectra behind various thickness of iron measured by the BC501A detector on the beam axis for 68-MeV p-Li neutrons

Table 1.12 Neutron spectra behind 0cm thick iron measured by the BC501A detector for 68-MeV p-Li neutrons

Energy (MeV)	Flux *	Error (%)	Flux	Error (%)
20cm off axis			40cm off axis	
1.0E+1	3.691E+1	3.2	1.843E+0	7.1
6.8E+1	6.570E+1	4.4	4.089E+0	8.7
6.6E+1	8.288E+1	3.8	5.269E+0	7.2
6.4E+1	4.212E+1	4.2	3.137E+0	8.3
6.2E+1	2.565E+1	5.9	2.388E+0	12.2
5.8E+1	2.572E+1	6.8	1.965E+0	9.3
5.6E+1	2.565E+1	6.8	1.940E+0	11.4
5.4E+1	2.754E+1	5.4	2.286E+0	8.5
5.2E+1	2.937E+1	5.7	2.858E+0	7.5
4.8E+1	3.290E+1	5.0	3.180E+0	6.7
4.6E+1	3.860E+1	5.4	3.559E+0	9.9
4.4E+1	4.822E+1	6.4	4.050E+0	8.0
4.2E+1	4.283E+1	6.4	3.554E+0	7.0
4.0E+1	3.164E+1	6.0	3.532E+0	7.0
3.9E+1	3.023E+1	6.0	3.530E+0	8.0
3.8E+1	3.037E+1	6.2	3.586E+0	9.0
3.7E+1	3.162E+1	6.2	3.713E+0	9.4
3.6E+1	3.316E+1	6.2	3.883E+0	8.0
3.5E+1	3.108E+1	6.8	3.474E+0	9.0
3.4E+1	3.023E+1	6.8	3.474E+0	9.5
3.3E+1	3.039E+1	6.8	3.658E+0	9.5
3.2E+1	3.234E+1	6.8	3.667E+0	10.7
3.1E+1	3.294E+1	6.8	3.740E+0	10.1
3.0E+1	3.027E+1	6.7	3.740E+0	10.6
2.9E+1	3.027E+1	6.7	3.752E+0	7.6
2.8E+1	3.456E+1	4.6	3.752E+0	8.8
2.7E+1	3.013E+1	4.6	3.100E+0	10.1
2.6E+1	3.282E+1	5.4	3.605E+0	11.6
2.5E+1	3.013E+1	5.4	3.605E+0	11.1
2.4E+1	3.222E+1	5.4	3.474E+0	11.1
2.3E+1	3.370E+1	5.4	3.120E+0	11.1
2.2E+1	3.022E+1	5.4	3.294E+0	11.1
2.1E+1	3.370E+1	5.4	3.120E+0	11.1
2.0E+1	3.022E+1	5.4	3.294E+0	11.1
1.9E+1	3.370E+1	5.4	3.120E+0	11.1
1.8E+1	3.022E+1	5.4	3.294E+0	11.1
1.7E+1	3.370E+1	5.4	3.120E+0	11.1
1.6E+1	3.022E+1	5.4	3.294E+0	11.1
1.5E+1	3.370E+1	5.4	3.120E+0	11.1
1.4E+1	3.022E+1	5.4	3.294E+0	11.1
1.3E+1	3.370E+1	5.4	3.120E+0	11.1
1.2E+1	3.022E+1	5.4	3.294E+0	11.1
1.1E+1	3.370E+1	5.4	3.120E+0	11.1
1.0E+1	3.022E+1	5.4	3.294E+0	11.1
9.0E+0	1.792E+1	3.7	2.274E+0	5.8
8.0E+0	1.244E+1	7.7	2.274E+0	5.8

\* Read as  $7.0 \times 10^{-2} \text{ Lenergy}^{-1} \mu\text{C}^{-1}$

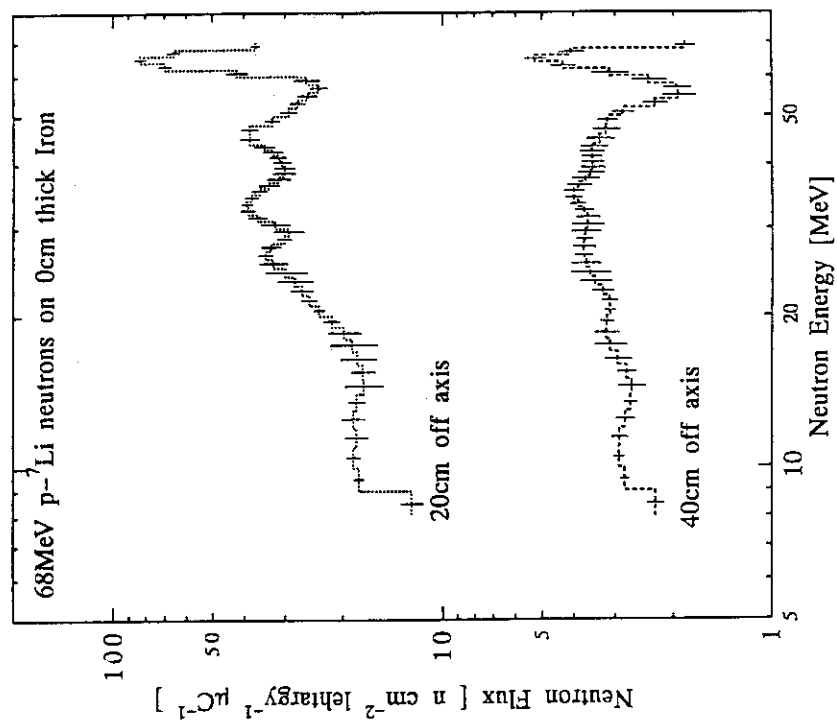


Fig.1.12 Neutron spectra behind 0cm thick iron measured by the BC501A detector on 20- and 40-cm off axis for 68-MeV p-Li neutrons

Table 1.13 Neutron spectra behind 20cm thick iron measured by the BC501A detector for 68-MeV p-Li neutrons

Energy (MeV)	Flux *	Error (%)	Flux	Error (%)	Flux	Error (%)	Flux	Error (%)
	beam axis	20cm off axis	20cm off axis	20cm off axis	40cm off axis	40cm off axis	40cm off axis	40cm off axis
7.0E+1	1.749E+2	5.0	5.167E+0	8.4	3.192E+0	3.1	2.945E+0	3.5
6.8E+1	1.935E+2	7.7	1.032E+1	14.0	1.636E+1	8.0	1.803E+1	5.5
6.6E+1	2.948E+2	4.7	1.803E+1	12.9	1.390E+0	13.8	1.950E+0	3.6
6.4E+1	2.329E+2	3.8	1.340E+1	10.0	8.997E+0	8.8	1.523E+0	6.2
6.2E+1	1.507E+2	10.9	8.997E+0	10.9	8.997E+0	10.9	8.997E+0	4.8
6.0E+1	1.356E+2	10.9	8.997E+0	10.9	8.997E+0	10.9	8.997E+0	3.5
5.8E+1	1.172E+2	3.8	1.172E+2	3.8	1.172E+2	3.8	1.172E+2	2.6
5.6E+1	1.172E+2	3.8	1.172E+2	3.8	1.172E+2	3.8	1.172E+2	2.6
5.4E+1	1.172E+2	3.8	1.172E+2	3.8	1.172E+2	3.8	1.172E+2	2.6
5.2E+1	1.172E+2	3.8	1.172E+2	3.8	1.172E+2	3.8	1.172E+2	2.6
5.0E+1	1.020E+3	4.0	5.39E+2	3.0	1.191E+1	1.1	1.264E+1	1.1
4.8E+1	1.150E+3	4.6	6.605E+2	2.8	1.311E+1	1.1	1.333E+1	1.1
4.6E+1	8.350E+3	4.9	6.606E+2	2.4	1.345E+1	1.1	1.358E+1	1.1
4.4E+1	4.150E+3	5.5	5.866E+2	2.6	1.370E+1	1.1	1.385E+1	1.1
4.2E+1	4.830E+3	5.5	5.866E+2	2.6	1.370E+1	1.1	1.385E+1	1.1
4.0E+1	2.948E+3	6.7	5.388E+2	2.9	1.399E+1	1.1	1.421E+1	1.1
3.8E+1	2.829E+3	7.8	5.978E+2	3.4	1.423E+1	1.1	1.423E+1	1.1
3.6E+1	2.735E+3	8.1	5.483E+2	4.0	1.413E+1	1.1	1.424E+1	1.1
3.4E+1	2.663E+3	7.8	5.483E+2	4.1	1.423E+1	1.1	1.424E+1	1.1
3.2E+1	2.664E+3	7.8	5.454E+2	4.2	1.424E+1	1.1	1.424E+1	1.1
3.0E+1	2.677E+3	6.0	4.059E+2	4.1	1.388E+1	1.1	1.323E+1	1.1
2.8E+1	2.445E+3	6.0	3.056E+2	4.1	1.287E+1	1.1	1.252E+1	1.1
2.6E+1	2.633E+3	6.0	3.392E+2	4.5	1.217E+1	1.1	1.217E+1	1.1
2.4E+1	2.633E+3	6.0	3.392E+2	4.5	1.147E+1	1.1	1.147E+1	1.1
2.2E+1	1.963E+3	6.5	1.93E+2	5.5	1.142E+1	1.1	1.142E+1	1.1
2.0E+1	1.947E+3	6.5	1.940E+2	5.5	1.140E+1	1.1	1.140E+1	1.1
1.8E+1	1.988E+3	7.8	1.988E+2	5.5	1.066E+2	5.9	1.066E+2	5.0
1.6E+1	1.975E+3	8.7	1.995E+2	5.7	1.036E+2	6.7	1.036E+2	5.0
1.4E+1	1.824E+3	13.9	9.919E+1	7.7	9.919E+1	7.7	9.919E+1	5.6
1.2E+1	1.562E+3	17.0	9.919E+1	7.7	9.919E+1	7.7	9.919E+1	5.6
1.0E+1	1.422E+3	11.1	9.889E+1	7.7	9.889E+1	7.7	9.889E+1	5.6
8.0E+0	1.344E+3	11.1	9.889E+1	7.7	9.889E+1	7.7	9.889E+1	5.6
6.0E+0	1.056E+2	15.7	9.645E+1	13.3	9.645E+1	13.3	9.645E+1	12.4
4.0E+0	1.909E+1	1.8	5.056E+0	1.8	5.056E+0	1.8	5.056E+0	1.8
2.0E+0	1.860E+2	30.1	6.902E+1	4.9	6.902E+1	4.9	6.902E+1	4.9
0.0E+0	6.659E+2	2.3	6.569E+1	4.9	6.569E+1	4.9	6.569E+1	4.9
8.0E+0	6.159E+2	13.3	6.289E+1	2.6	6.289E+1	2.6	6.289E+1	2.6
6.0E+0	5.428E+2	18.0	6.089E+1	1.8	6.089E+1	1.8	6.089E+1	1.8
4.0E+0	4.990E+2	18.0	5.961E+1	2.3	5.961E+1	2.3	5.961E+1	2.3
2.0E+0	4.958E+2	15.1	5.855E+1	4.2	5.855E+1	4.2	5.855E+1	4.2
0.0E+0	4.957E+2	19.7	6.659E+1	4.7	6.659E+1	4.7	6.659E+1	4.7
8.0E+0	4.740E+2	12.1	5.244E+1	6.5	5.244E+1	6.5	5.244E+1	6.5
6.0E+0	4.025E+2	10.6	4.491E+1	4.1	4.491E+1	4.1	4.491E+1	4.1
4.0E+0	2.624E+2	16.3	4.155E+1	4.9	4.155E+1	4.9	4.155E+1	4.9

\* unit:  $n \text{ cm}^{-2} \text{ lethargy}^{-1} \mu\text{C}^{-1}$

Read as  $7.0 \times 10^0$

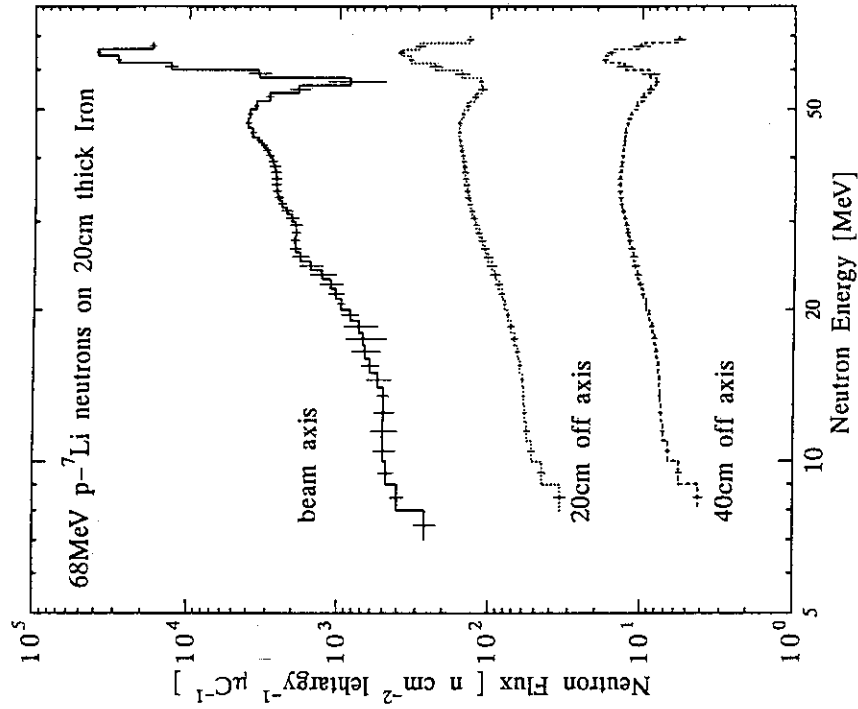


Fig.1.13 Neutron spectra behind 20cm thick iron measured by the BC501A detector on the beam axis, 20- and 40-cm off axis for 68-MeV p-Li neutrons

Table 1.14 Neutron spectra behind 40cm thick iron measured by the BC501A detector for 68-MeV p-Li neutrons

Energy (MeV)	Flux *	Error (%)	Flux	Error (%)	Flux	Error (%)
beam axis	20cm off axis		40cm off axis		beam axis	
7.0E+1	2.495E+1	13.8	3.943E+0	13.1	8.477E+0	26.1
6.8E+1	1.317E+3	8.6	5.952E+2	8.9	1.034E+1	14.0
6.6E+1	3.213E+3	6.6	1.426E+2	6.1	2.627E+0	16.1
6.4E+1	1.069E+3	15.0	1.739E+2	12.1	9.624E+0	35.4
6.2E+1	2.624E+2	30.1	1.532E+1	13.2	4.867E+0	11.8
6.0E+1	1.533E+2	2.2	1.932E+1	19.2	5.586E+0	11.1
5.8E+1	2.344E+2	1.2	1.824E+1	12.2	6.091E+0	11.3
5.6E+1	2.779E+2	5.4	9.967E+1	4.1	6.463E+0	5.2
5.4E+1	3.067E+2	7.6	5.755E+1	4.3	6.971E+0	4.6
5.2E+1	5.05E+1	6.0	6.067E+1	5.0	7.000E+0	4.4
5.0E+1	3.230E+2	6.0	6.162E+1	5.2	6.866E+0	4.9
4.8E+1	3.219E+2	7.0	5.955E+1	5.2	6.701E+0	4.2
4.6E+1	2.959E+2	8.4	6.425E+1	5.3	6.579E+0	4.6
4.4E+1	6.696E+2	8.6	5.526E+1	5.8	6.339E+0	5.2
4.2E+1	5.474E+2	5.5	5.555E+1	5.8	6.228E+0	5.9
4.0E+1	4.127E+2	3.2	4.233E+2	10.9	6.610E+0	6.0
3.8E+1	2.047E+2	0.4	1.111E+2	12.9	5.991E+0	7.6
3.6E+1	9.425E+2	12.2	4.913E+1	7.6	5.911E+0	7.1
3.4E+1	2.018E+2	10.4	4.444E+1	7.3	5.790E+0	7.0
3.2E+1	1.922E+2	1.4	4.444E+1	7.4	5.652E+0	7.0
3.0E+1	1.922E+2	1.4	4.444E+1	7.5	5.549E+0	7.0
2.8E+1	1.651E+2	8.2	8.613E+1	8.6	6.096E+0	6.5
2.6E+1	1.600E+2	1.1	1.621E+2	1.1	6.430E+0	1.0
2.4E+1	1.192E+2	1.2	1.084E+2	2.1	2.043E+0	1.2
2.2E+1	1.081E+2	1.0	8.01E+1	2.1	9.144E+0	1.0
2.0E+1	8.955E+1	1.2	9.555E+1	1.2	8.074E+0	1.0
1.8E+1	6.747E+1	1.2	18.992E+1	24.7	1.713E+1	17.9
1.6E+1	5.188E+1	1.0	1.922E+2	21.0	2.430E+1	21.9
1.4E+1	3.488E+1	1.2	1.084E+2	32.2	2.043E+1	21.9
1.2E+1	1.035E+2	1.4	1.035E+2	1.1	9.533E+0	1.0
1.0E+1	8.955E+1	1.2	9.555E+1	1.6	1.807E+1	2.2
8.0E+0	6.490E+1	1.7	1.713E+1	1.1	1.398E+1	1.1
7.0E+0	6.517E+1	23.4	5.538E+1	6.3	1.344E+1	13.4
					5.544E+1	15.9
					5.644E+1	13.0
					5.688E+1	9.3
					6.519E+1	6.0
					6.00E+0	9.0
					6.448E+0	2.2
					2.665E+0	2.8
					2.665E+0	1.6

\* unit:  $\text{n cm}^{-2} \text{Leihtergy}^{-1} \mu\text{C}^{-1}$

Read as  $7.0 \times 10^0$

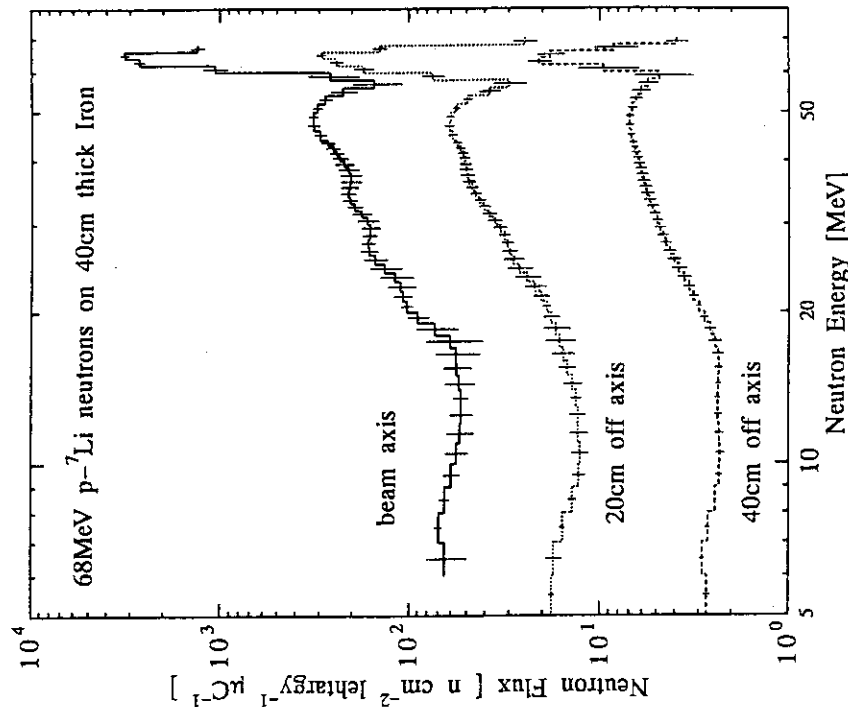


Fig.1.14 Neutron spectra behind 40cm thick iron measured by the BC501A detector on the beam axis, 20- and 40-cm off axis for 68-MeV p-Li neutrons

Table 1.15 Neutron spectra behind 25, 50, 100 and 150cm thick concrete shield measured by the BC501A detector for 43-MeV p-Li neutrons

Energy (MeV)	Flux *	Error (%)	Flux	Error (%)	Flux	Error (%)	Flux	Error (%)
25 cm thick	25 cm	50 cm	100 cm	150 cm				
4.4E+1	6.744E+3	9.3	9.291E+2	10.0	7.982E+0	6.3	2.026E-1	10.9
4.3E+1	3.17E+4	4.5	1.609E+3	4.8	1.658E+1	3.7	3.907E-1	7.7
4.2E+1	1.965E+4	1.5	2.215E+3	1.6	2.741E+1	1.9	6.249E-1	5.7
4.1E+1	2.265E+4	1.8	2.429E+3	1.7	3.590E+1	1.0	8.164E-1	3.8
4.0E+1	2.023E+4	3.1	2.112E+3	2.8	3.730E+1	2.2	8.651E-1	2.2
3.9E+1	1.396E+4	4.1	1.451E+3	3.6	3.104E+1	4.0	7.466E-1	6.9
3.8E+1	7.428E+3	4.1	7.942E+2	3.3	2.133E+1	5.0	5.400E-1	15.0
3.7E+1	3.133E+3	3.8	3.710E+2	3.1	2.133E+1	3.8	5.66E-1	20.7
3.6E+1	1.325E+3	3.2	1.905E+2	1.0	8.372E+0	2.4	3.514E-1	15.1
3.5E+1	1.019E+3	17.3	1.55E+2	13.9	6.416E+0	6.0	2.110E-1	5.5
3.4E+1	1.274E+3	33.1	1.635E+2	11.2	5.779E+0	6.7	1.996E-1	13.0
3.3E+1	1.611E+3	10.5	1.829E+2	9.8	5.528E+0	6.2	1.934E-1	15.7
3.2E+1	1.878E+3	9.4	1.933E+2	9.7	5.311E+0	6.2	1.657E-1	15.0
3.1E+1	2.054E+3	8.4	2.052E+2	9.3	5.036E+0	6.4	1.847E-1	17.3
3.0E+1	2.147E+3	7.6	2.01E+2	8.9	4.96E+0	6.5	1.626E-1	13.1
2.9E+1	2.168E+3	8.0	2.058E+2	9.6	4.537E+0	7.5	1.532E-1	13.0
2.8E+1	2.130E+3	10.3	1.939E+2	12.6	4.291E+0	10.1	1.462E-1	15.9
2.7E+1	1.936E+3	14.4	1.756E+2	18.3	4.037E+0	10.4	1.410E-1	18.5
2.6E+1	1.930E+3	19.0	1.578E+2	25.1	3.766E+0	19.4	1.358E-1	20.9
2.5E+1	1.888E+3	21.9	1.425E+2	30.4	3.404E+0	23.3	1.288E-1	22.2
2.4E+1	1.725E+3	21.7	1.330E+2	30.4	3.033E+0	24.4	1.184E-1	21.8
2.3E+1	1.665E+3	17.4	1.295E+2	24.4	2.676E+0	21.5	1.046E-1	18.9
2.2E+1	1.640E+3	10.3	1.202E+2	14.0	2.389E+0	14.7	8.81E-2	13.9
2.1E+1	1.644E+3	2.2	1.324E+2	3.0	2.166E+0	3.6	4.671E-2	4.9
2.0E+1	1.649E+3	7.6	1.333E+2	10.3	2.023E+0	12.1	5.705E-2	12.0
1.9E+1	1.635E+3	12.6	1.297E+2	17.6	1.931E+0	20.9	4.810E-2	22.0
1.8E+1	1.555E+3	12.7	1.033E+2	18.4	1.847E+0	21.5	4.529E-2	22.0
1.7E+1	1.417E+3	7.5	1.033E+2	11.7	1.757E+0	21.8	4.671E-2	13.9
1.6E+1	1.267E+3	2.1	8.752E+1	3.2	1.645E+0	3.6	4.872E-2	6.9
1.5E+1	1.157E+3	3.5	7.839E+1	5.6	1.545E+0	5.7	4.830E-2	5.1
1.4E+1	1.108E+3	1.7	7.448E+1	2.7	1.463E+0	2.7	4.499E-2	8.5
1.3E+1	1.089E+3	8.6	8.043E+1	12.4	1.394E+0	12.6	4.405E-2	17.5
1.2E+1	1.054E+3	12.4	8.144E+1	17.7	1.333E+0	19.7	3.714E-2	25.1
1.1E+1	9.850E+2	13.0	7.837E+1	17.9	1.297E+0	19.9	3.589E-2	26.7
1.0E+1	9.110E+2	11.1	7.365E+1	15.1	1.314E+0	15.6	3.780E-2	19.9
9.0E+0	8.461E+2	5.7	6.797E+1	7.7	1.378E+0	7.0	4.511E-2	2.8
8.0E+0	7.555E+2	9.9	5.690E+1	14.4	1.441E+0	10.5	5.828E-2	22.4
7.0E+0	6.756E+2	22.3	4.823E+1	38.2	1.522E+0	22.3	6.872E-2	42.0
6.0E+0	6.938E+2	25.4	5.012E+1	28.2	1.655E+0	15.7	6.311E-2	54.7
5.0E+0	6.344E+2	42.9	3.966E+1	73.6	1.570E+0	27.7		
4.0E+0								

\* unit: n cm<sup>-2</sup> Lenergy<sup>-1</sup> μ C<sup>-1</sup>

Read as 4.4 × 10<sup>-1</sup>

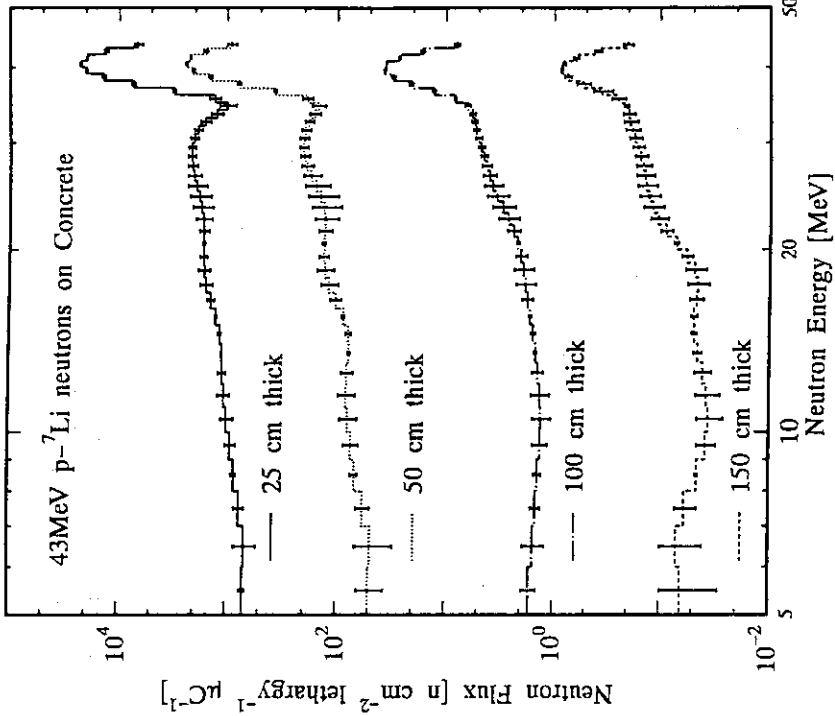


Fig.1.15 Neutron spectra behind various thicknesses of concrete measured by the BC501A detector on the beam axis for 43-MeV p-Li neutrons

Table 1.16 Neutron spectra behind 25cm thick concrete measured by the BC501A detector for 43-MeV p-Li neutrons

Energy (MeV)	Flux * ( $\mu\text{C}^{-1}$ )	Error (%)	Flux 20cm off axis	Error (%)	Flux 40cm off axis	Error (%)
4.4E+1	6.744E+3	9.3	1.029E+2	55.7	1.240E+1	20.0
4.3E+1	1.317E+4	4.5	1.864E+2	64.4	2.332E+1	21.5
4.2E+1	1.965E+4	1.5	3.223E+2	39.8	3.197E+1	16.8
4.1E+1	2.265E+4	1.8	4.607E+2	11.9	3.461E+1	6.8
4.0E+1	2.023E+4	3.1	5.036E+2	10.4	3.263E+1	8.3
3.9E+1	1.396E+4	4.1	4.150E+2	24.0	2.852E+1	17.1
3.8E+1	1.428E+3	4.1	2.740E+2	29.4	1.322E+1	17.1
3.7E+1	3.133E+3	3.8	1.732E+2	21.6	1.833E+1	9.6
3.6E+1	1.325E+3	1.2	1.304E+2	9.8	1.551E+1	4.1
3.5E+1	1.019E+3	17.3	1.189E+2	10.3	1.463E+1	5.5
3.4E+1	1.274E+3	13.1	1.165E+2	9.7	1.454E+1	5.3
3.3E+1	1.611E+3	10.5	1.156E+2	8.1	1.452E+1	4.5
3.2E+1	1.878E+3	9.4	1.144E+2	7.1	1.438E+1	4.3
3.1E+1	2.054E+3	8.4	1.127E+2	7.3	1.416E+1	4.6
3.0E+1	2.147E+3	7.6	1.105E+2	8.5	1.391E+1	5.2
2.9E+1	2.168E+3	8.0	1.078E+2	10.4	1.365E+1	6.4
2.8E+1	2.130E+3	14.4	1.048E+2	13.9	1.342E+1	7.9
2.7E+1	2.043E+3	14.4	1.018E+2	15.9	1.324E+1	9.5
2.6E+1	1.930E+3	19.0	9.920E+1	18.1	1.310E+1	10.7
2.5E+1	1.818E+3	21.9	9.722E+1	18.8	1.302E+1	10.9
2.4E+1	1.725E+3	21.7	9.514E+1	17.3	1.299E+1	9.9
2.3E+1	1.665E+3	17.4	9.452E+1	13.7	1.291E+1	7.7
2.2E+1	1.640E+3	10.3	9.336E+1	7.8	1.306E+1	4.4
2.1E+1	1.642E+3	2.2	9.200E+1	2.0	1.309E+1	1.3
2.0E+1	1.649E+3	7.6	9.030E+1	5.1	1.304E+1	2.6
1.9E+1	1.630E+3	12.6	8.799E+1	8.2	1.286E+1	4.0
1.8E+1	1.551E+3	12.7	8.433E+1	12.5	1.223E+1	2.7
1.7E+1	1.478E+3	7.5	8.127E+1	5.6	1.166E+1	1.4
1.6E+1	1.261E+3	2.2	7.751E+1	2.9	1.132E+1	1.1
1.5E+1	1.157E+3	3.5	7.452E+1	2.2	1.102E+1	1.3
1.4E+1	1.108E+3	1.7	7.164E+1	3.7	1.112E+1	1.8
1.3E+1	1.083E+3	8.1	6.964E+1	6.7	1.103E+1	3.3
1.2E+1	1.055E+3	12.4	6.788E+1	8.9	1.100E+1	4.3
1.1E+1	9.850E+2	13.0	6.622E+1	9.4	1.102E+1	3.4
1.0E+1	9.110E+2	11.1	6.503E+1	7.5	1.114E+1	3.4
9.0E+0	8.461E+2	5.7	6.352E+1	1.2	1.130E+1	0.6
8.0E+0	7.555E+2	9.9	5.906E+1	14.2	1.109E+1	6.0
7.0E+0	6.756E+2	22.3	4.854E+1	38.5	9.770E+0	15.0
6.0E+0	6.938E+2	5.4	4.244E+1	42.9		
4.0E+0						

\* unit:  $n \text{ cm}^{-2} \text{ Leitnergy}^{-1} \mu\text{C}^{-1}$   
o Read as  $4.4 \times 10^{-1}$

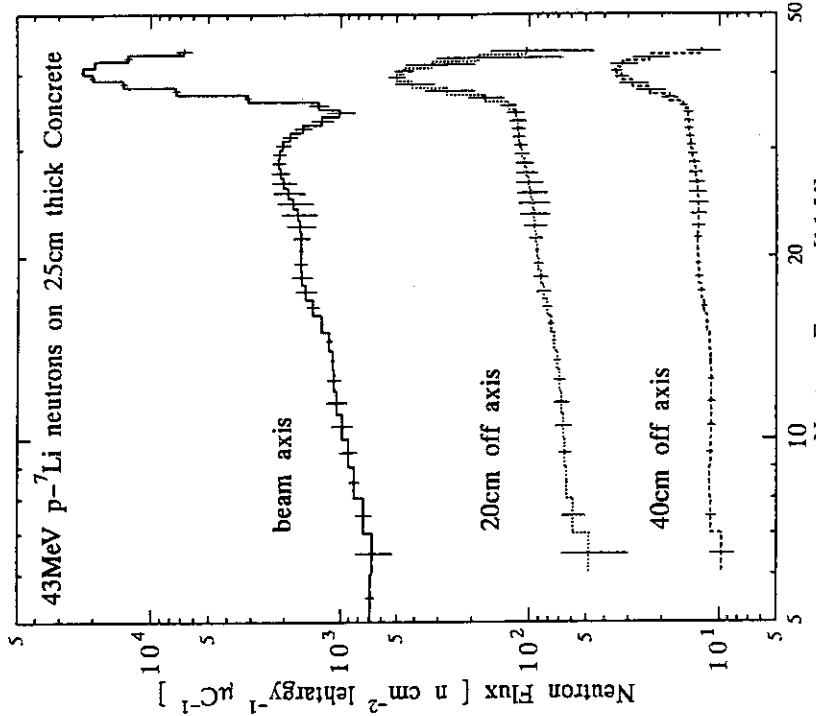


Fig.1.16

Neutron spectra behind 25cm thick concrete measured by the BC501A detector on the beam axis, 20- and 40-cm off axis for 43-MeV p-Li neutrons

Table 1.17 Neutron spectra behind 50cm thick concrete measured by the BC501A detector for 43-MeV p-Li neutrons

Energy (MeV)	Flux *	Error (%)	Flux	Error (%)	Flux	Error (%)
	beam axis		20cm off axis		40cm off axis	
4. 4E+1	9. 291E+2	10. 9	7. 643E+1	30. 4	1. 148E+1	20. 0
4. 3E+1	1. 609E+3	4. 8	1. 393E+2	34. 9	2. 235E+1	20. 8
4. 2E+1	2. 429E+3	1. 6	2. 224E+2	23. 3	3. 336E+1	14. 9
4. 1E+1	2. 429E+3	1. 7	2. 958E+2	7. 4	4. 001E+1	5. 5
4. 0E+1	2. 112E+3	2. 8	3. 163E+2	6. 7	4. 012E+1	6. 3
3. 9E+1	1. 451E+3	3. 6	2. 661E+2	15. -	3. 390E+1	13. 5
3. 8E+1	1. 942E+2	3. 3	1. 792E+2	18. -	2. 466E+1	15. 2
3. 7E+1	3. 710E+2	3. -	1. 072E+2	14. -	1. 692E+1	9. 8
3. 6E+1	1. 905E+2	11. 0	7. 055E+1	7. -	1. 283E+1	4. 6
3. 5E+1	1. 515E+2	13. 9	5. 886E+1	7. 8	1. 140E+1	6. 8
3. 4E+1	1. 635E+2	11. 2	5. 551E+1	7. 5	1. 095E+1	6. 6
3. 3E+1	1. 829E+2	19. 8	5. 362E+1	6. 4	1. 064E+1	5. 7
3. 2E+1	1. 973E+2	9. 3	5. 230E+1	6. 6	1. 027E+1	5. 4
3. 1E+1	2. 052E+2	9. 3	5. 074E+1	7. 9	9. 362E+0	5. 7
3. 0E+1	2. 071E+2	8. 9	5. 074E+1	7. 9	9. 362E+0	6. 8
2. 9E+1	2. 028E+2	9. 6	4. 911E+1	9. 9	8. 812E+0	8. 6
2. 8E+1	1. 919E+2	12. 6	4. 751E+1	12. 5	8. 207E+0	11. 3
2. 7E+1	1. 756E+2	18. 3	4. 559E+1	15. 3	7. 606E+0	14. 5
2. 6E+1	1. 578E+2	25. 1	4. 440E+1	17. 6	7. 097E+0	17. 3
2. 5E+1	1. 425E+2	30. 4	4. 265E+1	18. 6	6. 766E+0	18. 5
2. 4E+1	1. 330E+2	30. 4	4. 063E+1	17. 7	6. 657E+0	17. 0
2. 3E+1	1. 295E+2	24. 4	3. 820E+1	14. 5	6. 575E+0	12. 9
2. 2E+1	1. 302E+2	14. 0	3. 575E+1	8. 9	6. 027E+0	7. 1
2. 1E+1	1. 324E+2	3. 0	3. 312E+1	2. 2	7. 326E+0	1. 8
2. 0E+1	1. 333E+2	10. 3	3. 061E+1	6. 5	7. 502E+0	4. 0
1. 9E+1	1. 297E+2	17. 6	2. 843E+1	11. 1	7. 403E+0	6. 3
1. 8E+1	1. 192E+2	18. 4	2. 662E+1	11. 1	6. 978E+0	6. 4
1. 7E+1	1. 033E+2	11. 7	2. 535E+1	7. 8	6. 344E+0	4. 5
1. 6E+1	8. 752E+1	3. 2	2. 424E+1	3. 9	5. 747E+0	2. 4
1. 5E+1	7. 839E+1	5. 6	2. 314E+1	2. 8	5. 398E+0	1. 9
1. 4E+1	7. 748E+1	2. 7	2. 198E+1	5. 2	5. 338E+0	3. 3
1. 3E+1	8. 043E+1	12. -	2. 085E+1	9. 8	5. 433E+0	5. 8
1. 2E+1	8. 144E+1	17. 7	1. 988E+1	13. 3	5. 513E+0	7. 5
1. 1E+1	7. 837E+1	17. 9	1. 921E+1	14. 0	5. 508E+0	7. 7
1. 0E+1	7. 365E+1	15. 1	1. 899E+1	11. 1	5. 412E+0	6. 1
9. 0E+0	6. 797E+1	7. 7	1. 943E+1	1. 5	5. 059E+0	1. 0
8. 0E+0	5. 690E+1	14. 4	2. 016E+1	18. 1	4. 087E+0	14. 1
7. 0E+0	4. 823E+1	38. 2	1. 947E+1	41. 8		
6. 0E+0	5. 012E+1	28. 2				
5. 0E+0	3. 196E+1	73. 6				
4. 0E+0						

\* unit:  $n \text{ cm}^{-2} \text{ Lethargy}^{-1} \mu \text{ C}^{-1}$

† Read as  $4.4 \times 10^4$

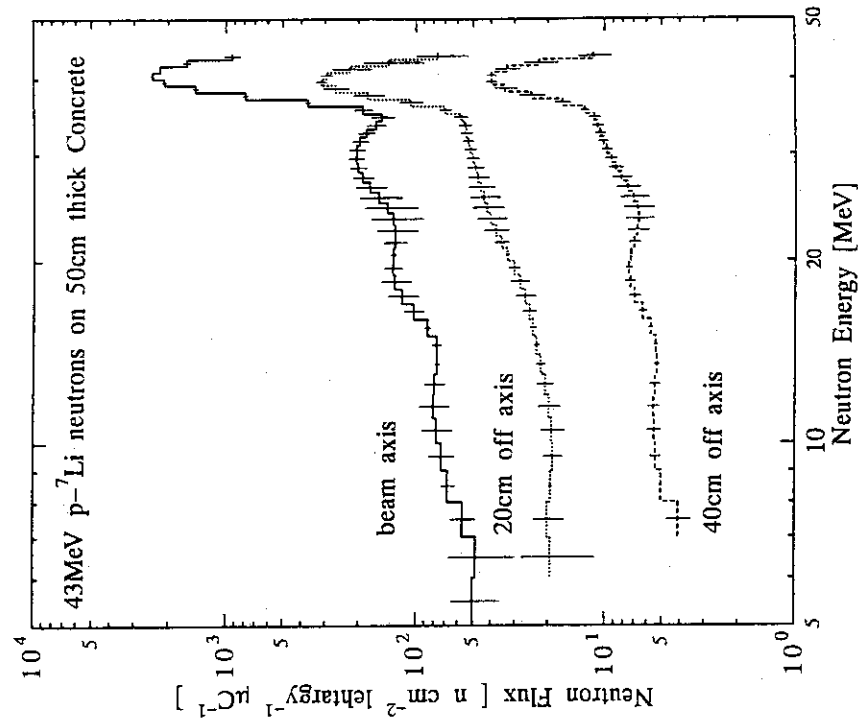


Fig.1.17 Neutron spectra behind 50cm thick concrete measured by the BC501A detector on the beam axis, 20- and 40-cm off axis for 43-MeV p-Li neutrons

Table 1.18 Neutron spectra behind 25, 50, 100, 150 and 200cm thick concrete shield measured by the BC501A detector for 68-MeV p-Li neutrons

Energy (MeV)	Flux *	Error (%)	Flux	Error (%)	Flux	Error (%)	Flux	Error (%)	Flux	Error (%)	Flux	Error (%)
25 cm thick	50 cm thick	100 cm thick	150 cm thick	200 cm thick	25 cm thick	50 cm thick	100 cm thick	150 cm thick	200 cm thick	25 cm thick	50 cm thick	
7.0E+1	1.600E+4	8.6	5.347E-1	8.6	5.240E+0	8.6	2.424E+0	8.6	2.424E+0	8.6	2.424E+0	8.6
6.8E+1	1.6239E+4	8.6	5.240E+0	8.6	2.424E+0	8.6	2.424E+0	8.6	2.424E+0	8.6	2.424E+0	8.6
6.6E+1	1.6576E+4	8.6	5.240E+0	8.6	2.424E+0	8.6	2.424E+0	8.6	2.424E+0	8.6	2.424E+0	8.6
6.4E+1	1.6914E+4	8.6	5.240E+0	8.6	2.424E+0	8.6	2.424E+0	8.6	2.424E+0	8.6	2.424E+0	8.6
6.2E+1	1.7252E+4	8.6	5.240E+0	8.6	2.424E+0	8.6	2.424E+0	8.6	2.424E+0	8.6	2.424E+0	8.6
6.0E+1	1.7600E+4	8.6	5.240E+0	8.6	2.424E+0	8.6	2.424E+0	8.6	2.424E+0	8.6	2.424E+0	8.6
5.8E+1	1.7948E+4	8.6	5.240E+0	8.6	2.424E+0	8.6	2.424E+0	8.6	2.424E+0	8.6	2.424E+0	8.6
5.6E+1	1.8296E+4	8.6	5.240E+0	8.6	2.424E+0	8.6	2.424E+0	8.6	2.424E+0	8.6	2.424E+0	8.6
5.4E+1	1.8644E+4	8.6	5.240E+0	8.6	2.424E+0	8.6	2.424E+0	8.6	2.424E+0	8.6	2.424E+0	8.6
5.2E+1	1.9000E+4	8.6	5.240E+0	8.6	2.424E+0	8.6	2.424E+0	8.6	2.424E+0	8.6	2.424E+0	8.6
5.0E+1	1.9356E+4	8.6	5.240E+0	8.6	2.424E+0	8.6	2.424E+0	8.6	2.424E+0	8.6	2.424E+0	8.6
4.8E+1	1.9712E+4	8.6	5.240E+0	8.6	2.424E+0	8.6	2.424E+0	8.6	2.424E+0	8.6	2.424E+0	8.6
4.6E+1	2.0068E+4	8.6	5.240E+0	8.6	2.424E+0	8.6	2.424E+0	8.6	2.424E+0	8.6	2.424E+0	8.6
4.4E+1	2.0424E+4	8.6	5.240E+0	8.6	2.424E+0	8.6	2.424E+0	8.6	2.424E+0	8.6	2.424E+0	8.6
4.2E+1	2.0780E+4	8.6	5.240E+0	8.6	2.424E+0	8.6	2.424E+0	8.6	2.424E+0	8.6	2.424E+0	8.6
4.0E+1	2.1136E+4	8.6	5.240E+0	8.6	2.424E+0	8.6	2.424E+0	8.6	2.424E+0	8.6	2.424E+0	8.6
3.8E+1	2.1492E+4	8.6	5.240E+0	8.6	2.424E+0	8.6	2.424E+0	8.6	2.424E+0	8.6	2.424E+0	8.6
3.6E+1	2.1848E+4	8.6	5.240E+0	8.6	2.424E+0	8.6	2.424E+0	8.6	2.424E+0	8.6	2.424E+0	8.6
3.4E+1	2.2204E+4	8.6	5.240E+0	8.6	2.424E+0	8.6	2.424E+0	8.6	2.424E+0	8.6	2.424E+0	8.6
3.2E+1	2.2560E+4	8.6	5.240E+0	8.6	2.424E+0	8.6	2.424E+0	8.6	2.424E+0	8.6	2.424E+0	8.6
3.0E+1	2.2916E+4	8.6	5.240E+0	8.6	2.424E+0	8.6	2.424E+0	8.6	2.424E+0	8.6	2.424E+0	8.6
2.8E+1	2.3272E+4	8.6	5.240E+0	8.6	2.424E+0	8.6	2.424E+0	8.6	2.424E+0	8.6	2.424E+0	8.6
2.6E+1	2.3628E+4	8.6	5.240E+0	8.6	2.424E+0	8.6	2.424E+0	8.6	2.424E+0	8.6	2.424E+0	8.6
2.4E+1	2.3984E+4	8.6	5.240E+0	8.6	2.424E+0	8.6	2.424E+0	8.6	2.424E+0	8.6	2.424E+0	8.6
2.2E+1	2.4340E+4	8.6	5.240E+0	8.6	2.424E+0	8.6	2.424E+0	8.6	2.424E+0	8.6	2.424E+0	8.6
2.0E+1	2.4696E+4	8.6	5.240E+0	8.6	2.424E+0	8.6	2.424E+0	8.6	2.424E+0	8.6	2.424E+0	8.6
1.8E+1	2.5052E+4	8.6	5.240E+0	8.6	2.424E+0	8.6	2.424E+0	8.6	2.424E+0	8.6	2.424E+0	8.6
1.6E+1	2.5408E+4	8.6	5.240E+0	8.6	2.424E+0	8.6	2.424E+0	8.6	2.424E+0	8.6	2.424E+0	8.6
1.4E+1	2.5764E+4	8.6	5.240E+0	8.6	2.424E+0	8.6	2.424E+0	8.6	2.424E+0	8.6	2.424E+0	8.6
1.2E+1	2.6120E+4	8.6	5.240E+0	8.6	2.424E+0	8.6	2.424E+0	8.6	2.424E+0	8.6	2.424E+0	8.6
1.0E+1	2.6476E+4	8.6	5.240E+0	8.6	2.424E+0	8.6	2.424E+0	8.6	2.424E+0	8.6	2.424E+0	8.6
8.0E+0	2.6832E+4	8.6	5.240E+0	8.6	2.424E+0	8.6	2.424E+0	8.6	2.424E+0	8.6	2.424E+0	8.6
6.0E+0	2.7188E+4	8.6	5.240E+0	8.6	2.424E+0	8.6	2.424E+0	8.6	2.424E+0	8.6	2.424E+0	8.6
4.0E+0	2.7544E+4	8.6	5.240E+0	8.6	2.424E+0	8.6	2.424E+0	8.6	2.424E+0	8.6	2.424E+0	8.6
2.0E+0	2.7900E+4	8.6	5.240E+0	8.6	2.424E+0	8.6	2.424E+0	8.6	2.424E+0	8.6	2.424E+0	8.6
0.0E+0	2.8256E+4	8.6	5.240E+0	8.6	2.424E+0	8.6	2.424E+0	8.6	2.424E+0	8.6	2.424E+0	8.6

\* Read as  $7.0 \times 10^{-2}$   $\text{cm}^{-2} \text{Leahy}^{-1} \mu\text{C}^{-1}$

b

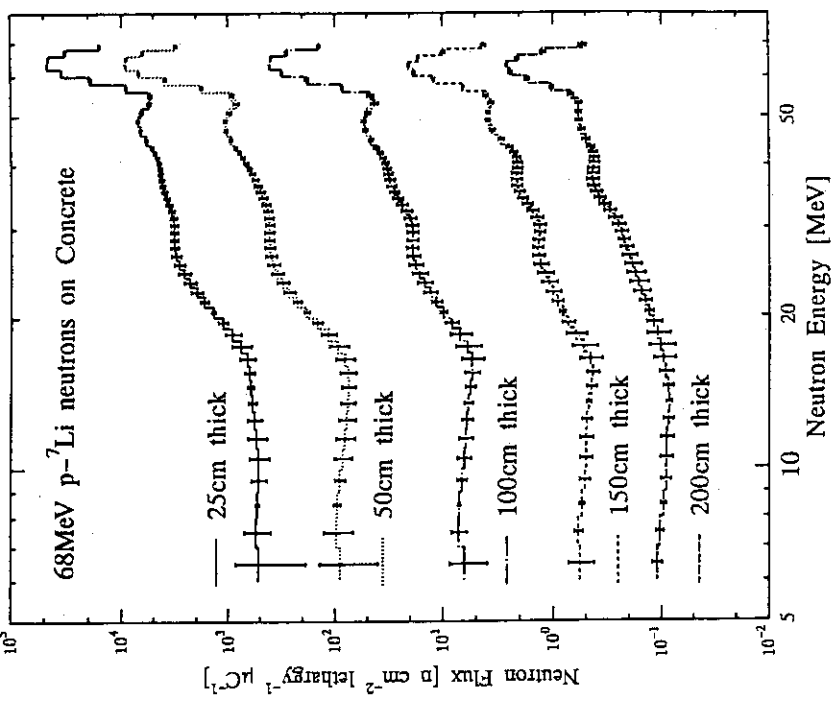


Fig.1.18

Neutron spectra behind various thickness of concrete measured by the BC501A detector on the beam axis for 68-MeV p-Li neutrons

Table 1.19 Neutron spectra behind 25cm thick concrete measured by the BC501A detector for 68-MeV p-Li neutrons

Energy (MeV)	Flux * beam axis	Error (%)	Flux		Error (%)	Flux	Error (%)
			20cm off axis	40cm off axis			
7.0E+1	1.600E+4	2.1	1.075E+2	1.08	5.036E+1	1.3	1
7.8E+1	1.239E+4	1.7	1.057E+2	1.39	5.936E+1	2.1	2
6.6E+1	4.576E+4	0.9	4.950E+2	0.4	2.360E+1	1.3	0
6.4E+1	4.658E+4	0.8	5.337E+2	1.08	3.368E+1	1.07	0
6.2E+1	4.478E+4	1.7	1.767E+2	1.52	1.346E+1	1.34	1
5.8E+1	9.141E+3	2.2	1.221E+2	1.96	1.407E+1	1.79	0
5.4E+1	5.437E+3	2.0	1.221E+2	1.96	1.580E+1	1.36	3
5.2E+1	6.558E+3	3.3	1.752E+2	8.47	1.669E+1	3.2	3
5.0E+1	7.050E+3	2.8	2.044E+2	4.5	1.857E+1	3.4	3
4.8E+1	6.736E+3	2.8	2.139E+2	4.5	2.023E+1	3.8	3
4.6E+1	5.920E+3	2.9	2.236E+2	4.1	2.221E+1	4.32	1
4.4E+1	5.297E+3	3.3	2.260E+2	4.1	2.244E+1	4.32	1
4.3E+1	4.688E+3	3.3	2.251E+2	3.8	2.244E+1	3.8	3
4.2E+1	4.524E+3	4.6	2.247E+2	4.4	2.244E+1	3.4	3
4.1E+1	4.351E+3	5.4	2.254E+2	5.1	2.244E+1	3.4	3
4.0E+1	4.273E+3	5.4	2.254E+2	5.3	2.244E+1	3.4	3
3.8E+1	3.767E+3	5.4	2.254E+2	5.3	2.244E+1	3.4	3
3.7E+1	3.545E+3	3.2	2.254E+2	5.3	2.244E+1	3.4	3
3.6E+1	3.433E+3	3.2	2.254E+2	5.3	2.244E+1	3.4	3
3.5E+1	3.321E+3	3.2	2.254E+2	5.3	2.244E+1	3.4	3
3.4E+1	3.209E+3	3.2	2.254E+2	5.3	2.244E+1	3.4	3
3.3E+1	3.097E+3	3.2	2.254E+2	5.3	2.244E+1	3.4	3
3.2E+1	2.985E+3	3.2	2.254E+2	5.3	2.244E+1	3.4	3
3.1E+1	2.873E+3	3.2	2.254E+2	5.3	2.244E+1	3.4	3
3.0E+1	2.761E+3	3.2	2.254E+2	5.3	2.244E+1	3.4	3
2.9E+1	2.649E+3	3.2	2.254E+2	5.3	2.244E+1	3.4	3
2.8E+1	2.537E+3	3.2	2.254E+2	5.3	2.244E+1	3.4	3
2.7E+1	2.425E+3	3.2	2.254E+2	5.3	2.244E+1	3.4	3
2.6E+1	2.313E+3	3.2	2.254E+2	5.3	2.244E+1	3.4	3
2.5E+1	2.201E+3	3.2	2.254E+2	5.3	2.244E+1	3.4	3
2.4E+1	2.089E+3	3.2	2.254E+2	5.3	2.244E+1	3.4	3
2.3E+1	1.977E+3	3.2	2.254E+2	5.3	2.244E+1	3.4	3
2.2E+1	1.865E+3	3.2	2.254E+2	5.3	2.244E+1	3.4	3
2.1E+1	1.753E+3	3.2	2.254E+2	5.3	2.244E+1	3.4	3
2.0E+1	1.641E+3	3.2	2.254E+2	5.3	2.244E+1	3.4	3
1.9E+1	1.529E+3	3.2	2.254E+2	5.3	2.244E+1	3.4	3
1.8E+1	1.417E+3	3.2	2.254E+2	5.3	2.244E+1	3.4	3
1.7E+1	1.305E+3	3.2	2.254E+2	5.3	2.244E+1	3.4	3
1.6E+1	1.193E+3	3.2	2.254E+2	5.3	2.244E+1	3.4	3
1.5E+1	1.081E+3	3.2	2.254E+2	5.3	2.244E+1	3.4	3
1.4E+1	9.69E+2	3.2	2.254E+2	5.3	2.244E+1	3.4	3
1.3E+1	8.57E+2	3.2	2.254E+2	5.3	2.244E+1	3.4	3
1.2E+1	7.45E+2	3.2	2.254E+2	5.3	2.244E+1	3.4	3
1.1E+1	6.33E+2	3.2	2.254E+2	5.3	2.244E+1	3.4	3
1.0E+1	5.21E+2	3.2	2.254E+2	5.3	2.244E+1	3.4	3
9.0E+0	4.09E+2	3.2	2.254E+2	5.3	2.244E+1	3.4	3
8.0E+0	3.07E+2	3.2	2.254E+2	5.3	2.244E+1	3.4	3
7.0E+0	2.05E+2	3.2	2.254E+2	5.3	2.244E+1	3.4	3

unit:  $n \text{ cm}^{-2} \text{ lethargy}^{-1} \mu \text{C}^{-1}$   
Read as  $7.0 \times 10$

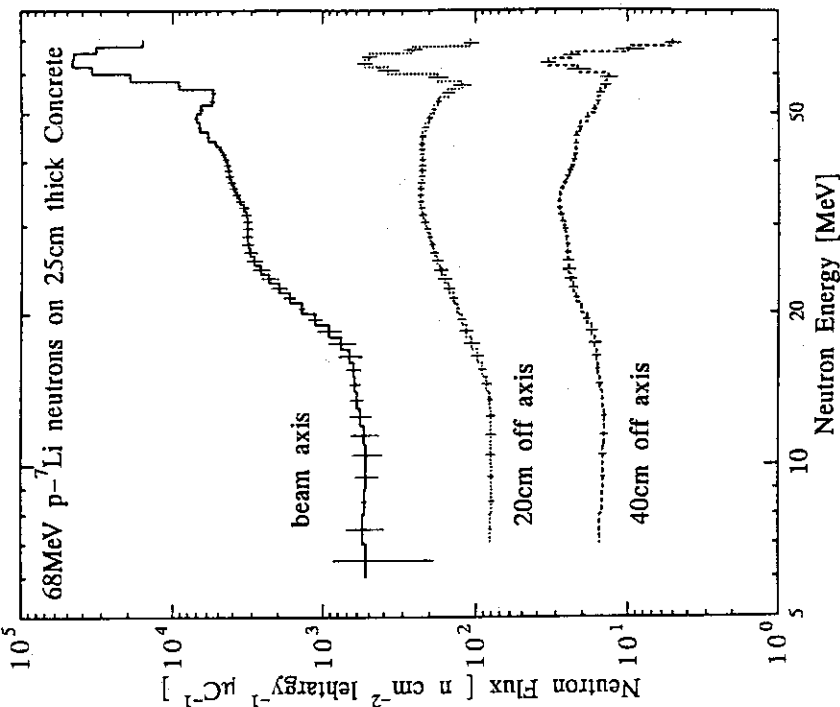


Fig.1.19 Neutron spectra behind 25cm thick concrete measured by the BC501A detector on the beam axis, 20- and 40-cm off axis for 68-MeV p-Li neutrons

Table 1.20 Neutron spectra behind 50cm thick concrete measured by the BC501A detector for 68-MeV p-Li neutrons

Energy (MeV)	Flux *	Error (%)	Flux	Error (%)	Flux	Error (%)	Flux	Error (%)
7.0E+0	3.117E+3	2.5	1.766E+2	4.7	8.311E+1	1.1	1.99E+0	1.0
6.8E+0	6.407E+3	2.5	1.771E+2	4.7	8.99E+1	1.3	1.90E+0	1.0
6.6E+0	9.058E+3	2.5	1.986E+2	5.5	5.900E+1	6.9	1.739E+0	1.0
6.4E+0	9.240E+3	2.5	1.986E+2	5.5	5.739E+1	5.7	1.539E+0	1.0
6.2E+0	6.949E+3	2.5	1.562E+2	15.0	3.04E+1	1.7	1.78E+0	1.0
6.0E+0	3.924E+3	2.5	1.757E+2	15.0	2.553E+1	1.0	1.68E+0	1.0
5.8E+0	1.790E+3	2.5	1.329E+2	18.4	2.098E+1	1.2	1.22E+0	1.0
5.6E+0	9.298E+2	2.5	1.524E+2	6.4	2.240E+1	2.0	1.40E+0	1.0
5.4E+0	8.462E+2	2.5	1.662E+2	4.4	2.404E+1	4.6	1.60E+0	1.0
5.2E+0	9.845E+2	2.5	1.662E+2	4.4	2.485E+1	3.5	1.74E+0	1.0
5.0E+0	1.073E+3	3.5	1.735E+2	4.4	2.613E+1	3.7	1.87E+0	1.0
4.8E+0	1.053E+3	3.5	1.754E+2	4.3	2.553E+1	4.0	1.87E+0	1.0
4.6E+0	9.530E+2	3.5	1.734E+2	4.3	2.423E+1	3.3	1.82E+0	1.0
4.4E+0	7.926E+2	3.5	1.929E+2	4.5	2.520E+1	3.6	1.82E+0	1.0
4.2E+0	7.340E+2	3.5	1.953E+2	4.5	2.502E+1	4.5	1.82E+0	1.0
4.0E+0	6.823E+2	3.5	1.552E+2	6.2	2.708E+1	4.5	1.82E+0	1.0
3.8E+0	5.984E+2	3.5	1.481E+2	6.9	2.659E+1	4.5	1.82E+0	1.0
3.6E+0	5.634E+2	3.5	1.481E+2	6.9	2.801E+1	4.6	1.82E+0	1.0
3.4E+0	5.307E+2	3.5	1.441E+2	6.9	2.863E+1	4.6	1.82E+0	1.0
3.2E+0	4.471E+2	3.5	1.349E+2	6.6	2.736E+1	4.5	1.82E+0	1.0
3.0E+0	4.610E+2	3.5	1.279E+2	6.6	2.645E+1	4.5	1.82E+0	1.0
2.8E+0	4.273E+2	3.5	1.299E+2	6.6	2.449E+1	4.5	1.82E+0	1.0
2.6E+0	4.123E+2	3.5	1.299E+2	6.6	2.334E+1	4.5	1.82E+0	1.0
2.4E+0	4.130E+2	3.5	1.090E+2	9.8	1.008E+2	2.2	1.239E+0	1.0
2.2E+0	4.140E+2	3.5	1.090E+2	9.8	5.872E+1	6.0	2.142E+0	1.0
2.0E+0	4.105E+2	3.5	1.051E+2	9.8	6.165E+1	6.4	2.038E+0	1.0
1.8E+0	4.105E+2	3.5	1.051E+2	9.8	6.134E+1	6.4	2.038E+0	1.0
1.6E+0	3.989E+2	3.5	1.212E+2	9.0	8.759E+1	7.3	1.938E+0	1.0
1.4E+0	3.977E+2	3.5	1.212E+2	9.0	8.836E+1	8.3	1.842E+0	1.0
1.2E+0	3.471E+2	3.5	1.315E+2	7.7	8.890E+1	8.3	1.747E+0	1.0
1.0E+0	3.100E+2	3.5	1.315E+2	7.7	7.373E+1	8.3	1.649E+0	1.0
8.0E+0	2.666E+2	3.5	1.909E+2	9.0	6.420E+1	8.5	1.452E+0	1.0
6.0E+0	1.846E+2	3.5	1.909E+2	9.0	6.002E+1	8.5	1.359E+0	1.0
4.0E+0	1.466E+2	3.5	1.909E+2	9.0	5.240E+1	10.2	1.185E+0	1.0
2.0E+0	1.160E+2	3.5	1.909E+2	9.0	4.851E+1	11.5	1.104E+0	1.0
1.0E+0	1.044E+2	3.5	1.909E+2	9.0	4.399E+1	9.9	1.031E+0	1.0
0.5E+0	1.088E+2	3.5	1.909E+2	9.0	4.049E+1	9.2	9.566E+0	1.0
0.2E+0	1.133E+2	3.5	1.909E+2	9.0	3.571E+1	9.0	8.566E+0	1.0
0.1E+0	1.178E+2	3.5	1.909E+2	9.0	3.449E+1	7.9	8.326E+0	1.0
0.05E+0	1.223E+2	3.5	1.909E+2	9.0	3.340E+1	7.7	8.111E+0	1.0
0.02E+0	1.268E+2	3.5	1.909E+2	9.0	3.287E+1	7.2	8.021E+0	1.0
0.01E+0	1.313E+2	3.5	1.909E+2	9.0	3.237E+1	7.2	8.047E+0	1.0
0.005E+0	1.358E+2	3.5	1.909E+2	9.0	3.222E+1	7.2	8.087E+0	1.0

\* Read as  $7.0 \times 10^{-3}$  unit:  $n \text{ cm}^{-2} \text{ lethargy}^{-1} \mu\text{C}^{-1}$

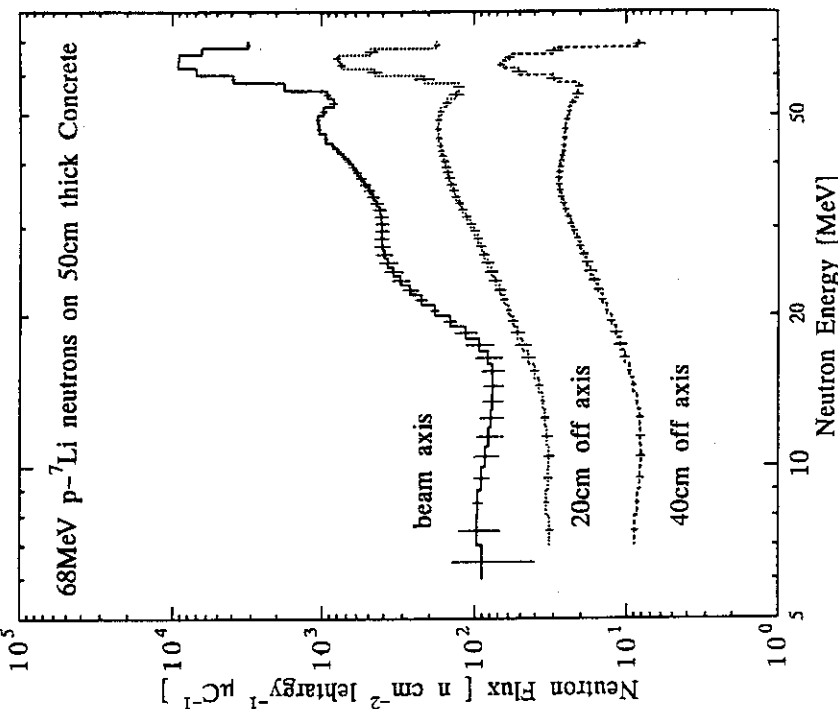


Fig.1.20 Neutron spectra behind 50cm thick concrete measured by the BC501A detector on the beam axis, 20- and 40-cm off axis for 68-MeV p-Li neutrons

Table 1.21 Reaction rates behind iron measured by the Bonner sphere spectrometer for 43-MeV p-Li neutrons

Counter	Reaction rate (in $\mu \text{ C}^{-1}$ )		
	20cm thick	40cm thick	100cm thick
Bare	1. 082E+3*	2. 320E+2	2. 290E+1
1. 5 cm+Cd	7. 708E+3	3. 094E+3	1. 855E+2
3 cm	2. 134E+4	7. 542E+3	3. 941E+2
5 cm	2. 280E+4	9. 210E+3	4. 716E+2
9 cm	1. 788E+4	4. 565E+3	1. 598E+2

\* Read as  $1.082 \times 10^3$

Table 1.22 Reaction rates behind iron measured by the Bonner sphere spectrometer for 68-MeV p-Li neutrons

Counter	Reaction rate (in $\mu \text{ C}^{-1}$ )		
	20cm thick	40cm thick	100cm thick
Bare	9. 205E+2*	4. 948E+2	7. 238E+1
1. 5 cm+Cd	1. 087E+4	7. 587E+3	6. 287E+2
3 cm	3. 317E+4	1. 858E+4	1. 302E+3
5 cm	5. 131E+4	2. 249E+4	1. 343E+3
9 cm	3. 847E+4	1. 344E+4	5. 402E+2

\* Read as  $9.205 \times 10^2$

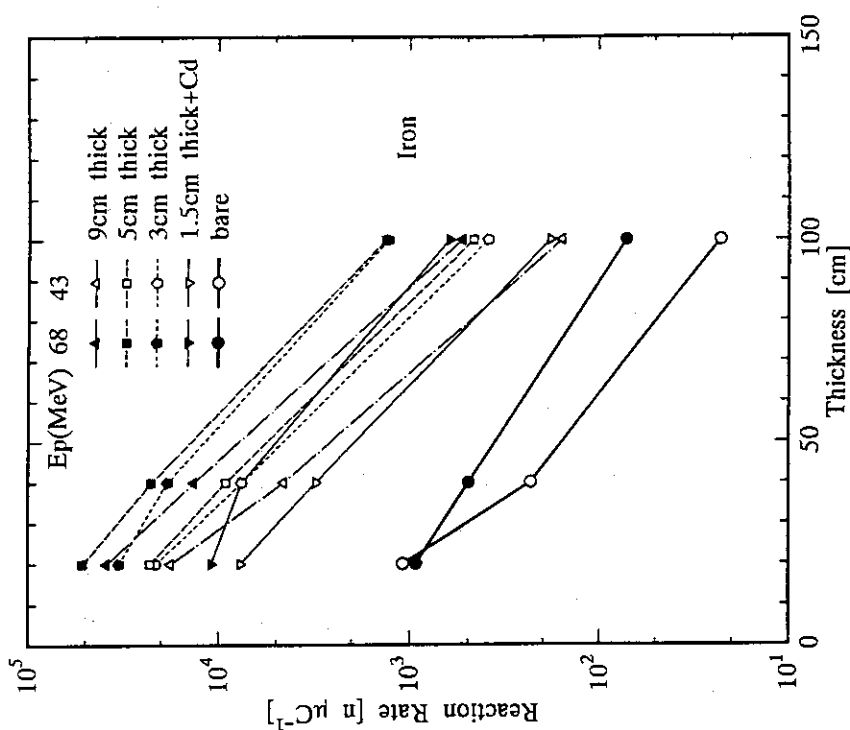


Fig.1.21 Reaction rates behind iron measured by the Bonner sphere spectrometer for 43- and 68-MeV p-Li neutrons

Table 1.23 Reaction rates behind concrete measured by the Bonner sphere spectrometer for 43-MeV p-Li neutrons

Counter	Reaction rate ( $\text{n} \mu \text{C}^{-1}$ )	25cm thick	50cm thick	100cm thick	150cm thick
Bare	5. 200E+3*	1. 317E+3	6. 449E+1	2. 729E+0	
1. 5cm	5. 984E+3	1. 252E+3	4. 842E+1	2. 285E+0	
3cm	8. 937E+4	1. 594E+3	6. 017E+1	2. 886E+0	
5cm	1. 195E+4	1. 903E+3	6. 623E+1	3. 024E+0	
9cm	1. 111E+4	1. 620E+3	5. 271E+1	2. 363E+0	

\* Read as  $5.200 \times 10^3$

Table 1.24

Reaction rates behind concrete measured by the Bonner sphere spectrometer for 68-MeV p-Li neutrons

Counter	Reaction rate ( $\text{n} \mu \text{C}^{-1}$ )	50cm thick	100cm thick	150cm thick
Bare	2. 044E+3*	2. 739E+2	1. 833E+1	
1. 5cm	2. 164E+3	-	-	
1. 5cmCd	-	1. 442E+2	1. 061E+1	
3cm	3. 043E+3	3. 146E+2	2. 422E+1	
5cm	3. 722E+3	3. 625E+2	2. 861E+1	
9cm	3. 251E+3	3. 076E+2	2. 464E+1	

\* Read as  $2.044 \times 10^3$

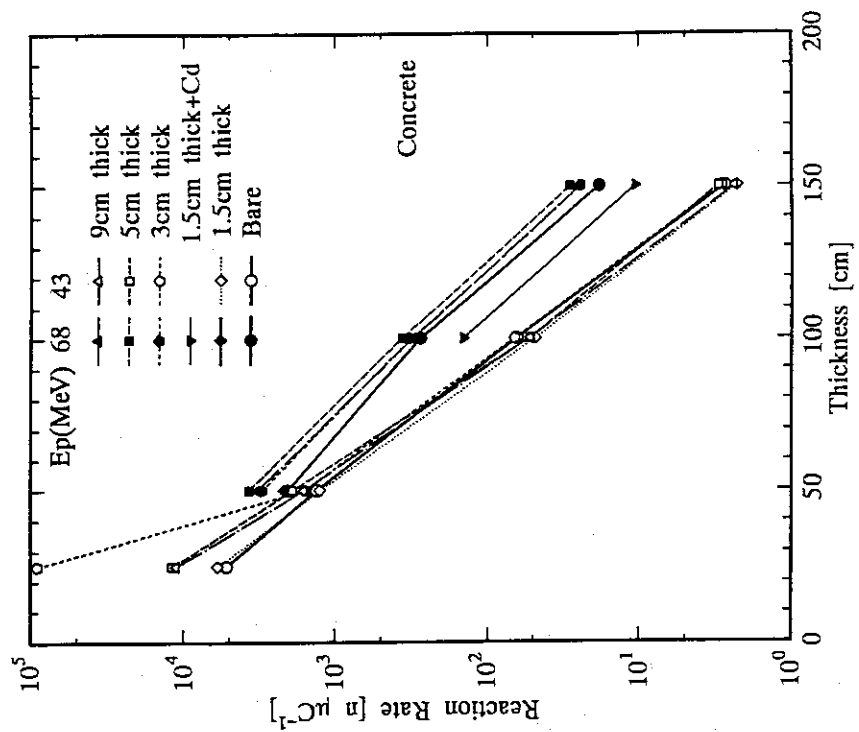


Fig.1.22 Reaction rates behind concrete measured by the Bonner sphere spectrometer for 43- and 68-MeV p-Li neutrons

Table 1.25 Neutron spectra behind iron measured by the Bonner sphere spectrometer for 43-MeV p-Li neutrons

Energy (MeV)	Neutron Flux (in cm <sup>-2</sup> lethargy <sup>-1</sup> μC <sup>-1</sup> )
4.50E+1*	2.740E+3 9.760E+1 8.940E-2
3.50E+1	6.395E+2 2.277E+1 5.349E-2
2.75E+1	5.945E+2 2.677E+1 1.415E-2
2.25E+1	4.454E+2 1.203E+1 5.843E-3
1.75E+1	3.016E+2 1.088E+1 5.141E-3
1.35E+1	2.027E+2 6.209E+0 1.069E-2
1.00E+1	1.245E+2 4.294E+0 7.898E-3
6.70E+0	1.316E+2 5.434E+0 1.549E-2
4.49E+0	1.753E+2 1.629E+1 7.986E-2
3.01E+0	2.725E+2 2.354E+1 6.793E-2
2.02E+0	3.424E+2 5.151E+1 1.369E-1
1.35E+0	4.830E+2 8.128E+1 2.440E-1
9.07E-1	7.111E+2 1.965E+2 3.249E+0
4.98E-1	8.604E+2 3.787E+2 1.147E+1
2.24E-1	4.851E+2 2.073E+2 9.915E+0
8.65E-2	2.700E+2 1.570E+2 1.200E+1
1.50E-2	4.618E+1 1.798E+1 1.015E+0
3.35E-3	2.620E+1 1.238E+1 8.151E-1
4.54E-4	2.930E+1 3.361E+0 1.190E+0
2.26E-5	1.769E+1 3.892E+0 6.792E-1
5.04E-6	8.083E+0 1.233E+0 4.982E-2
1.12E-6	5.673E+0 1.036E+0 2.216E-1
4.14E-7	3.083E+0 6.747E-1 3.199E-2
1.0E-10	

\* Read as  $4.50 \times 10^1$

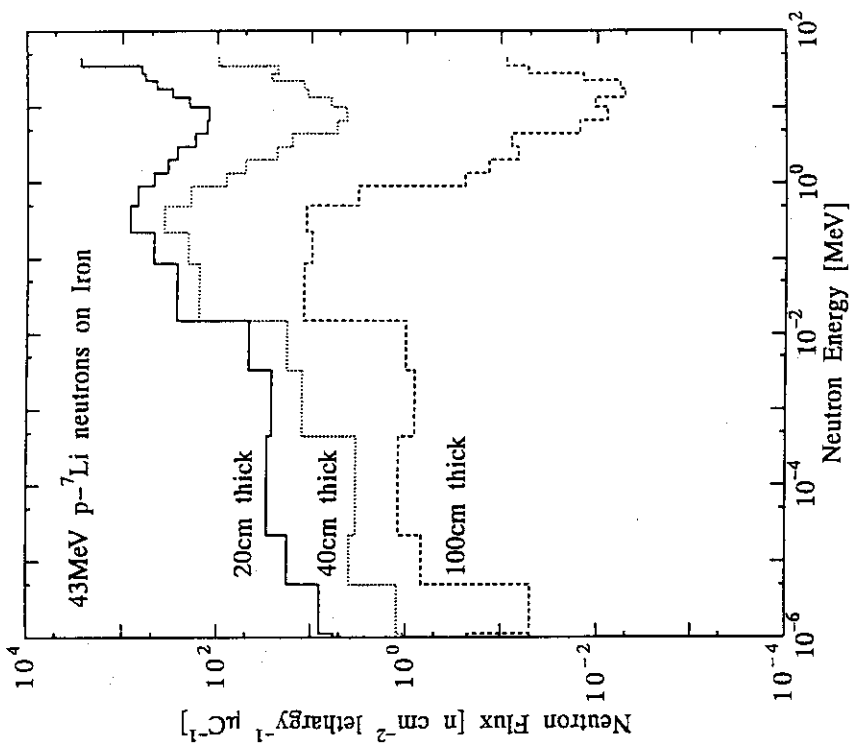


Fig.1.23 Neutron spectra behind various thick iron measured by the Bonner sphere spectrometer for 43-MeV p-Li neutrons

Table 1.26 Neutron spectra behind iron measured by the Bonner sphere spectrometer for 68-MeV p-Li neutrons

Energy (MeV)	Neutron Flux (in cm <sup>-2</sup> Lethargy <sup>-1</sup> μC <sup>-1</sup> )
	20cm thick    40cm thick    100cm thick
8. 00E+1*	1. 190E+3    1. 752E+2    5. 770E+0
6. 50E+1	6. 935E+3    9. 746E+2    1. 593E+1
5. 50E+1	2. 458E+3    2. 874E+2    3. 469E+0
4. 50E+1	1. 866E+3    2. 185E+2    4. 852E+0
3. 50E+1	1. 345E+3    1. 310E+2    2. 727E+0
2. 75E+1	8. 752E+2    1. 051E+2    4. 563E+0
2. 25E+1	5. 086E+2    4. 134E+1    1. 570E+0
1. 75E+1	4. 332E+2    5. 888E+1    8. 451E-1
1. 35E+1	2. 940E+2    3. 836E+1    2. 413E+0
1. 00E+1	2. 683E+2    4. 429E+1    6. 809E-1
6. 70E+0	3. 227E+2    4. 553E+1    4. 022E-1
4. 49E+0	5. 317E+2    6. 325E+1    7. 252E-1
3. 01E+0	7. 730E+2    1. 312E+2    1. 394E+0
2. 02E+0	1. 032E+3    1. 754E+2    1. 894E+0
1. 35E+0	1. 471E+3    3. 185E+2    2. 629E+0
9. 07E-1	1. 937E+3    6. 238E+2    9. 968E+0
4. 98E-1	1. 776E+3    9. 477E+2    3. 244E+1
2. 24E-1	7. 556E+2    5. 293E+2    2. 462E+1
8. 65E-2	2. 506E+2    2. 938E+2    4. 171E+1
1. 50E-2	3. 540E+1    4. 733E+1    5. 577E+0
3. 35E-3	2. 018E+1    3. 383E+1    4. 850E+0
4. 54E-4	1. 072E+1    1. 424E+1    2. 132E+0
2. 26E-5	4. 297E+0    5. 617E+0    1. 515E+0
5. 04E-6	3. 210E+0    3. 107E+0    4. 835E-1
1. 12E-6	3. 045E+0    2. 191E+0    2. 606E-1
4. 14E-7	3. 437E+0    1. 201E+0    1. 855E-1
1. 0E-10	Read as 8. 00 × 10 <sup>-1</sup>

- 29 -

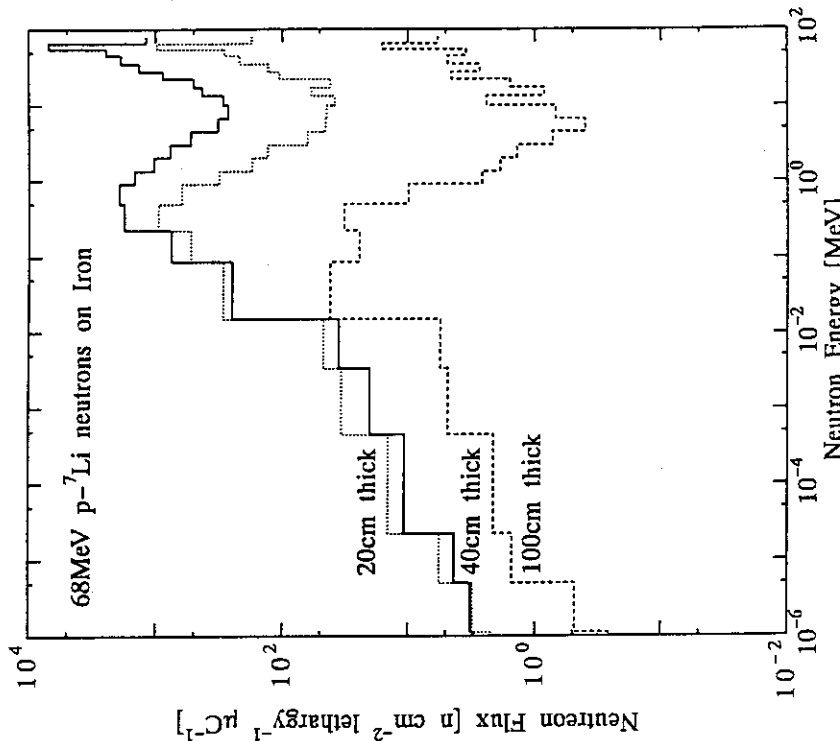


Fig.1.24 Neutron spectra behind various thick iron measured by the Bonner sphere spectrometer for 68-MeV p-Li neutrons

Table 1.27 Neutron spectra behind concrete measured by the Bonner sphere spectrometer for 43-MeV p-Li neutrons

Energy (MeV)	Neutron Flux (n cm <sup>-2</sup> lethargy <sup>-1</sup> μ C <sup>-1</sup> )			
	25cm thick	50cm thick	100cm thick	150cm thick
4. 50E+1 *	5. 500E+3	7. 250E+2	1. 636E+1	4. 229E-1
3. 50E+1	1. 073E+3	1. 564E+2	6. 268E+0	2. 288E-1
2. 75E+1	1. 113E+3	1. 315E+2	3. 573E+0	1. 504E-1
2. 25E+1	8. 812E+2	9. 571E+1	2. 492E+0	1. 628E-1
1. 75E+1	5. 741E+2	6. 533E+1	1. 642E+0	5. 817E-2
1. 35E+1	4. 005E+2	4. 633E+1	1. 370E+0	4. 111E-2
1. 00E+1	2. 936E+2	4. 195E+1	1. 173E+0	3. 869E-2
6. 70E+0	2. 543E+2	3. 656E+1	1. 648E+0	9. 705E-2
4. 49E+0	2. 001E+2	3. 344E+1	1. 111E+0	5. 715E-2
3. 01E+0	2. 428E+2	4. 345E+1	1. 946E+0	9. 173E-2
2. 02E+0	1. 875E+2	3. 181E+1	1. 327E+0	5. 963E-2
1. 35E+0	1. 529E+2	1. 751E+1	4. 833E-1	3. 533E-2
9. 07E-1	1. 593E+2	2. 609E+1	7. 886E-1	3. 736E-2
4. 98E-1	9. 488E+1	1. 392E+1	4. 285E-1	1. 648E-2
2. 24E-1	8. 161E+1	1. 163E+1	2. 062E-1	1. 415E-2
8. 65E-2	6. 455E+1	8. 349E+0	2. 927E-1	1. 011E-2
1. 50E-2	4. 638E+1	7. 128E+0	2. 642E-1	1. 162E-2
3. 35E-3	5. 408E+1	8. 594E+0	2. 629E-1	1. 777E-2
4. 54E-4	5. 612E+1	1. 085E+1	5. 137E-1	2. 236E-2
2. 26E-5	4. 454E+1	1. 071E+1	1. 941E-1	1. 446E-2
5. 04E-6	3. 377E+1	1. 169E+1	5. 963E-1	2. 941E-2
1. 12E-6	3. 770E+1	1. 402E+1	7. 425E-1	2. 216E-2
4. 14E-7	2. 168E+1	4. 895E+0	2. 470E-1	1. 077E-2
1. 0E-10				

\* Read as 4. 50 × 10<sup>1</sup>

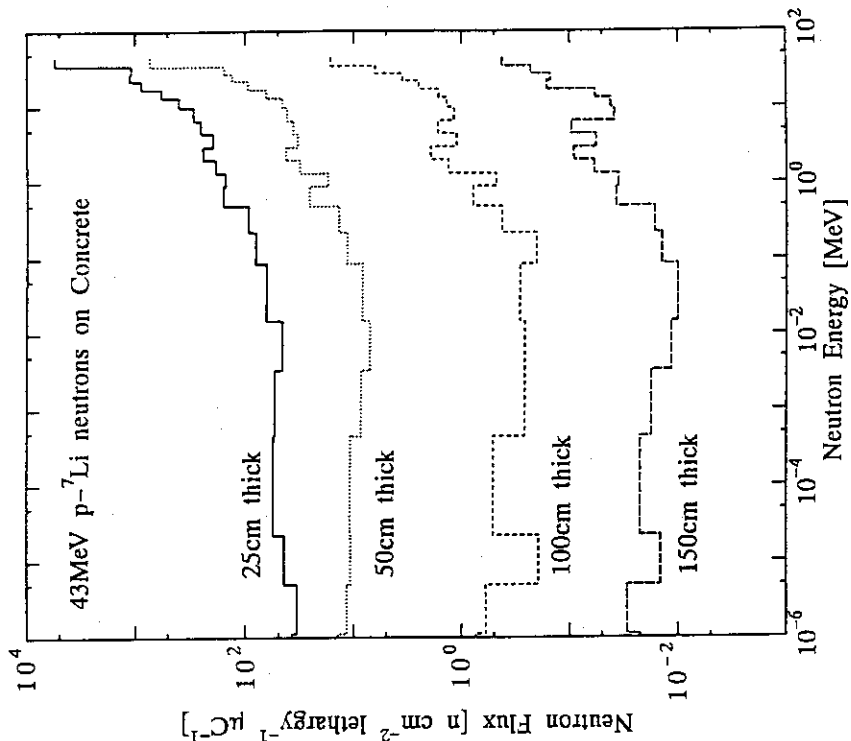


Fig.1.25 Neutron spectra behind various thick concrete measured by the Bonner sphere spectrometer for 43-MeV p-Li neutrons

Table 1.28 Neutron spectra behind concrete measured by the Bonner sphere spectrometer for 68-MeV p-Li neutrons

Energy (MeV)	Neutron Flux (in cm <sup>-2</sup> Lethargy <sup>-1</sup> μ C <sup>-1</sup> )		
	50cm thick	100cm thick	150cm thick
8. 00E+1*	6. 847E+2	1. 672E+1	5. 783E-1
6. 50E+1	2. 149E+3	8. 793E+1	7. 227E+0
5. 50E+1	4. 819E+2	2. 080E+1	1. 521E+0
4. 50E+1	3. 065E+2	1. 947E+1	1. 497E+0
3. 50E+1	2. 126E+2	6. 419E+0	8. 229E-1
2. 75E+1	1. 297E+2	9. 617E+0	8. 429E-1
2. 25E+1	8. 866E+1	1. 319E+1	1. 741E-1
1. 75E+1	6. 503E+1	5. 109E+0	2. 950E-1
1. 35E+1	5. 277E+1	5. 126E+0	2. 519E-1
1. 00E+1	5. 301E+1	4. 466E+0	2. 170E-1
6. 70E+0	6. 303E+1	7. 345E+0	9. 470E-1
4. 49E+0	6. 096E+1	9. 705E+0	7. 831E-1
3. 01E+0	8. 678E+1	1. 185E+1	8. 971E-1
2. 02E+0	5. 923E+1	1. 022E+1	9. 924E-1
1. 35E+0	4. 131E+1	5. 903E+0	5. 577E-1
9. 07E-1	5. 760E+1	7. 619E+0	5. 229E-1
4. 98E-1	3. 245E+1	4. 203E+0	4. 408E-1
2. 24E-1	2. 648E+1	4. 166E+0	2. 668E-1
8. 65E-2	1. 825E+1	1. 913E+0	5. 147E-2
1. 50E-2	1. 768E+1	1. 073E+0	7. 830E-2
3. 35E-3	1. 690E+1	7. 998E-1	1. 341E-1
4. 54E-4	1. 910E+1	9. 285E-1	9. 107E-2
2. 26E-5	1. 806E+1	7. 614E-1	7. 314E-2
5. 04E-6	1. 554E+1	1. 206E+0	6. 624E-2
1. 12E-6	1. 638E+1	2. 419E+0	4. 131E-2
4. 14E-7	8. 259E+0	1. 290E+0	9. 931E-2
1. 0E-10	Read as 8. 00 × 10 <sup>1</sup>		

- 31 -

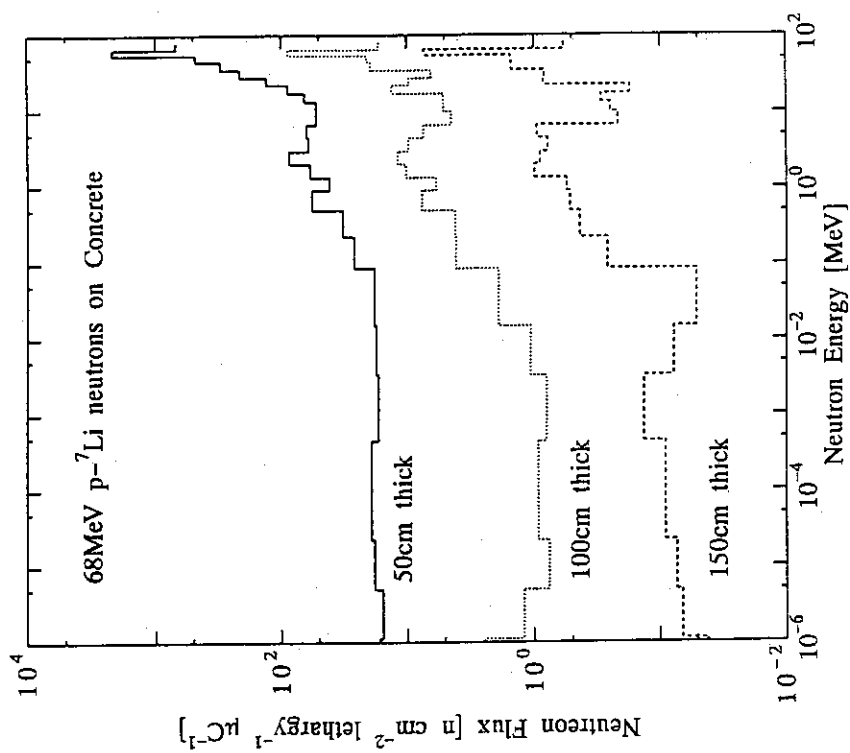


Fig.1.26 Neutron spectra behind various thick concrete measured by the Bonner sphere spectrometer for 68-MeV p-Li neutrons

Table 1.29 Fission rates of  $^{232}\text{Th}$  and  $^{238}\text{U}$  behind iron for 43-MeV p-Li neutrons

Position $Z^*$ (cm)	$R^b$ (cm)	Fission reaction rate $^{232}\text{Th}$		
		(n $\mu\text{C}^{-1}$ )	(%)	(n $\mu\text{C}^{-1}$ ) (%)
0	0	8.01E+4 <sup>c</sup>	(0.59)	3.21E+4 (0.24)
10	0	2.43E+4	(1.0)	1.02E+4 (0.89)
20	0	5.64E+3	(1.8)	2.49E+3 (0.99)
40	0	2.97E+2	(3.4)	1.16E+2 (3.3)
70	0	6.96E+0	(9.8)	1.79E+0 (28.)
0	20	1.00E+2	(4.3)	
10	20	2.47E+2	(5.7)	
20	20	1.95E+2	(3.5)	6.12E+1 (17.)
40	20	5.14E+1	(5.0)	1.77E+1 (14.)
70	20	3.61E+0	(20.)	1.53E+0 (21.)

\* Thickness of iron shields

<sup>b</sup> Distance from the beam axis

<sup>c</sup> Read as  $8.01 \times 10^4$

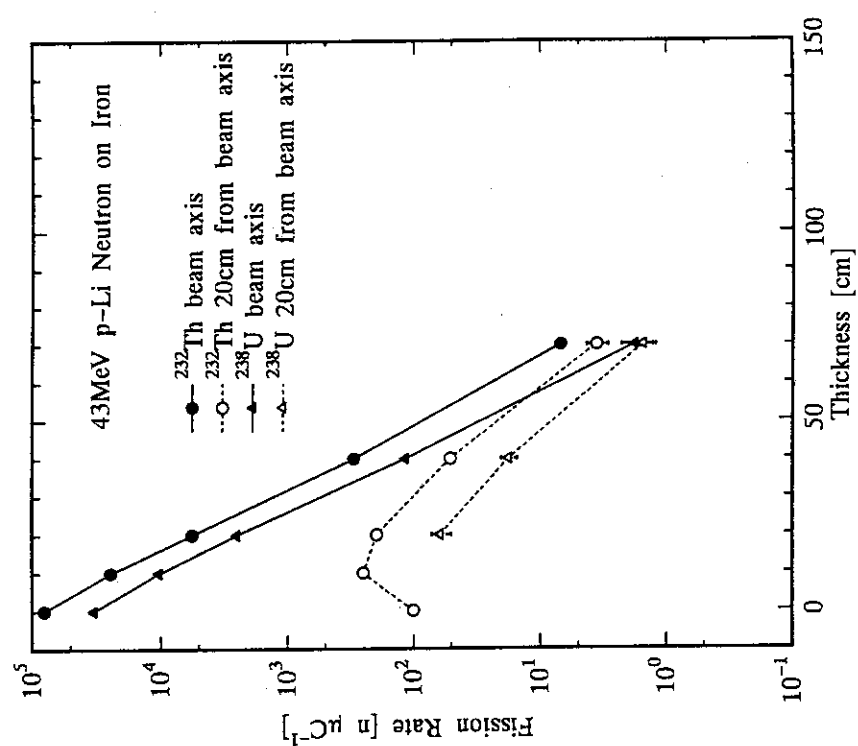


Fig.1.27 Fission rates of  $^{232}\text{Th}$  and  $^{238}\text{U}$  behind iron on the beam axis and 20-cm off axis for 43-MeV p-Li neutrons

Table 1.30 Fission rates of  $^{232}\text{Th}$  and  $^{238}\text{U}$  behind iron for 68-MeV p-Li neutrons

Position $Z^a$ $R^b$ (cm)	Fission reaction rate $^{232}\text{U}$ (n $\mu\text{C}^{-1}$ )	Fission reaction rate $^{232}\text{Th}$ (n $\mu\text{C}^{-1}$ )	(%)
0 0	1.18E+5 <sup>c</sup>	0.38	(0.49)
20 0	1.53E+4	(0.66)	7.70E+3 (0.90)
40 0	1.23E+3	(2.3)	5.47E+2 (3.3)
70 0	3.18E+1	(7.1)	1.08E+1 (12.)
100 0	2.59E+0	(11.)	8.51E-1 (19.)
20 20	7.14E+1	(4.0)	4.69E+1 (4.7)
40 20	1.68E+2	(3.4)	1.15E+2 (4.0)
70 20	1.58E+1	(6.0)	7.12E+0 (8.6)
100 20	2.57E+0	(9.3)	9.07E-1 (15.)
130 20	1.08E+0	(12.)	4.59E-1 (18.)

<sup>a</sup> Thickness of iron shields  
<sup>b</sup> Distance from the beam axis  
<sup>c</sup> Read as  $1.18 \times 10^5$

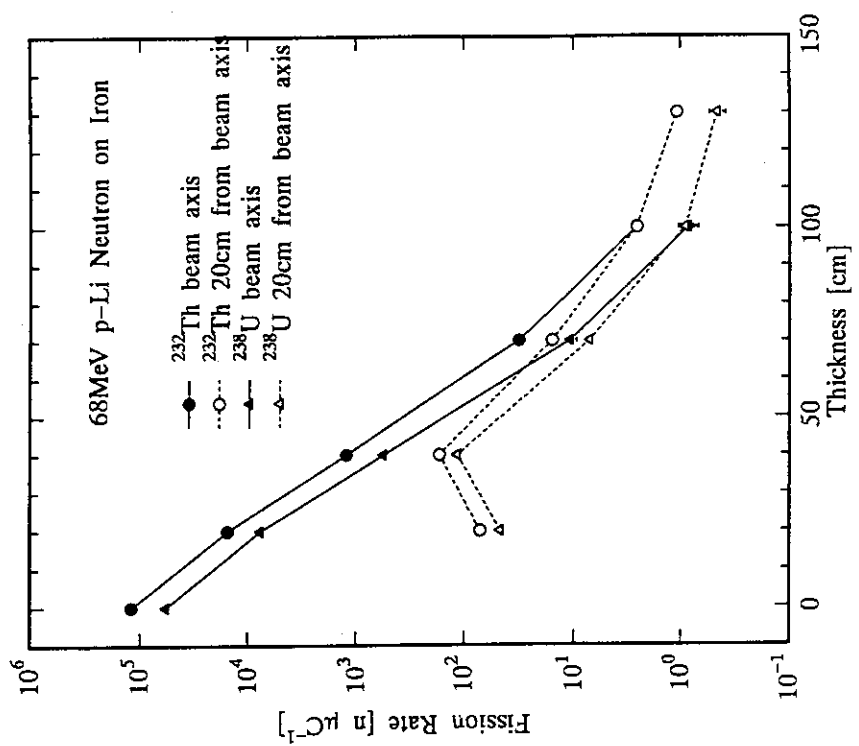


Fig.1.28 Fission reaction rates of  $^{232}\text{Th}$  and  $^{238}\text{U}$  behind iron on the beam axis and 20-cm off axis for 68-MeV p-Li neutrons

Table 1.31 Fission rates of  $^{232}\text{Th}$  and  $^{238}\text{U}$  behind concrete for 43-MeV p-Li neutrons

Position $Z^*$ (cm)	$R^*$ (cm)	Fission reaction rate $^{232}\text{Th}$		
		(n $\mu\text{C}^{-1}$ )	(X)	(n $\mu\text{C}^{-1}$ ) (%)
0	0	7.28E+4 <sup>c</sup>	(0.40)	3.07E+4 (0.60)
25	0	1.15E+4	(1.4)	4.32E+3 (4.8)
50	0	1.26E+3	(5.6)	5.23E+2 (4.9)
100	0	1.98E+1	(8.0)	7.80E+0 (24.)
150	0	1.72E+0	(17.)	
0	20	3.24E+2	(6.4)	6.24E+1 (16.)
25	20	4.78E+2	(15.)	1.48E+2 (12.)
50	20	1.90E+2	(8.4)	7.58E+1 (8.8)
100	20	1.37E+1	(17.)	5.73E+0 (27.)
150	20	1.33E+0	(20.)	

\* Thickness of Concrete shields

♦ Distance from the beam axis

<sup>c</sup> Read as  $7.28 \times 10^4$

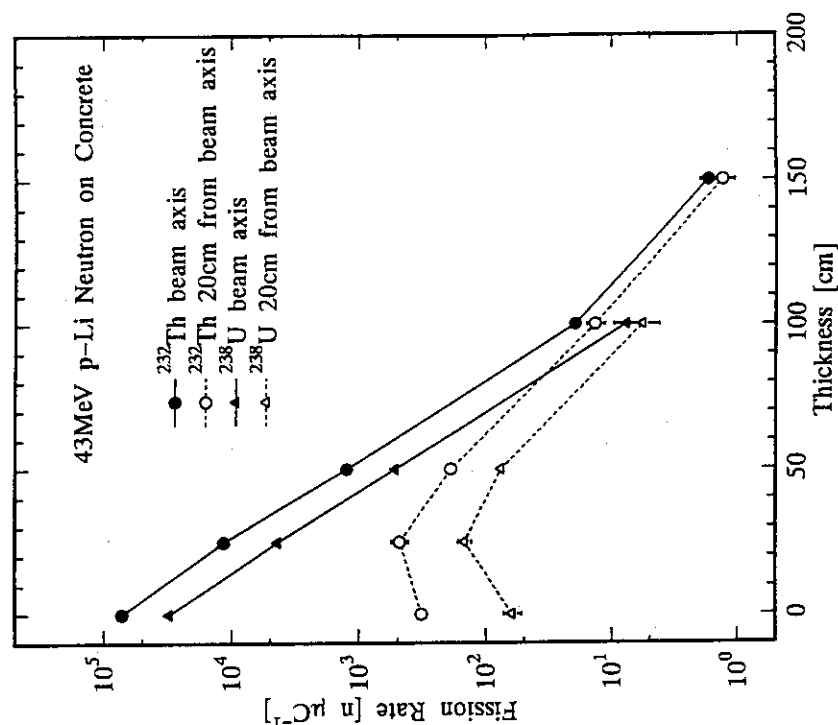


Fig.1.29 Fission rates of  $^{232}\text{Th}$  and  $^{238}\text{U}$  behind concrete on the beam axis and 20-cm off axis for 43-MeV p-Li neutrons

Table 1.32 Fission rates of  $^{232}\text{Th}$  and  $^{238}\text{U}$  behind concrete for 68-MeV p-Li neutrons

Position $Z^*$ (cm)	$R^*$ (cm)	Fission reaction rate		
		$^{232}\text{U}$ (n $\mu\text{C}^{-1}$ )	(%)	$^{232}\text{Th}$ (n $\mu\text{C}^{-1}$ ) (%)
0	0	1.18E+5 <sup>c</sup>	(0.38)	5.71E+4 (0.49)
25	0	2.37E+4	(1.7)	1.41E+4 (2.2)
50	0	4.63E+3	(1.1)	2.43E+3 (1.4)
100	0	1.72E+2	(4.8)	9.23E+1 (6.4)
150	0	9.47E+0	(7.5)	4.93E+0 (10.)
25	20	1.28E+3	(3.9)	2.82E+2 (8.1)
50	20	7.82E+2	(1.9)	1.96E+2 (3.7)
100	20	8.30E+1	(3.3)	3.86E+1 (4.7)
150	20	7.41E+0	(6.7)	3.46E+0 (9.5)

\* Thickness of Concrete shields

<sup>b</sup> Distance from the beam axis

<sup>c</sup> Read as  $1.18 \times 10^6$

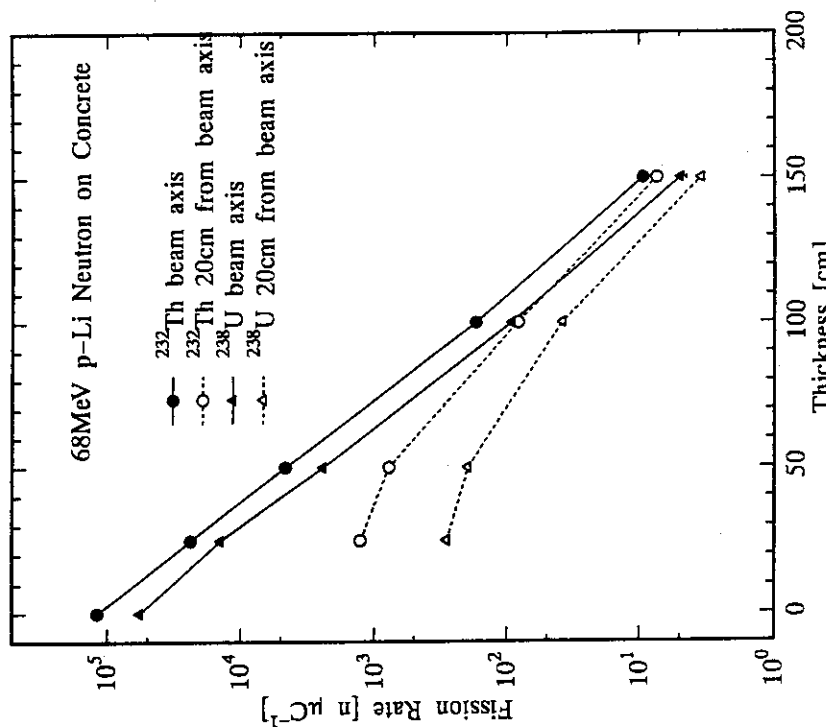


Fig. 1.30 Fission rates of  $^{232}\text{Th}$  and  $^{238}\text{U}$  behind concrete on the beam axis and 20-cm off axis for 68-MeV p-Li neutrons

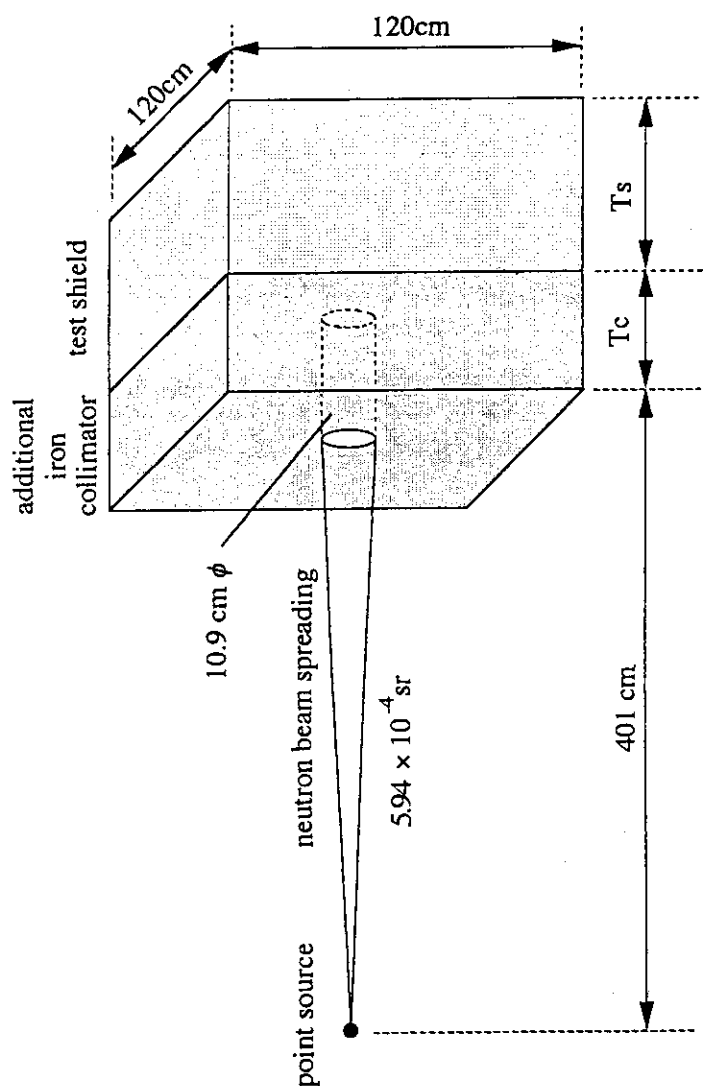


Fig.1.31 Calculation geometry for the Monte Carlo codes  
The values of shield thickness,  $T_s$  and collimator thickness,  $T_c$  are  
tabulated in Table I.1.

Table 1.33 Fission cross sections of  $^{232}\text{Th}$  and  $^{238}\text{U}$ 

Energy boundary (MeV)	Cross section (b) $^{232}\text{Th}$	Energy boundary (MeV)	Cross section (b) $^{238}\text{U}$
4.00E+2 *5.7915E-1	1.3016E+0	1.22E+1	3.1267E-1 9.7859E-1
3.75E+2 6.6380E-1	1.3128E+0	1.00E+1	3.3658E-1 9.9039E-1
3.50E+2 7.4080E-1	1.3296E+0	8.19E+0	3.876E-1 9.7573E-1
3.25E+2 7.6801E-1	1.3394E+0	6.70E+0	1.9331E-1 6.5639E-1
3.00E+2 7.8376E-1	1.3434E+0	5.49E+0	1.4968E-1 5.3713E-1
2.75E+2 8.0047E-1	1.3334E+0	4.49E+0	1.4654E-1 5.6118E-1
2.50E+2 8.0915E-1	1.3254E+0	3.68E+0	1.4599E-1 5.3383E-1
2.25E+2 8.1796E-1	1.3224E+0	3.01E+0	1.2197E-1 5.3862E-1
2.00E+2 7.3489E-1	1.3244E+0	2.46E+0	1.2712E-1 5.4919E-1
1.80E+2 7.7471E-1	1.3194E+0	2.02E+0	0.3155E-1 4.9559E-1
1.60E+2 7.5311E-1	1.3227E+0	1.65E+0	0.8389E-2 3.1461E-1
1.40E+2 8.0410E-1	1.3516E+0	1.355E+0	1.355E-2 5.1671E-2
1.20E+2 7.8314E-1	1.3583E+0	1.11E+0	1.7806E-3 1.8998E-2
1.10E+2 8.0839E-1	1.4180E+0	9.07E-1	5.9640E-4 6.5292E-3
1.00E+2 8.4285E-1	1.4493E+0	7.43E-1	1.1930E-4 1.0334E-3
9.00E+1 8.6533E-1	1.4845E+0	4.98E-1	1.2951E-5 2.5770E-4
8.00E+1 8.7328E-1	1.5234E+0	3.34E-1	0.0 9.659E-5
7.00E+1 8.9851E-1	1.5383E+0	2.24E-1	0.0 9.9000E-5
6.50E+1 9.0406E-1	1.5893E+0	1.50E-1	0.0 3.9529E-5
6.00E+1 8.7266E-1	1.6395E+0	8.65E-2	0.0 6.1955E-5
5.50E+1 7.9173E-1	1.6442E+0	3.18E-2	0.0 6.685E-5
5.00E+1 8.2918E-1	1.6656E+0	1.50E-2	0.0 1.1000E-4
4.50E+1 8.3477E-1	1.6856E+0	7.10E-3	0.0 6.7200E-6
4.00E+1 7.8466E-1	1.6738E+0	3.35E-3	0.0 4.0000E-8
3.50E+1 7.5686E-1	1.6621E+0	1.58E-3	0.0 4.5624E-8
3.00E+1 6.5466E-1	1.6173E+0	4.54E-4	0.0 8.7118E-8
2.75E+1 6.4635E-1	1.5873E+0	1.01E-4	0.0 1.865E-7
2.50E+1 6.4801E-1	1.5777E+0	2.26E-5	0.0 3.095E-7
2.25E+1 5.8063E-1	1.4448E+0	1.07E-5	0.0 4.476E-7
1.96E+1 5.0863E-1	1.2333E+0	5.04E-6	0.0 6.4623E-7
1.75E+1 4.4226E-1	1.2344E+0	2.38E-6	0.0 9.3423E-7
1.49E+1 3.7120E-1	1.1388E+0	1.12E-6	0.0 1.4397E-6
1.35E+1 3.1923E-1	1.0034E+0	4.14E-7	0.0 6.3656E-6

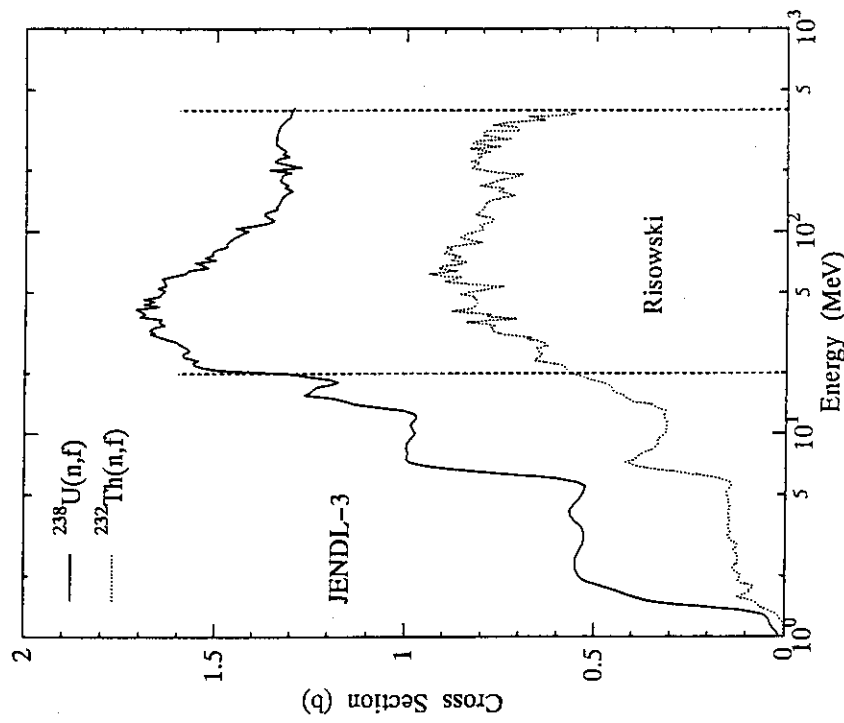
\* Read as  $4.00 \times 10^{-2}$ Lower energy boundary is  $1.00 \times 10^{-10}$  (MeV)

Fig.1.32

Fission cross sections of  $^{232}\text{Th}$  and  $^{238}\text{U}$ . The cross sections up to 20 MeV is taken from JENDL-3, those between 20 and 400 MeV have been measured by Lisowski et al.

## 2. Neutron Fluxes in and around Iron Beam Stop Irradiated by 500 MeV Protons

### (Summary)

- 1) Accelerator (Organization) : Proton Synchrotron (KEK)
- 2) Projectile (Energy) : Proton (500 MeV)
- 3) Target : Iron
- 4) Shielding material : Iron and Concrete
- 5) Geometry : Beam Stop of Rectangular Parallelepiped,  
Forward and Lateral Shields
- 6) Instrument : Activation Detectors (Fe, Al, Cu, Au, C)
- 7) Measured Quantities : Saturated Activity

### 2.1 Experimental Arrangement

Cross-sectional plane view of a beam stop for the experiment<sup>1)</sup> is shown in Fig. 2.1. The beam stop consisted of an iron beam catcher of rectangular parallelepiped and an iron shielding box of rectangular parallelepiped. Activation detectors were packed in iron pipes of 55.0 cm long and 2.0 cm inner diameter and put into the hole bored in the beam stop.

Plan view of a beam dump room for the experiment<sup>2)</sup> is shown in Fig. 2.2. In the figure, a concrete wall thickness in the beam direction is 2 m and a lateral wall thickness is 1.5 m. Activation detectors were set inside and outside the concrete shielding wall at 0, 65, 80, 90 and 100 degree around the beam stop. The origin for the directions was set at 5 cm from the entrance point of proton beam toward the beam direction.

### 2.2 Methods of Measurement and Instrument

Saturated activity distributions were measured with a 40 cm<sup>3</sup> Ge(Li) gamma-ray detector. Activation detectors of Fe, Al, Cu and Au were used in the beam stop. Physical properties of activation detectors used for the experiment are listed in Table 2.1.

Activation detectors of C and Al were used in the beam dump room. Physical properties of the activation detectors are listed in Table 2.2.

### 2.3 Beam Conditions

The 500 MeV proton beam impinged on the beam stop perpendicularly at its center. For the measurements in the beam stop, the beam profile was about 6.0 cm (FWHM) in the horizontal and 3.0 cm (FWHM) in the vertical direction. For the measurements in the beam dump room, the beam profile was about 3.0 cm (FWHM) in the horizontal and 1.5 cm (FWHM) in the vertical direction. The accuracy of absolute beam intensity was within 4%.

## 2.4 Measured Results

Measured distributions of saturated activities in the beam stop are shown in Figs. 2.3 through 2.5 and Tables 2.3 and 2.4. Measured distributions of saturated activities in the beam dump room are given in Table 2.5. All measured data in the beam stop and in the beam dump room are normalized by a condition of one proton incidence.

## 2.5 Model for Calculation

### a. Source Condition

The 500 MeV proton beam of mono-direction along the Z-axis impinges on the origin in Figs.

2.6 and 2.7.

### b. Calculation Geometry

The beam stop is expressed with a two-dimensional (R-Z) model shown in Fig. 2.6. The beam dump room is expressed with a three-dimensional (X,Y,Z) model shown in Fig. 2.7, however, it can be expressed with a two-dimensional (R-Z) model.

### c. Material Descriptions

Densities of iron and concrete, and atomic composition of concrete are given in Table 2.6.

## 2.6 Proposed Neutron Cross Sections

Neutron reaction cross sections except the  $^{12}\text{C}(\text{n},2\text{n})$  reaction have been calculated<sup>3)</sup> up to 500MeV. The resultant cross sections are shown in Figs 2.8 - 2.11 and are given in Tables 2.7 and 2.8. For the  $^{12}\text{C}(\text{n},2\text{n})$  reaction, we propose a simple cross section<sup>4)</sup> shown in Fig. 2.12.

## 2.7 Normalization between Calculation and Measurement

The calculated distributions in the beam stop and in the beam dump room are requested to be normalized by a condition of one proton incidence.

## 2.8 Notice

In the beam catcher, the detectors are activated by not only neutrons but protons. For example,  $\text{Fe} \Rightarrow ^{56}\text{Co}$  is mainly due to proton reaction. Therefore, direct contributions of protons to activation should be considered in the calculation. There are two ways to consider the contributions. One way is to use some proton spallation cross section data and the other is to calculate residual nuclei directly using a high energy particle transport code, such as, HETC and NMTC/JAERI. The proton reaction is negligible outside the beam catcher.

References

1. Arakita Y., Hirayama H., Inagaki T. and Miyajima M. : "Study of an Iron Beam Stop for 500 MeV Protons", Nucl. Instrum. Methods, 164, 255-265 (1979).
2. Ban S., Hirayama H. and Katoh K. : "Measurement of Secondary Neutron Fluxes around Beam Stop for 500 MeV protons", ibid., 184, 409-412 (1981).
3. Nakashima H., et al. : "Benchmark Problems for Intermediate and High Energy Accelerator Shielding", JAERI-Data/Code 94-012 (1994).
4. Patterson H. W. and Thomas R. H. : "Accelerator Health Physics", Academic Press (1973).

Table 2.1 Physical properties of activation detectors for measurements in the beam stop

Detector	Detector Shape	Dimension (cm)	Reaction
Fe	Cylinder	2.0 $\phi \times$ 1.0	$\text{Fe} \rightarrow ^{48}\text{V}$ , $\text{Fe} \rightarrow ^{52}\text{Mn}$ , $\text{Fe} \rightarrow ^{54}\text{Mn}$ , $\text{Fe} \rightarrow ^{56}\text{Co}$
Al	Cylinder	1.4 $\phi \times$ 0.5	$^{27}\text{Al}(\text{n}, \text{x})^{24}\text{Na}$
Cu	Cylinder	2.0 $\phi \times$ 0.5	$\text{Cu} \rightarrow ^{58}\text{Co}$
Au	Rectangular	1 $\times$ 1 $\times$ 0.05	$^{197}\text{Au}(\text{n}, \gamma)^{198}\text{Au}$

Table 2.2 Physical properties of activation detectors for measurements in the beam dump room

Detector	Detector Shape	Dimensions (cm)	Reaction
C	Cylinder	7 $\phi \times$ 4	$^{12}\text{C}(\text{n}, 2\text{n})^{11}\text{C}$
Al	Hollow Cylinder	9 $\phi \times$ 6.5 (Inside 7 $\phi \times$ 5)	$^{27}\text{Al}(\text{n}, \text{spal.})^{18}\text{F}$ , $^{27}\text{Al}(\text{n}, \alpha)^{24}\text{Na}$

Table 2.3 Saturated activity distributions of  $^{48}\text{V}$ ,  $^{52}\text{Mn}$ ,  $^{54}\text{Mn}$  and  $^{56}\text{Co}$  in beam stop

R (cm)	-2.5	12.5	27.5	Z(cm) 40	52.5	67.5	82.5
Fe → $^{48}\text{V}$							
0.0		5.22E-29	2.48E-30	1.06E-30	2.30E-31	5.94E-32	2.07E-32
7.0	6.92E-30 *		2.12E-30	1.06E-30	2.28E-31	6.23E-32	2.02E-32
14.0	6.87E-32	9.95E-31	6.17E-31	6.11E-31	1.58E-31	5.23E-32	2.30E-32
28.0		6.51E-32	8.68E-32		7.38E-32	3.68E-32	1.49E-32
44.0		5.41E-33	1.79E-32	1.72E-32	2.27E-32		
Fe → $^{52}\text{Mn}$							
0.0		4.23E-29	3.19E-30	6.11E-31	2.85E-31	7.87E-32	2.68E-32
7.0	4.88E-30	1.88E-29	2.76E-30	5.74E-31	2.73E-31	7.69E-32	2.28E-32
14.0	2.16E-31	1.65E-30	9.30E-31	3.58E-31	2.16E-31	7.15E-32	2.38E-32
28.0	8.68E-33	1.50E-31	2.02E-31	6.07E-32	1.15E-31	3.67E-32	1.51E-32
44.0		2.18E-32	2.81E-32		2.33E-32	1.12E-32	7.14E-33
Fe → $^{54}\text{Mn}$							
0.0		5.88E-28	6.73E-29	1.26E-29	6.21E-30	1.70E-30	6.84E-31
7.0	8.18E-29	2.80E-28	5.75E-29	1.24E-29	5.88E-30	2.07E-30	6.28E-31
14.0	1.77E-29	4.19E-29	1.79E-29	8.86E-30	5.17E-30	1.44E-30	6.93E-31
28.0	9.25E-30	1.20E-29	7.45E-30	2.09E-30	3.05E-30	1.02E-30	
44.0	4.93E-30	7.57E-30	2.08E-30	1.30E-30	8.24E-31		
56.0		6.03E-30	1.49E-30	1.11E-30	6.02E-31	4.41E-31	
Fe → $^{56}\text{Co}$ (Relative to $^{54}\text{Mn}$ )							
0.0		5.88E-28					
1.5	2.36E-28						
2.0		2.45E-28					
3.0	1.60E-28		1.71E-28				
4.0	6.19E-29		7.08E-29				
5.0	3.03E-29		4.09E-29				
6.0	8.32E-30		2.21E-29				
7.0		1.34E-29					

\* Read as  $6.92 \times 10^{-30}$  (n/proton).

Table 2.4 Saturated activity distributions of  $^{24}\text{Na}$ ,  $^{58}\text{Co}$  and  $^{198}\text{Au}$   
in beam stop

R (cm)	Z (cm)							
	-2.5	12.5	27.5	40	52.5	67.5	82.5	97.5
	$^{27}\text{Al}(\text{n}, \text{x})^{24}\text{Na}$							
0.0		1.82E-28	7.43E-30	1.46E-30	6.24E-31	4.07E-31	8.16E-32	2.49E-32
7.0	1.08E-29 *	2.53E-29	5.52E-30	1.78E-30	5.58E-31	2.78E-31	8.51E-32	1.77E-32
14.0	2.03E-30	4.87E-30	3.04E-30	9.32E-31	3.20E-31	2.22E-31	6.07E-32	2.43E-32
28.0	3.26E-31	6.79E-31	6.68E-31	4.22E-31	1.14E-31	8.47E-32	2.87E-32	
	$\text{Cu} \rightarrow ^{58}\text{Co}$							
0.0		1.21E-27	2.96E-29	5.49E-30	2.28E-30	8.58E-31		
7.0	1.29E-29	7.50E-29	2.01E-29	4.46E-30	1.98E-30	5.84E-31		
14.0	1.49E-30	8.05E-30	5.73E-30	2.54E-30	1.30E-30	4.67E-31		
28.0	2.79E-31	9.70E-31	1.25E-30	8.12E-31	7.71E-31	2.54E-31		
	$^{197}\text{Au}(\text{n}, \gamma)^{198}\text{Au}$							
0.0		4.33E-27	3.69E-27	2.23E-27	2.21E-28	1.47E-28	1.20E-28	3.45E-29
7.0	3.00E-27	4.15E-27	2.82E-27	2.46E-27	2.16E-28	1.58E-28	8.93E-29	3.39E-29
14.0		3.68E-27	2.19E-27	2.74E-27	2.42E-28	1.39E-28	1.15E-28	
28.0	2.03E-27	2.79E-27	1.34E-27	1.77E-27	1.80E-28	1.05E-28	6.14E-29	2.27E-29
44.0	4.69E-28	7.36E-28		6.04E-28	7.23E-29	2.83E-29	3.19E-29	1.22E-29
54.0	2.18E-28	2.47E-28	2.54E-28	2.32E-28	1.97E-29	1.84E-29	2.10E-29	

\* Read as  $1.08 \times 10^{-29}$  (n/proton).

Table 2.5 Experimental results of saturated activities around beam stop

Position	$^{11}\text{C}$ s $^{-1}$ per proton/s	$^{18}\text{F}$ s $^{-1}$ per proton/s	$^{24}\text{Na}$ s $^{-1}$ per proton/s
0° I <sup>a</sup>	1.96E-33 <sup>c</sup>	3.84E-34	2.99E-33
65° I	1.08E-33		
80° I	1.04E-33	1.73E-34	2.14E-33
90° I	1.18E-33	1.64E-34	2.13E-33
100° I	8.71E-34		
0° O <sup>b</sup>	1.15E-35	1.85E-36	1.46E-35
65° O	1.11E-35		
80° O	9.86E-36	1.74E-36	1.70E-35
90° O	7.25E-36	1.18E-36	1.43E-35
100° O	4.40E-36		

<sup>a</sup> Inside the concrete shield. <sup>b</sup> Outside. <sup>c</sup>  $1.96 \times 10^{-33}$ .

Table 2.6 Densities and atomic composition

Material	Density
Iron	7.8 g/cm $^3$
Concrete	2.35 g/cm $^3$
H	1.20%
O	54%
Si	31%
Ca	9.70%
Al	4.10%

Table 2.7 Group-wise neutron cross sections for the benchmark calculation

Energy (eV)	reaction cross section (barn)			Energy (eV)	reaction cross section (barn)		
	Fe(n, x) <sup>48</sup> V	Fe(n, x) <sup>52</sup> Mn	Fe(n, x) <sup>54</sup> Mn		Fe(n, x) <sup>48</sup> V	Fe(n, x) <sup>52</sup> Mn	Fe(n, x) <sup>54</sup> Mn
5.00E+08*	1.42E-02	9.87E-03	1.80E-02	1.22E+07	0.00E+00	0.00E+00	3.08E-02
4.50E+08	1.56E-02	1.06E-02	1.95E-02	1.00E+07	0.00E+00	0.00E+00	3.07E-02
4.00E+08	1.70E-02	1.10E-02	2.06E-02	8.19E+06	0.00E+00	0.00E+00	3.03E-02
3.75E+08	1.80E-02	1.11E-02	2.13E-02	6.70E+06	0.00E+00	0.00E+00	2.86E-02
3.50E+08	1.90E-02	1.14E-02	2.20E-02	5.49E+06	0.00E+00	0.00E+00	2.34E-02
3.25E+08	2.00E-02	1.20E-02	2.27E-02	4.49E+06	0.00E+00	0.00E+00	1.60E-02
3.00E+08	2.18E-02	1.26E-02	2.36E-02	3.68E+06	0.00E+00	0.00E+00	1.12E-02
2.75E+08	2.55E-02	1.34E-02	2.45E-02	3.01E+06	0.00E+00	0.00E+00	5.41E-03
2.50E+08	2.82E-02	1.42E-02	2.60E-02	2.46E+06	0.00E+00	0.00E+00	2.31E-03
2.25E+08	2.64E-02	1.52E-02	2.88E-02	2.02E+06	0.00E+00	0.00E+00	6.96E-04
2.00E+08	2.28E-02	1.63E-02	3.18E-02	1.65E+06	0.00E+00	0.00E+00	1.04E-04
1.80E+08	2.13E-02	1.78E-02	3.46E-02	1.35E+06	0.00E+00	0.00E+00	2.62E-05
1.60E+08	2.11E-02	2.07E-02	3.81E-02	1.11E+06	0.00E+00	0.00E+00	3.24E-06
1.40E+08	2.03E-02	2.57E-02	4.31E-02	9.07E+05	0.00E+00	0.00E+00	0.00E+00
1.20E+08	1.89E-02	3.14E-02	4.79E-02	7.43E+05	0.00E+00	0.00E+00	0.00E+00
1.10E+08	1.77E-02	3.69E-02	5.18E-02	4.98E+05	0.00E+00	0.00E+00	0.00E+00
1.00E+08	1.67E-02	4.45E-02	5.70E-02	3.34E+05	0.00E+00	0.00E+00	0.00E+00
9.00E+07	1.38E-02	5.00E-02	6.57E-02	2.24E+05	0.00E+00	0.00E+00	0.00E+00
8.00E+07	6.97E-03	5.00E-02	7.80E-02	1.50E+05	0.00E+00	0.00E+00	0.00E+00
7.00E+07	2.99E-03	4.66E-02	9.23E-02	8.65E+04	0.00E+00	0.00E+00	0.00E+00
6.50E+07	1.90E-03	4.04E-02	1.07E-01	3.18E+04	0.00E+00	0.00E+00	0.00E+00
6.00E+07	1.32E-03	3.16E-02	1.26E-01	1.50E+04	0.00E+00	0.00E+00	0.00E+00
5.50E+07	6.32E-04	2.31E-02	1.54E-01	7.10E+03	0.00E+00	0.00E+00	0.00E+00
5.00E+07	1.36E-04	1.85E-02	1.93E-01	3.35E+03	0.00E+00	0.00E+00	0.00E+00
4.50E+07	1.46E-05	1.70E-02	2.43E-01	1.58E+03	0.00E+00	0.00E+00	0.00E+00
4.00E+07	4.68E-07	1.43E-02	2.80E-01	4.54E+02	0.00E+00	0.00E+00	0.00E+00
3.50E+07	0.00E+00	7.54E-03	2.59E-01	1.01E+02	0.00E+00	0.00E+00	0.00E+00
3.00E+07	0.00E+00	2.23E-03	1.99E-01	2.26E+01	0.00E+00	0.00E+00	0.00E+00
2.75E+07	0.00E+00	8.97E-04	1.39E-01	1.07E+01	0.00E+00	0.00E+00	0.00E+00
2.50E+07	0.00E+00	1.55E-04	8.39E-02	5.04E+00	0.00E+00	0.00E+00	0.00E+00
2.25E+07	0.00E+00	4.99E-05	3.05E-02	2.38E+00	0.00E+00	0.00E+00	0.00E+00
1.96E+07	0.00E+00	1.83E-06	8.60E-03	1.12E+00	0.00E+00	0.00E+00	0.00E+00
1.75E+07	0.00E+00	0.00E+00	1.28E-02	4.14E-01	0.00E+00	0.00E+00	0.00E+00
1.49E+07	0.00E+00	0.00E+00	2.01E-02	1.00E-04	lower limit		
1.35E+07	0.00E+00	0.00E+00	2.67E-02				

\* Read as  $5.0 \times 10^8$

Table 2.8 Group-wise neutron cross sections for the benchmark calculation

Energy (eV)	reaction cross section (barn)		Energy (eV)	reaction cross section (barn)	
	Cu(n, x) <sup>58</sup> Co	<sup>27</sup> Al(n, alpha) <sup>24</sup> Na		<sup>27</sup> Al(n, x) <sup>18</sup> F	Cu(n, x) <sup>58</sup> Co
5.00E+08*	2.12E-02	6.17E-03	5.05E-03	1.22E+07	0.00E+00
4.50E+08	2.25E-02	6.65E-03	5.44E-03	1.00E+07	0.00E+00
4.00E+08	2.39E-02	7.04E-03	5.65E-03	8.19E+06	0.00E+00
3.75E+08	2.52E-02	7.32E-03	5.76E-03	6.70E+06	0.00E+00
3.50E+08	2.66E-02	7.52E-03	5.92E-03	5.49E+06	0.00E+00
3.25E+08	2.82E-02	7.62E-03	6.15E-03	4.49E+06	0.00E+00
3.00E+08	3.01E-02	7.63E-03	6.49E-03	3.68E+06	0.00E+00
2.75E+08	3.25E-02	7.86E-03	6.66E-03	3.01E+06	0.00E+00
2.50E+08	3.49E-02	8.29E-03	6.27E-03	2.46E+06	0.00E+00
2.25E+08	3.74E-02	8.87E-03	5.46E-03	2.02E+06	0.00E+00
2.00E+08	3.95E-02	9.72E-03	4.53E-03	1.65E+06	0.00E+00
1.80E+08	4.12E-02	1.04E-02	3.79E-03	1.35E+06	0.00E+00
1.60E+08	4.28E-02	1.15E-02	3.29E-03	1.11E+06	0.00E+00
1.40E+08	4.25E-02	1.34E-02	3.00E-03	9.07E+05	0.00E+00
1.20E+08	4.09E-02	1.52E-02	2.86E-03	7.43E+05	0.00E+00
1.10E+08	3.96E-02	1.64E-02	2.79E-03	4.98E+05	0.00E+00
1.00E+08	3.82E-02	1.72E-02	2.77E-03	3.34E+05	0.00E+00
9.00E+07	3.58E-02	1.65E-02	2.90E-03	2.24E+05	0.00E+00
8.00E+07	3.19E-02	1.43E-02	2.91E-03	1.50E+05	0.00E+00
7.00E+07	2.86E-02	1.18E-02	2.45E-03	8.65E+04	0.00E+00
6.50E+07	2.64E-02	1.02E-02	2.01E-03	3.18E+04	0.00E+00
6.00E+07	2.80E-02	8.93E-03	1.24E-03	1.50E+04	0.00E+00
5.50E+07	3.37E-02	8.37E-03	3.78E-04	7.10E+03	0.00E+00
5.00E+07	4.51E-02	7.73E-03	5.35E-05	3.35E+03	0.00E+00
4.50E+07	5.75E-02	6.04E-03	1.01E-06	1.58E+03	0.00E+00
4.00E+07	5.56E-02	3.36E-03	0.00E+00	4.54E+02	0.00E+00
3.50E+07	3.18E-02	2.00E-03	0.00E+00	1.01E+02	0.00E+00
3.00E+07	1.06E-02	3.66E-03	0.00E+00	2.26E+01	0.00E+00
2.75E+07	3.65E-03	6.79E-03	0.00E+00	1.07E+01	0.00E+00
2.50E+07	0.00E+00	1.63E-02	0.00E+00	5.04E+00	0.00E+00
2.25E+07	0.00E+00	3.30E-02	0.00E+00	2.38E+00	0.00E+00
2.00E+07	0.00E+00	5.48E-02	0.00E+00	1.12E+00	0.00E+00
1.96E+07	0.00E+00	9.09E-02	0.00E+00	4.14E-01	0.00E+00
1.75E+07	0.00E+00	1.20E-01	0.00E+00	1.00E-04	lower limit
1.49E+07	0.00E+00	1.25E-01	0.00E+00	0.00E+00	

\* Read as  $5.0 \times 10^8$

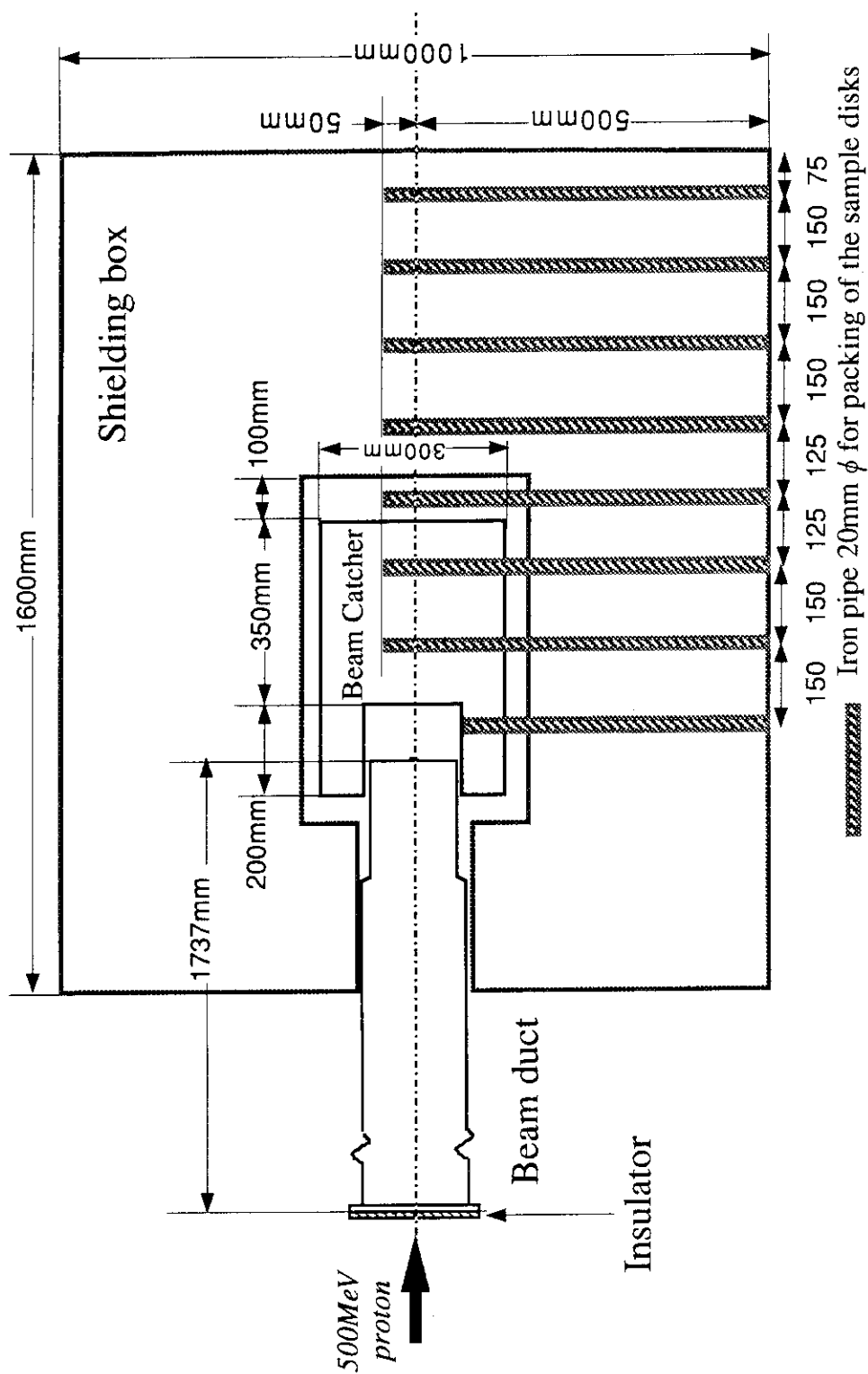


Fig. 2.1 Cross-sectional plane view of the beam stop

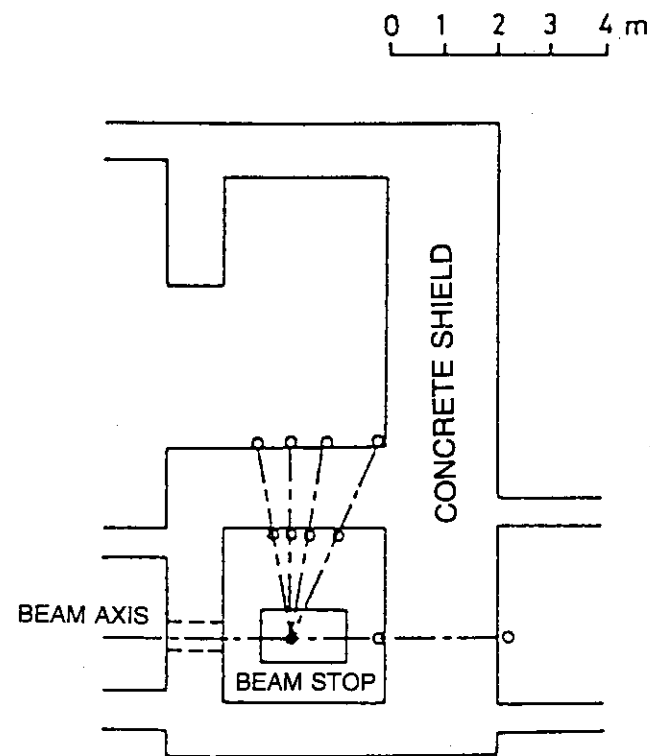


Fig. 2.2 Plan view of beam dump room

Open circles denote measurement points for directions  
0, 65, 80, 90 and 100 degree.

Brack circle denotes the origin for each direction.

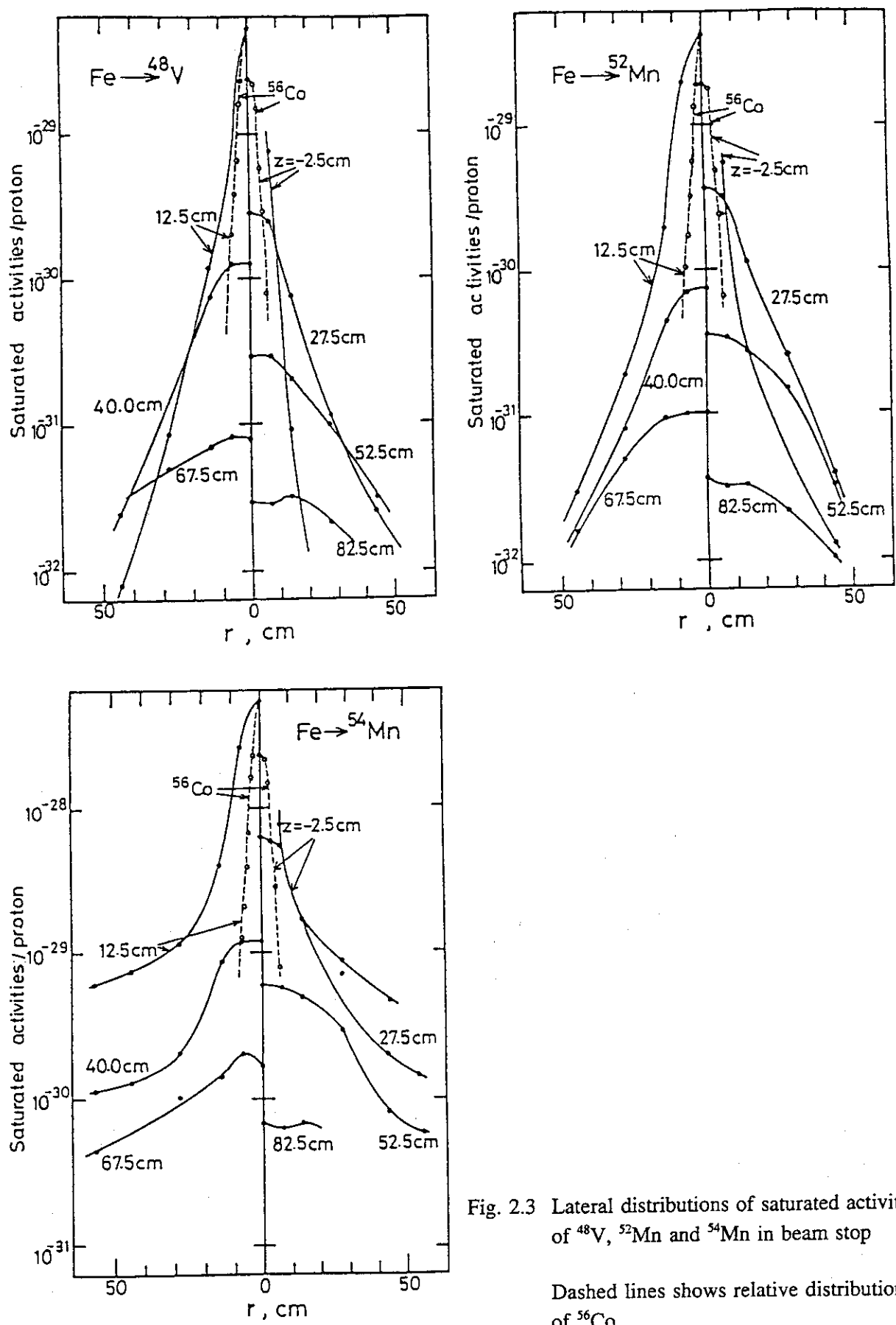


Fig. 2.3 Lateral distributions of saturated activities of  $^{48}\text{V}$ ,  $^{52}\text{Mn}$  and  $^{54}\text{Mn}$  in beam stop

Dashed lines shows relative distribution of  $^{56}\text{Co}$ .

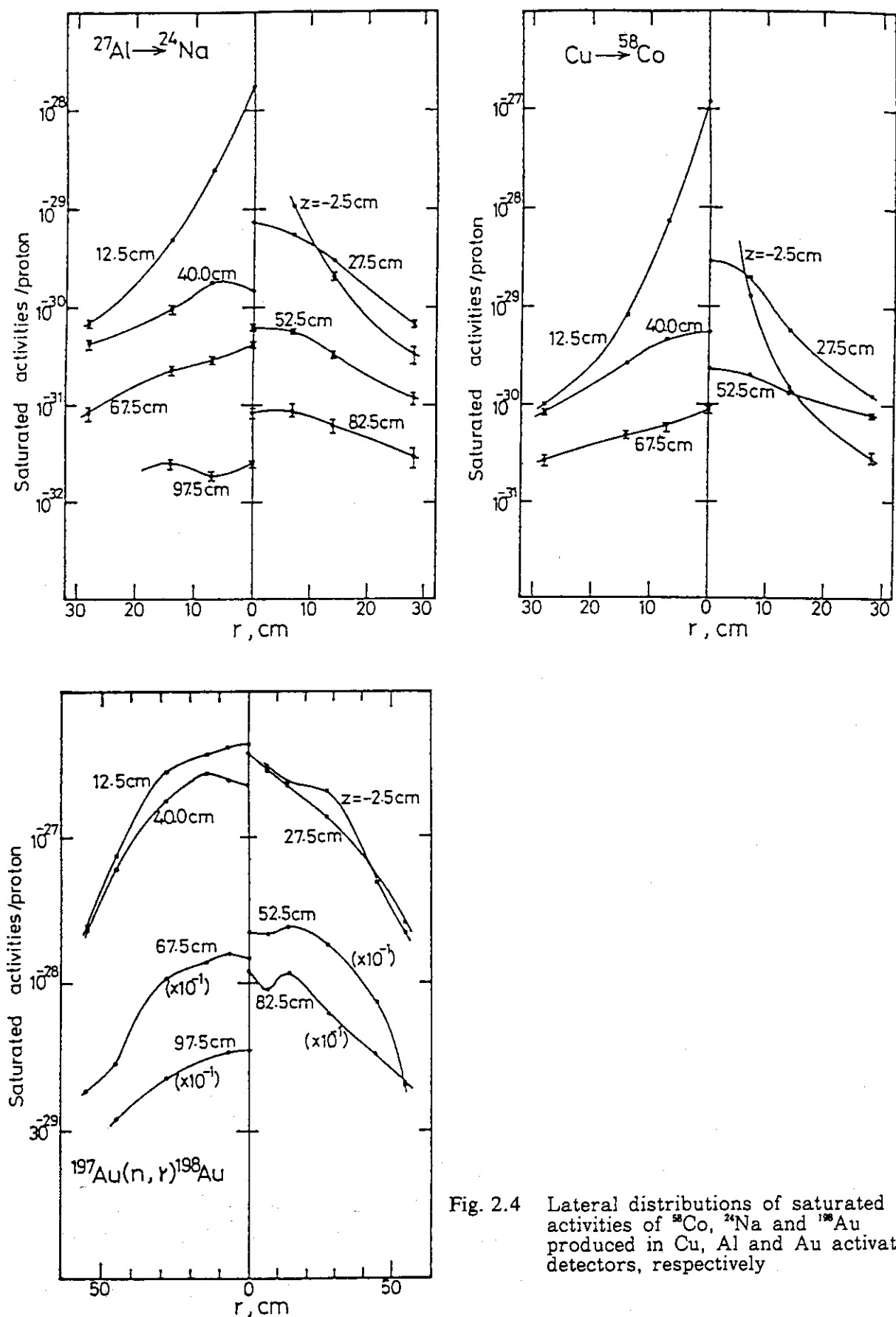


Fig. 2.4 Lateral distributions of saturated activities of  $^{58}\text{Co}$ ,  $^{24}\text{Na}$  and  $^{198}\text{Au}$  produced in Cu, Al and Au activation detectors, respectively

Saturated activities per proton

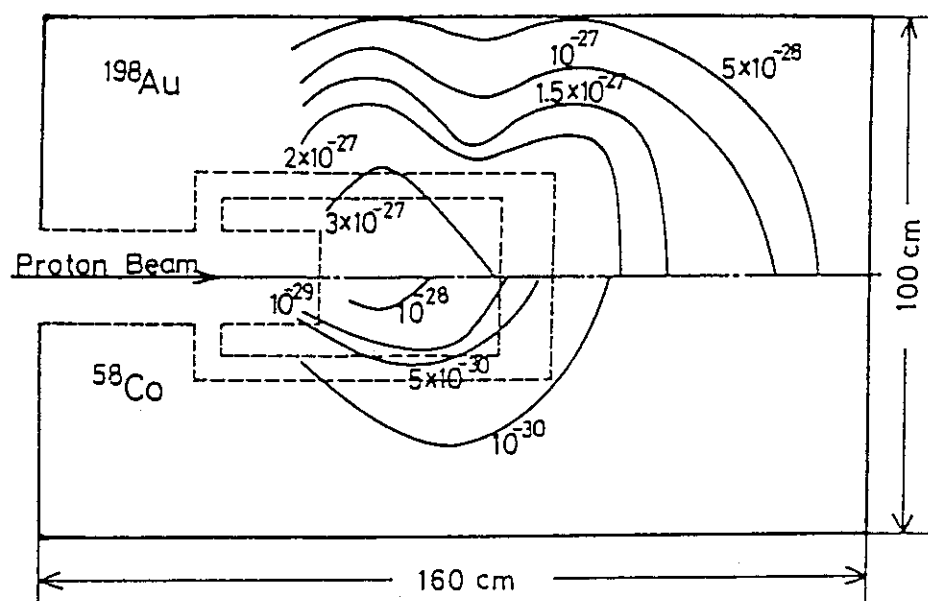


Fig. 2.5 Iso-activity-contours of  $^{58}\text{Co}$  and  $^{198}\text{Au}$  in beam stop

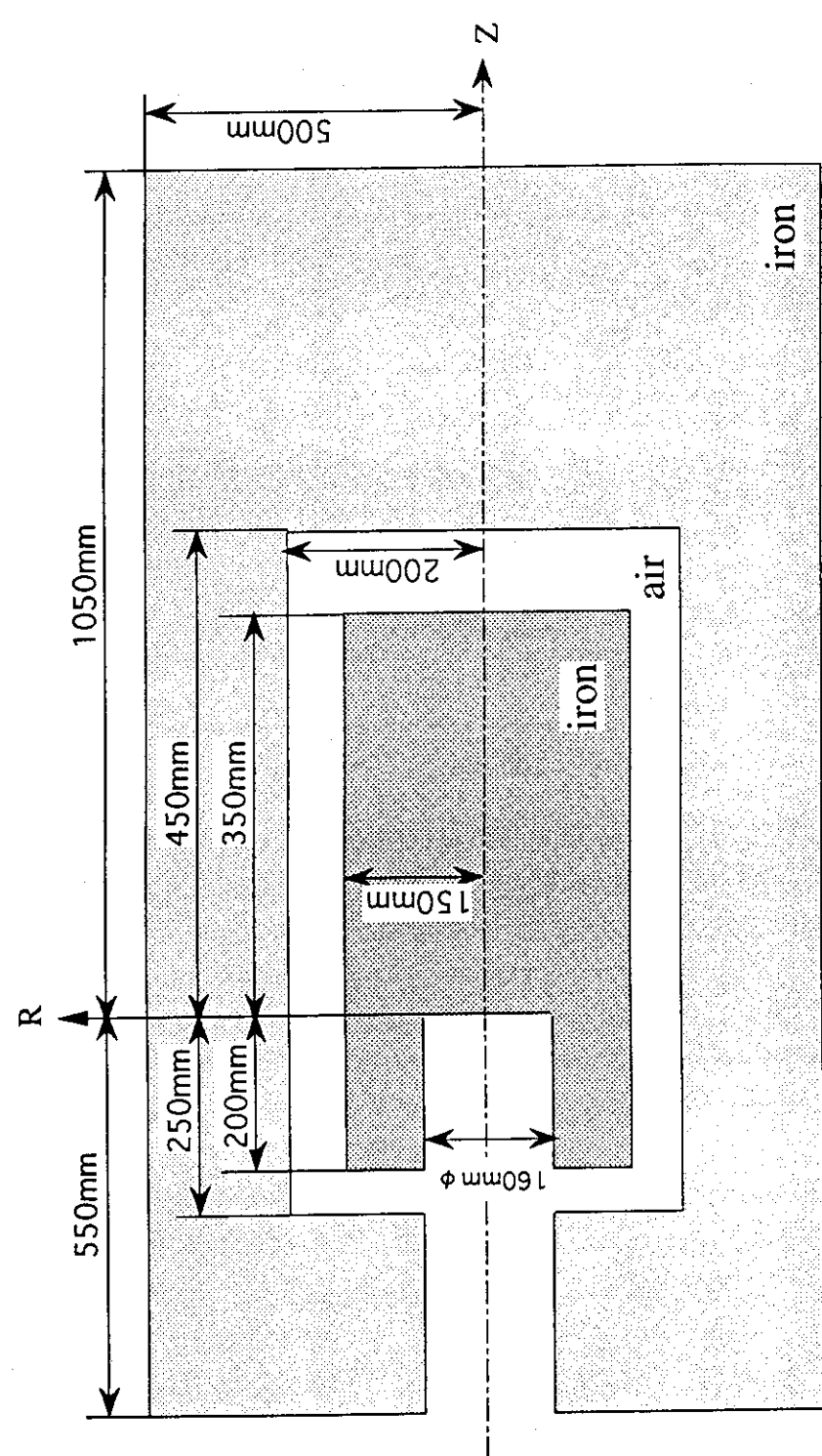


Fig. 2.6 Calculation model of the beam stop

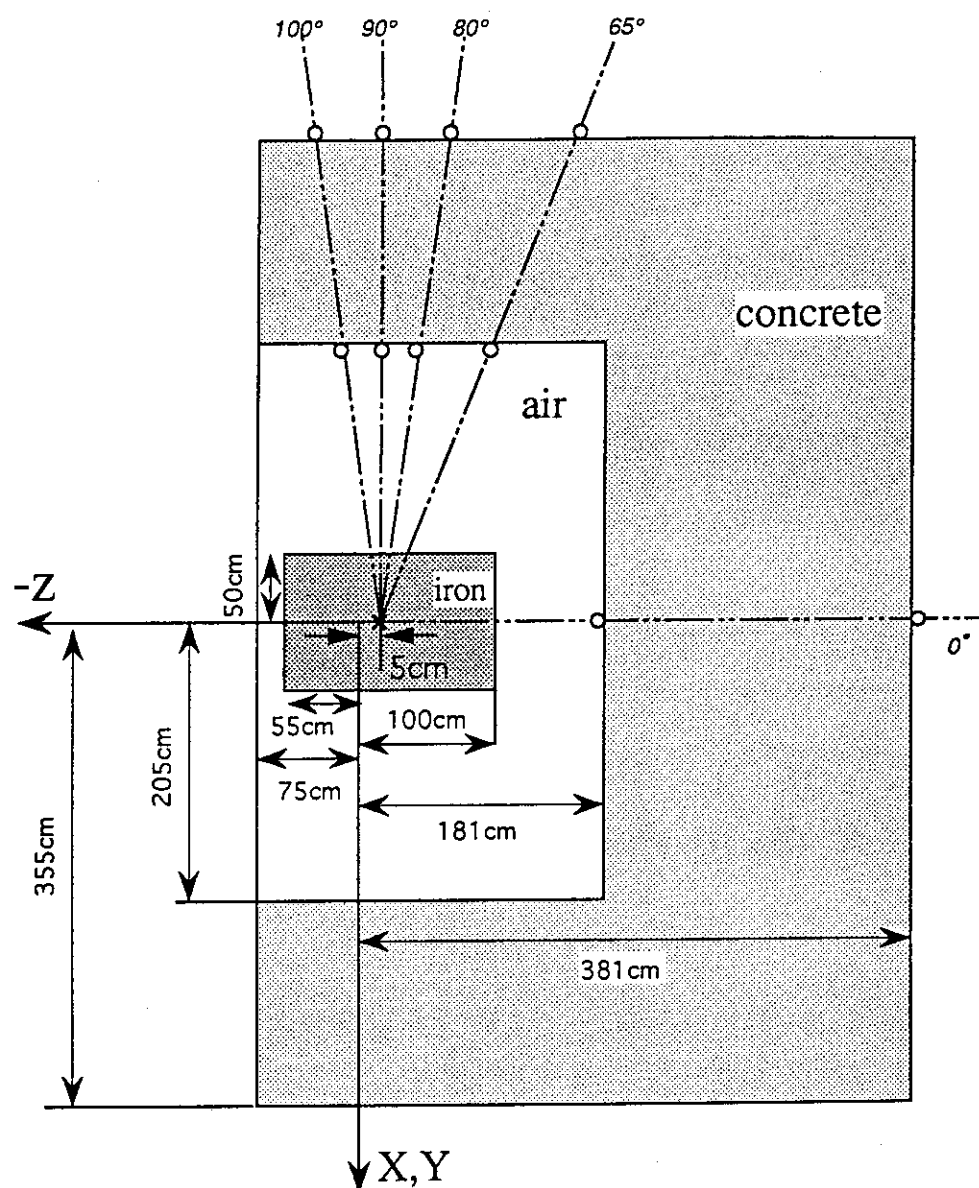
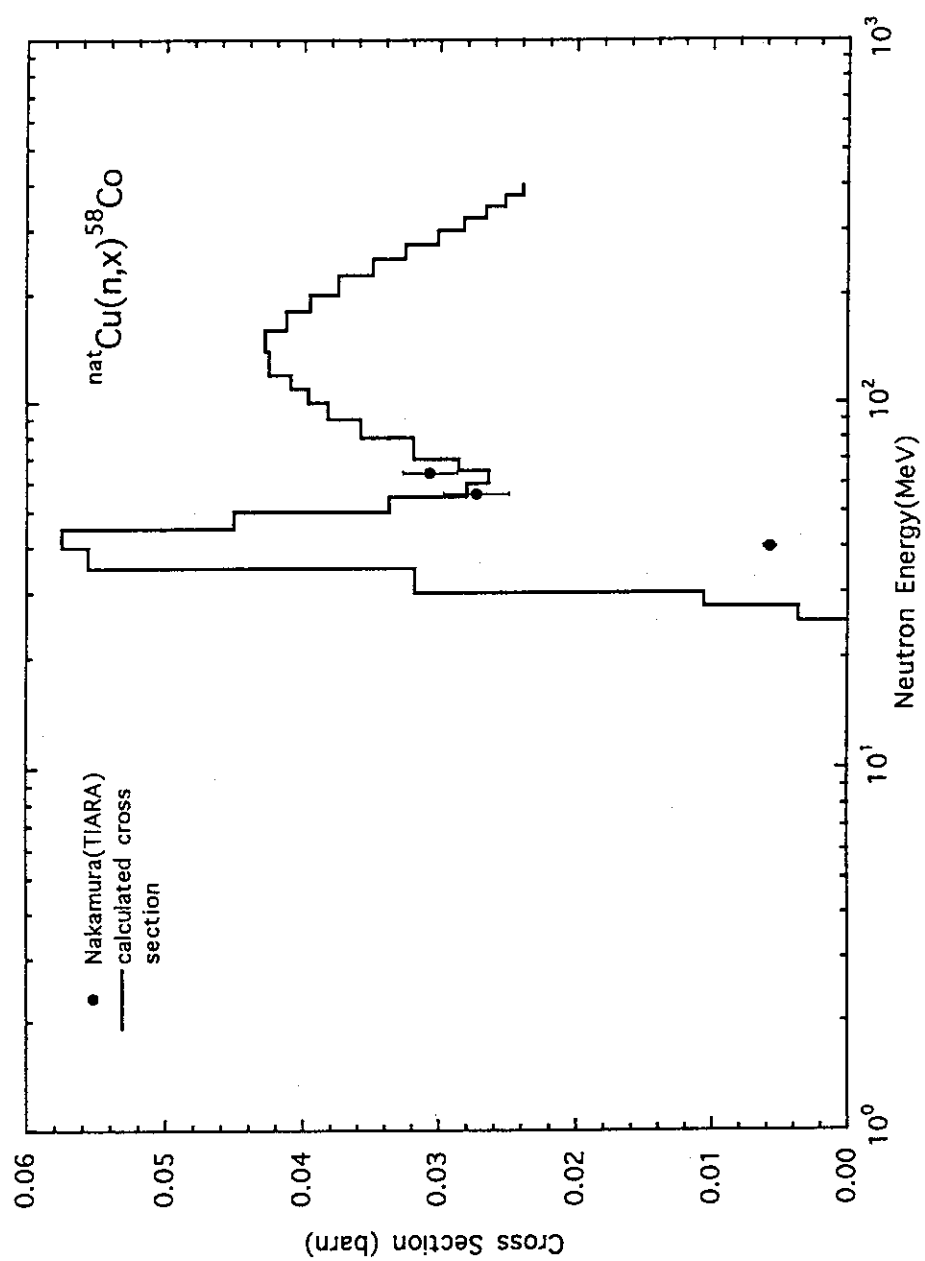
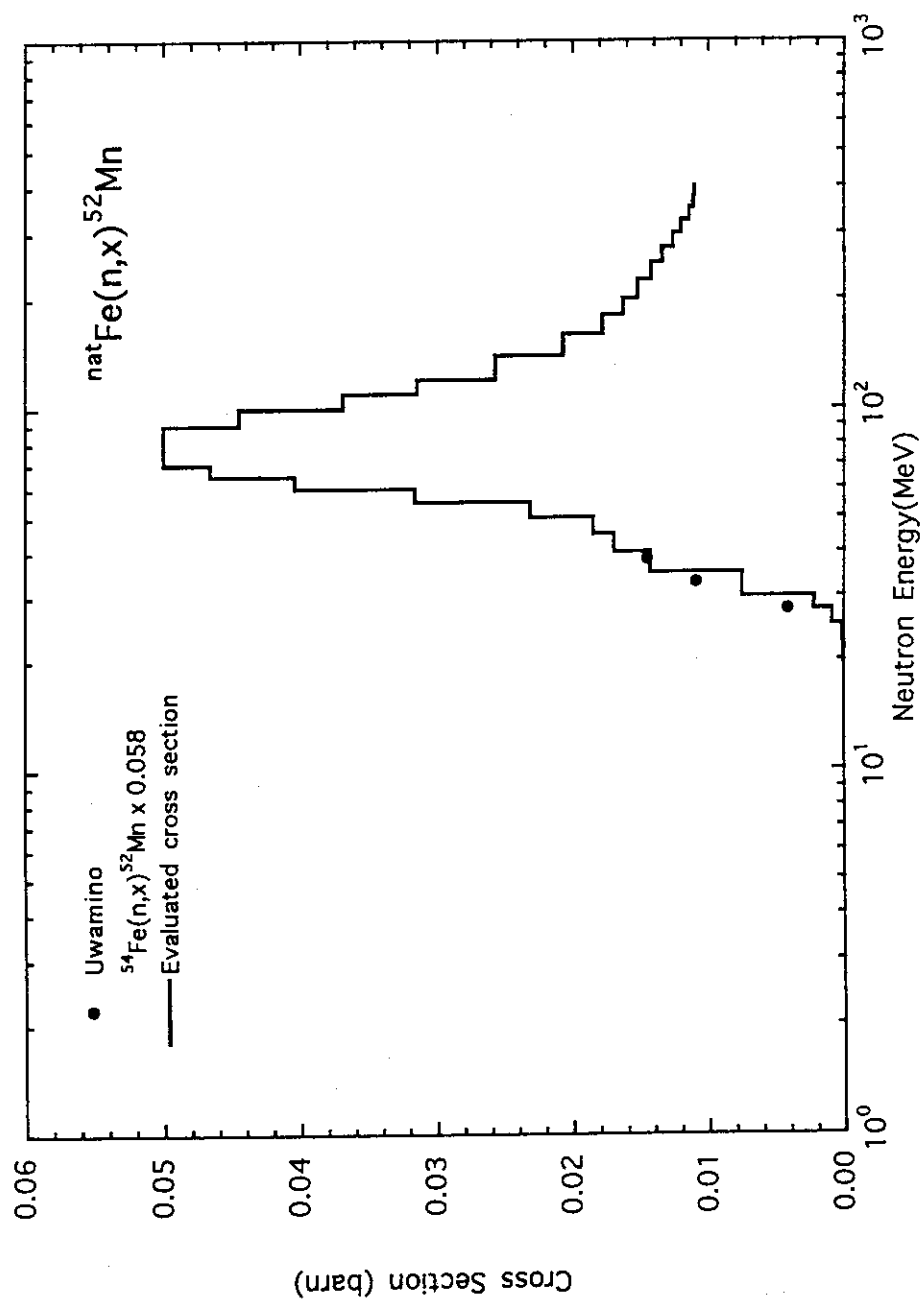


Fig. 2.7 Calculation model of the beam dump room

Fig. 2.8 <sup>nat</sup>Cu(n,x)<sup>58</sup>Co cross section

Nakamura's data will be published in the Journal of Nuclear and Science Technology.  
Solid line is calculated cross section for the benchmark calculation.

Fig. 2.9 <sup>nat</sup>Fe(n,x)<sup>52</sup>Mn cross section

Uwamino's data will be published in the Journal of Nuclear and Science Technology.  
 Solid line is calculated cross section for the benchmark calculation.  
 Uwamino's data is deduced with relative isotopic abundance (5.8%) of <sup>54</sup>Fe.

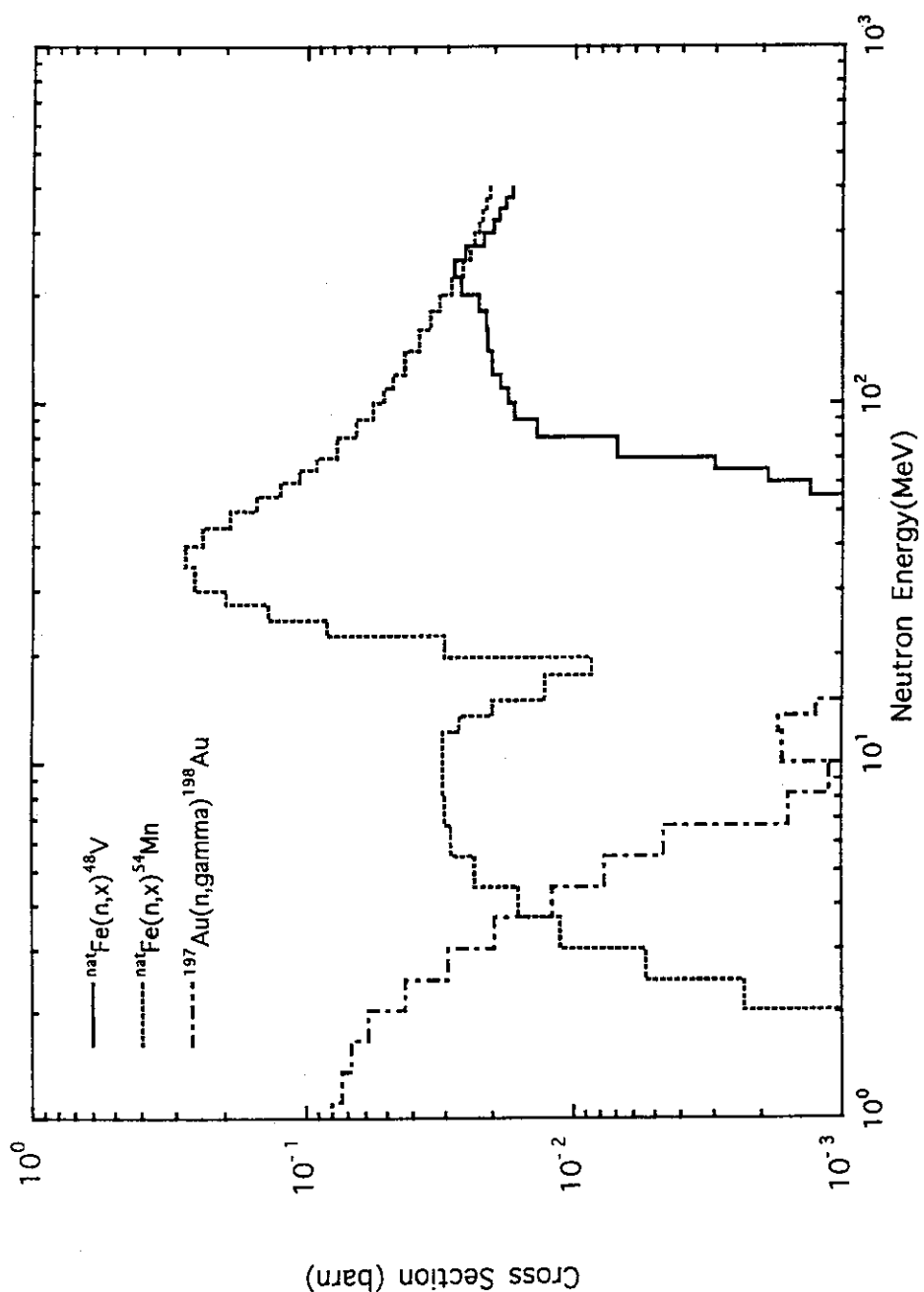


Fig. 2.10 Calculated cross sections of  ${}^{nat}\text{Fe}(n,x)^{48}\text{V}$ ,  ${}^{nat}\text{Fe}(n,x)^{54}\text{Mn}$  and  ${}^{197}\text{Au}(n,\gamma){}^{198}\text{Au}$  for the benchmark calculation

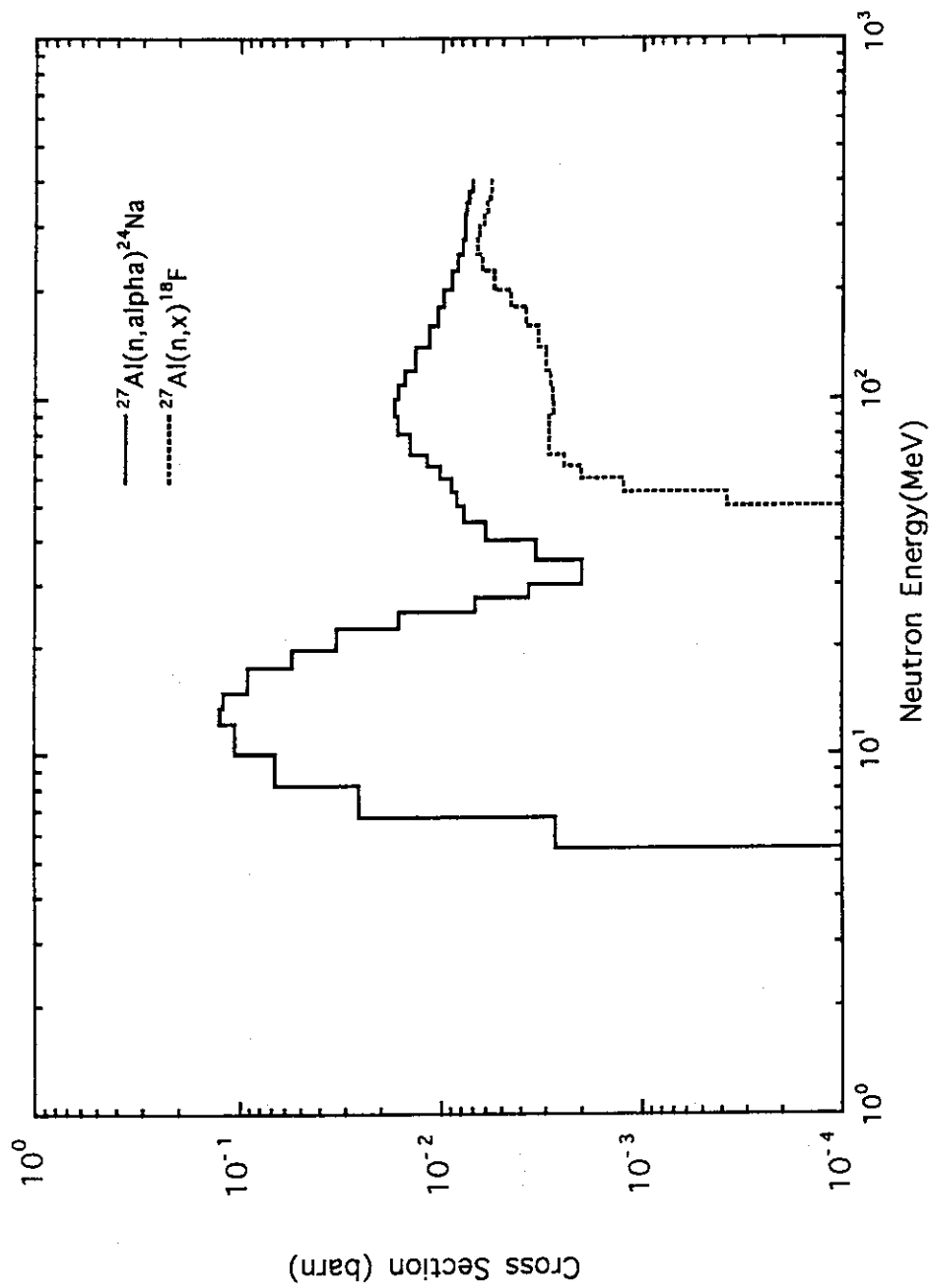


Fig. 2.11 Calculated cross sections of  $^{27}\text{Al}(n,\alpha)^{24}\text{Na}$  and  $^{27}\text{Al}(n,x)^{18}\text{F}$  for the benchmark calculation

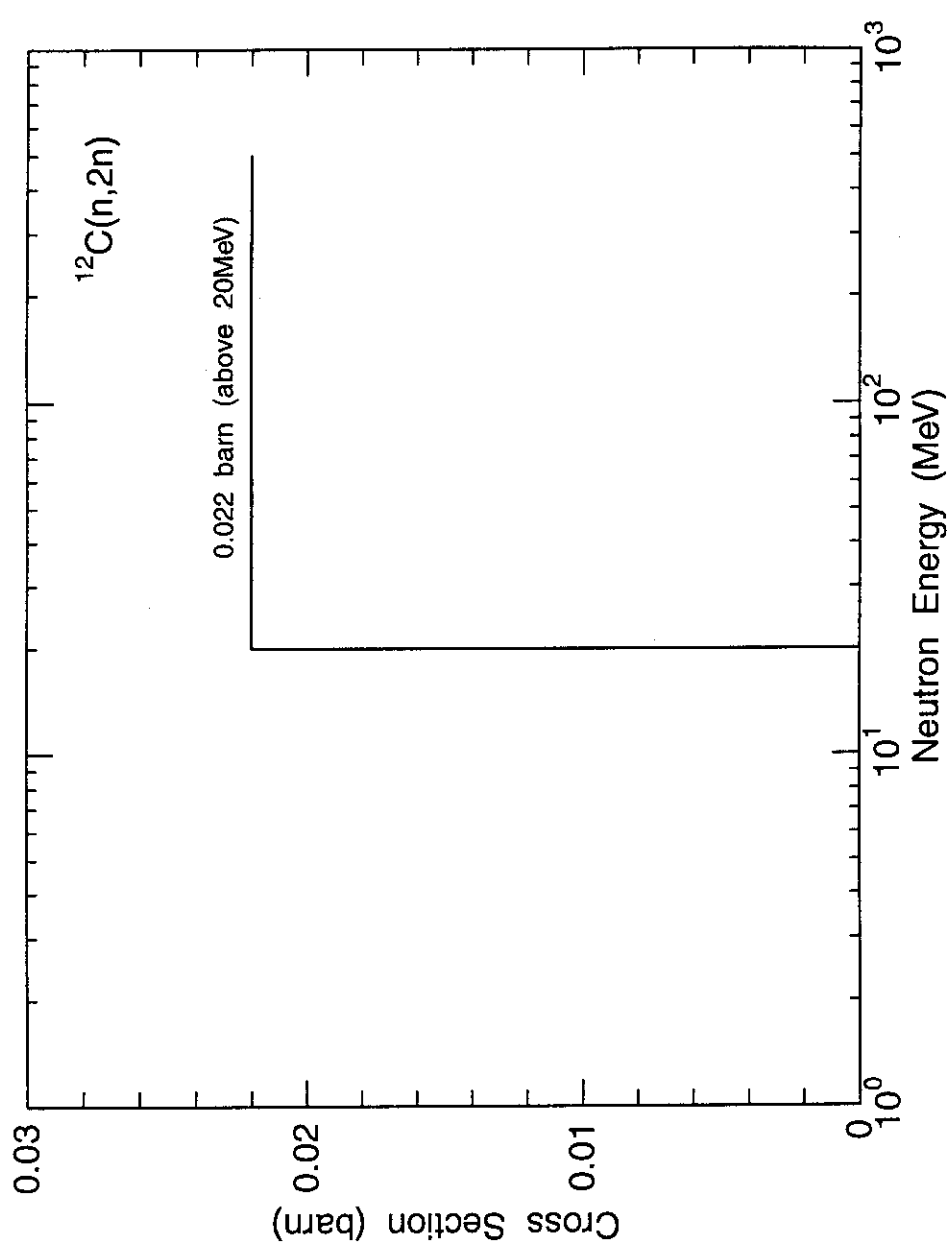


Fig. 2.12  $^{12}\text{C}(\text{n},2\text{n})$  cross section

### 3. Reaction Rate Distributions inside Thick Concrete Shield Irradiated by 6.2 GeV Protons

#### (Summary)

- 1) Accelerator (Organization) : Bevatron (LBL)
- 2) Projectile (Energy) : Proton (6.2 GeV)
- 3) Target : Ordinary Concrete
- 4) Shielding material : Ordinary Concrete (Target)
- 5) Geometry : Rectangular Slabs
- 6) Instrument : Activation Detector (Al, C, Au)
- 7) Measured Quantities : Relative Reaction Rate

#### 3.1 Experimental Arrangement

Experimental arrangement<sup>1)</sup> is shown in Fig. 3.1. A shielding assembly consisted of seven ordinary concrete slabs of 4 ft thickness. The concrete slabs were separated by 3-inch-wide gaps to allow insertion of detectors. All portions of these gaps, except slots actually used for detector placement, were filled with gypsum wallboard (approximately same density as concrete) to prevent neutron streaming along the gaps. (1 ft = 30.48 cm, 1 inch = 2.54 cm)

#### 3.2 Methods of Measurement

Gold-foils, aluminum-discs and carbon scintillators, in the form of 4 inch diameter by thicknesses between 1/32 and 1 inch, were used as activation detectors for measurement of radiation fields shown in Table 3.1. Both aluminum and carbon reactions can be initiated by protons of somewhat higher energies. The  $\gamma$ -ray activities of  $^{198}\text{Au}$  and  $^{24}\text{Na}$  were measured with a NaI crystal scintillation spectrometer, while the activities of  $^{11}\text{C}$  were measured by observing the positron decay inside the carbon scintillator. These detectors were placed at every 4-ft depth and every 1-ft from the beam axis in lateral direction. Aluminum-discs were used for measurements of incident proton energy dependence of attenuation profiles along the beam axis.

#### 3.3 Beam Conditions

The 6.2 GeV proton beam impinged on the shielding assembly perpendicularly to its front surface. The beam spot was kept within 2 inch in diameter, which was observed by using a scintillator-television system. The 4.2 and 2.2 GeV proton beams were used for the measurements of incident proton energy dependence of attenuation profiles.

#### 3.4 Measured Results

Lateral profiles of the detector count rates taken at each 4-ft depth are shown in Figs. 3.2 - 3.4 and given in Tables 3.2 - 3.4. Attenuation profiles of the three detectors measured along the beam axis are shown in Fig 3.5 and given in Table 3.5. The count rates in the figure are normalized at a depth

of 8 ft. The attenuation lengths in the table were obtained from the profile beyond 12 ft using the density for ordinary concrete, 2.4 g/cm<sup>3</sup>. Incident proton energy dependence of attenuation profiles is shown in Fig 3.6 and given in Table 3.6.

### 3.5 Model for Calculation

#### a. Source Condition

A proton beam impinges on the concrete surface perpendicularly at its center. The beam profile on the surface is circular, 5 cm in diameter. Incident proton energies are 6.2 GeV for the calculation of attenuation profiles along the beam axis and in lateral direction, and 2.2 and 4.2 GeV for the calculation of incident proton energy dependence of attenuation profiles.

#### b. Calculation Geometry

We propose to use a simple calculation geometry with a three-dimensional (X,Y,Z) model shown in Fig. 3.7. If it expresses a geometry with a two-dimensional (R-Z) model, the radius of a cylinder should be 11.23 ft (342.3 cm).

#### c. Material Descriptions

We propose to use the composition and the density of the NBS concrete given in Table 3.7 as those of the shielding assembly.

### 3.6 Normalization between Calculation and Measurement

Measured data are relative values, therefore, the relative attenuation profile is only requested for comparison. Calculated data for lateral profiles should be normalized by experimental value on the beam axis. Calculated attenuation profiles on the beam axis should be normalized by experimental value at a depth of 8 ft.

### 3.7 Notice

In the experiments, aluminum and carbon detectors are activated not only by neutrons but protons. Therefore, direct contributions of protons to activation should be considered in the calculation. There are two ways to consider the contributions. One way is to use some proton spallation cross section data and the other is to calculate residual nuclei directly using a high energy particle transport code, such as, HETC and NMTC/JAERI.

### References

1. Smith A. R. : "Some Experimental Shielding Studies at the 6.2-BeV Berkeley Bevatron", Proc. of the USAEC First Symposium on Accelerator Radiation Dosimetry and Experience, p.365, CONF-651109 (1965).

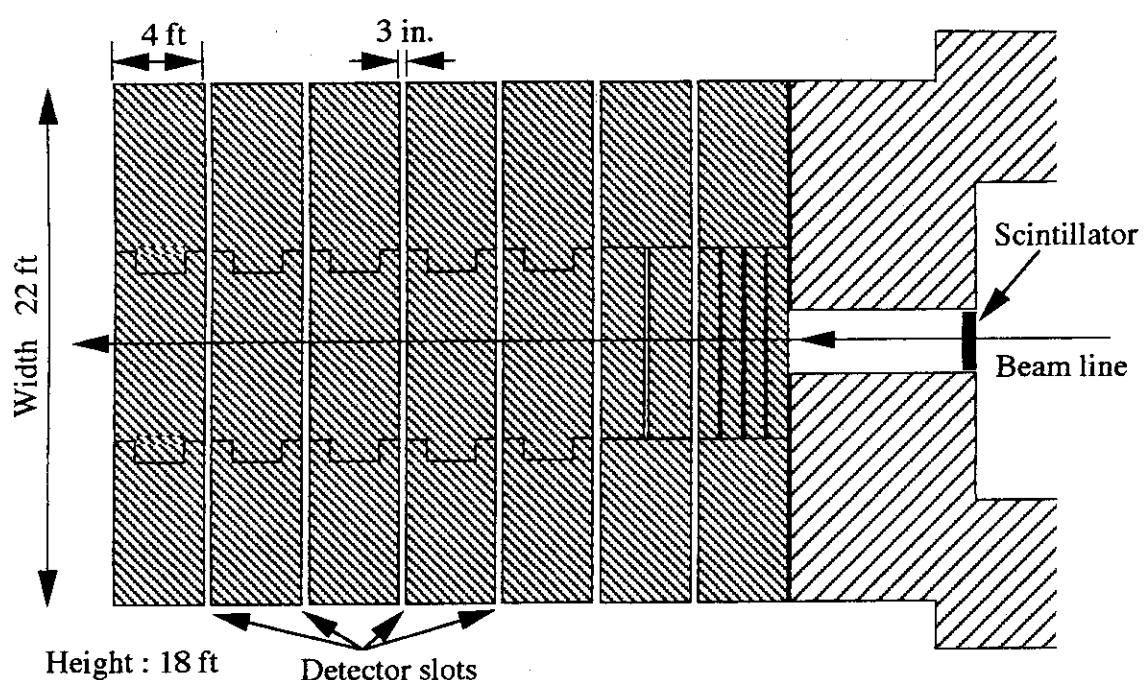


Fig. 3.1 Plan view of shield array

Table 3.1 Measured radiation fields and used reactions for each activation detectors

Detector	Radiation field	Reaction
Gold foil	thermal neutron	$^{197}\text{Au}(n,\gamma)^{198}\text{Au}$
Aluminum disc	neutrons of $E_n > 6.7 \text{ MeV}$	$^{27}\text{Al} \rightarrow ^{24}\text{Na}$
Carbon scintillator	neutrons of $E_n > 20.4 \text{ MeV}$	$^{12}\text{C} \rightarrow ^{11}\text{C}$

Table 3.2 Lateral-attenuation profiles for gold-foil detector

Distance from beam line [ft (m)]	Relative response [counts/min]					
	4 ft (1.22 m)	8 ft (2.44 m)	12 ft (3.66 m)	16 ft (4.88 m)	20 ft (6.10 m)	24 ft (7.32 m)
0 ( 0.00 )	1.9E+06 <sup>b</sup>	1.9E+05	2.7E+04	3.0E+03	2.4E+02	2.1E+01
1 ( 0.30 )	5.9E+05	9.6E+04	2.0E+04	2.4E+03	2.2E+02	1.9E+01
2 ( 0.61 )	1.8E+05	4.5E+04	1.3E+04	1.6E+03	1.8E+02	1.7E+01
3 ( 0.91 )	5.8E+04	2.0E+04	7.5E+03	9.2E+02	1.3E+02	1.3E+01
4 ( 1.22 )	2.1E+04	9.0E+03	3.7E+03	5.1E+02	8.4E+01	1.0E+01
5 ( 1.52 )	8.4E+03	4.1E+03	1.7E+03	2.9E+02	5.2E+01	7.4E+00
6 ( 1.83 )	3.6E+03	1.8E+03	7.9E+02	1.6E+02	3.2E+01	5.2E+00
7 ( 2.13 )	1.4E+03	7.4E+02	3.4E+02	9.0E+01	2.0E+01	3.5E+00
8 ( 2.44 )	5.9E+02	3.2E+02	1.6E+02	5.5E+01	1.3E+01	2.3E+00
9 ( 2.74 )	2.5E+02	1.4E+02	6.7E+01	3.4E+01	8.8E+00	1.7E+00
10 ( 3.05 )	1.1E+02	-	3.0E+01	2.2E+01	6.6E+00	1.3E+00

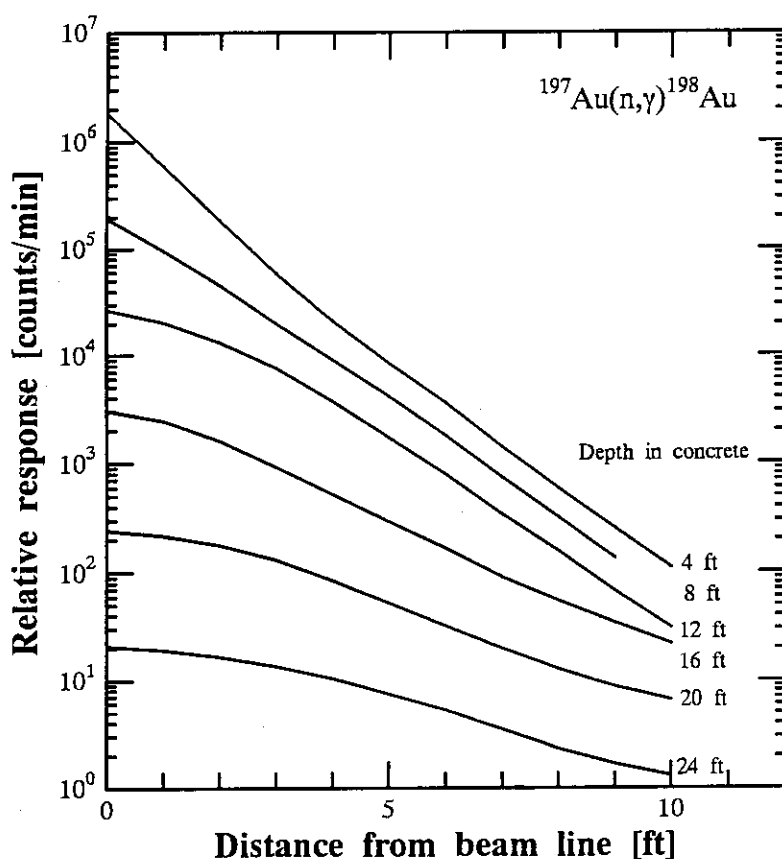
<sup>a</sup> Depth in concrete<sup>b</sup> Read as  $1.9 \times 10^6$ 

Fig. 3.2 Lateral-attenuation profiles for gold-foil detector

Table 3.3 Lateral-attenuation profiles for aluminum detector

Distance from beam line [ft (m)]	Relative response [counts/min]				
	4 ft <sup>a</sup> (1.22 m)	8 ft (2.44 m)	12 ft (3.66 m)	16 ft (4.88 m)	20 ft (6.10 m)
0 ( 0.00 )	5.8E+06 <sup>b</sup>	7.6E+05	6.5E+04	5.0E+03	2.5E+02
1 ( 0.30 )	1.0E+06	2.7E+05	3.6E+04	3.7E+03	2.1E+02
2 ( 0.61 )	2.5E+05	1.1E+05	1.8E+04	2.3E+03	1.6E+02
3 ( 0.91 )	8.2E+04	5.0E+04	9.3E+03	1.3E+03	1.1E+02
4 ( 1.22 )	3.0E+04	2.3E+04	4.9E+03	7.6E+02	7.2E+01
5 ( 1.52 )	1.3E+04	1.1E+04	2.7E+03	4.7E+02	4.4E+01
6 ( 1.83 )	5.5E+03	4.8E+03	1.5E+03	2.9E+02	2.5E+01
7 ( 2.13 )	2.5E+03	2.3E+03	8.0E+02	1.7E+02	1.4E+01
8 ( 2.44 )	1.2E+03	1.0E+03	4.4E+02	1.1E+02	8.8E+00
9 ( 2.74 )	5.5E+02	4.9E+02	2.4E+02	6.6E+01	6.0E+00
10 ( 3.05 )	2.5E+02	2.2E+02	1.3E+02	4.0E+01	4.3E+00

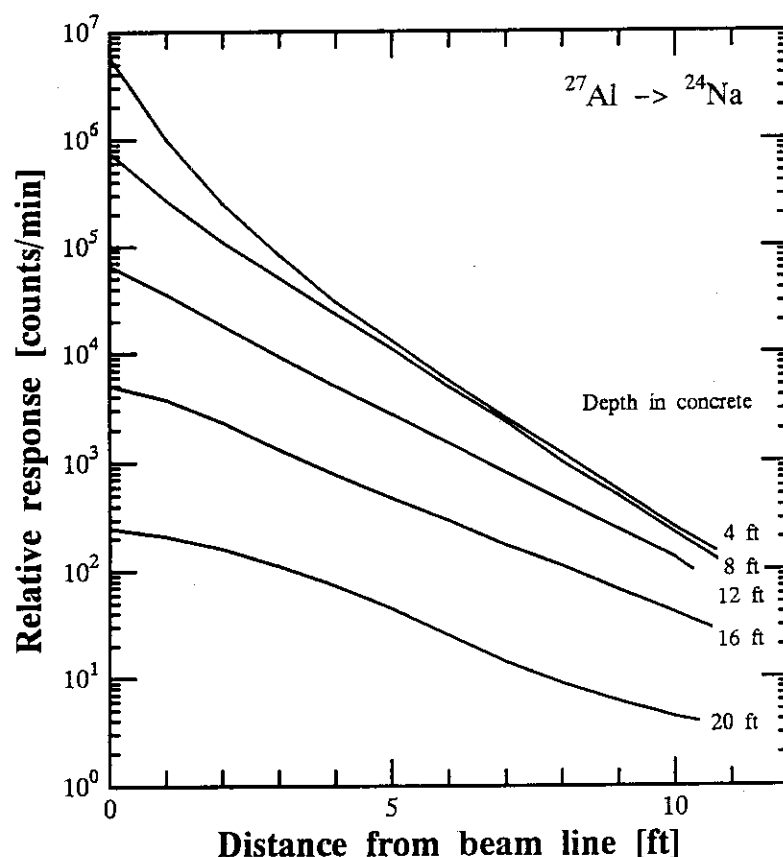
<sup>a</sup> Depth in concrete<sup>b</sup> Read as  $5.8 \times 10^6$ 

Fig. 3.3 Lateral-attenuation profiles for aluminum detector

Table 3.4 Lateral-attenuation profiles for carbon detector

Distance from beam line [ft (m)]	Relative response [counts/min]					
	4 ft <sup>a</sup> (1.22 m)	8 ft (2.44 m)	12 ft (3.66 m)	16 ft (4.88 m)	20 ft (6.10 m)	24 ft (7.32 m)
0 ( 0.00 )	6.0E+06 <sup>b</sup>	5.0E+05	2.9E+04	1.6E+03	9.2E+01	7.1E+00
1 ( 0.30 )	4.8E+05	1.2E+05	1.2E+04	9.5E+02	7.2E+01	5.5E+00
2 ( 0.61 )	1.1E+05	4.0E+04	5.4E+03	5.7E+02	5.2E+01	4.3E+00
3 ( 0.91 )	3.5E+04	1.6E+04	2.6E+03	3.1E+02	3.6E+01	3.2E+00
4 ( 1.22 )	1.2E+04	6.9E+03	1.3E+03	1.7E+02	2.3E+01	2.3E+00
5 ( 1.52 )	5.4E+03	3.3E+03	6.8E+02	9.8E+01	1.4E+01	1.6E+00
6 ( 1.83 )	2.8E+03	1.7E+03	3.6E+02	5.7E+01	8.1E+00	1.1E+00
7 ( 2.13 )	1.5E+03	9.4E+02	1.8E+02	3.5E+01	4.6E+00	-
8 ( 2.44 )	8.4E+02	5.3E+02	9.9E+01	2.2E+01	2.5E+00	-
9 ( 2.74 )	-	3.1E+02	5.6E+01	1.5E+01	1.3E+00	-
10 ( 3.05 )	-	1.9E+02	3.3E+01	1.0E+01	-	-

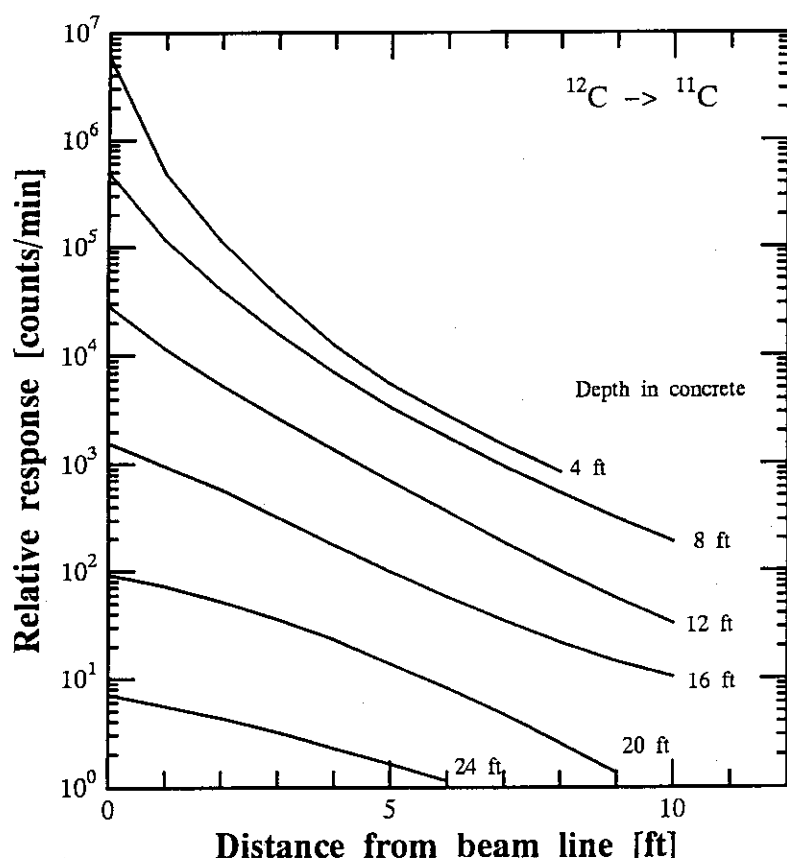
<sup>a</sup> Depth in concrete<sup>b</sup> Read as  $6.0 \times 10^6$ 

Fig. 3.4 Lateral-attenuation profiles for carbon detector

Table 3.5 Numerical data of plots in Fig.3.5 and attenuation lengths determined by their slopes beyond 12 ft thickness

Depth in shield [ft (m)]	$^{12}\text{C} \rightarrow ^{11}\text{C}$ <sup>a</sup>	$^{27}\text{Al} \rightarrow ^{24}\text{Na}$	$^{197}\text{Au}(n,\gamma)^{198}\text{Au}$
4 ( 1.22 )	1.1E+06 <sup>b</sup>	6.2E+05	4.9E+05
8 ( 2.44 )	7.2E+04	7.2E+04	7.2E+04
12 ( 3.66 )	4.4E+03	6.2E+03	9.8E+03
16 ( 4.88 )	2.5E+02	4.6E+02	9.3E+02
20 ( 6.10 )	1.5E+01	3.2E+01	7.1E+01
24 ( 7.32 )	1.2E+00	2.4E+00	5.8E+00
Attenuation length	108 g/cm <sup>2</sup>	114 g/cm <sup>2</sup>	120 g/cm <sup>2</sup>

<sup>a</sup> Reaction for estimation of flux

<sup>b</sup> Read as  $1.1 \times 10^6$

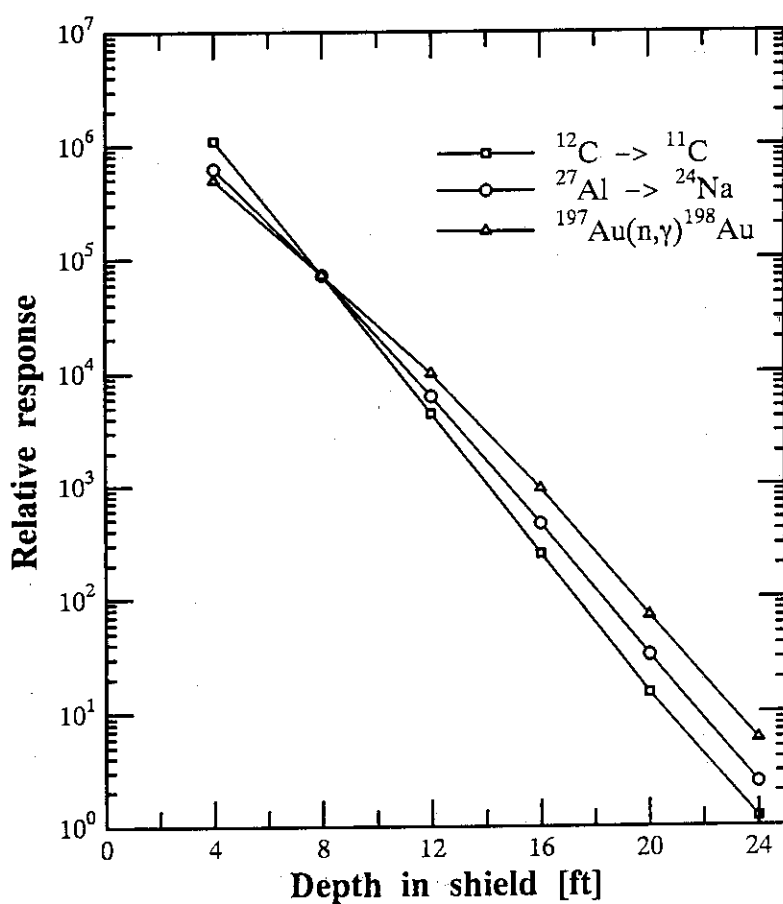


Fig. 3.5 Attenuation profiles along the beam axis measured with  $^{197}\text{Au}(n,\gamma)^{198}\text{Au}$ ,  $^{27}\text{Al} \rightarrow ^{24}\text{Na}$  and  $^{12}\text{C} \rightarrow ^{11}\text{C}$  reactions

Data are normalized at a depth of 8 ft in concrete.

Table 3.6 Numerical data of plots in Fig. 3.6 and attenuation lengths determined by their slopes beyond 12 ft thickness

Depth in shield [ft (m)]	Proton Energy		
	2.2 GeV <sup>a</sup>	4.2 GeV	6.2 GeV
4 ( 1.22 )	9.1E+05 <sup>b</sup>	6.6E+05	4.9E+05
8 ( 2.44 )	5.6E+04	5.6E+04	5.6E+04
12 ( 3.66 )	2.2E+03	3.5E+03	5.0E+03
16 ( 4.88 )	1.1E+02	2.2E+02	3.7E+02
20 ( 6.10 )	6.5E+00	1.4E+01	2.5E+01
24 ( 7.32 )	-	9.9E-01	1.9E+00
Attenuation length	99 g/cm <sup>2</sup>	108 g/cm <sup>2</sup>	114 g/cm <sup>2</sup>

<sup>a</sup> Incident proton energy

<sup>b</sup> Read as  $9.1 \times 10^5$

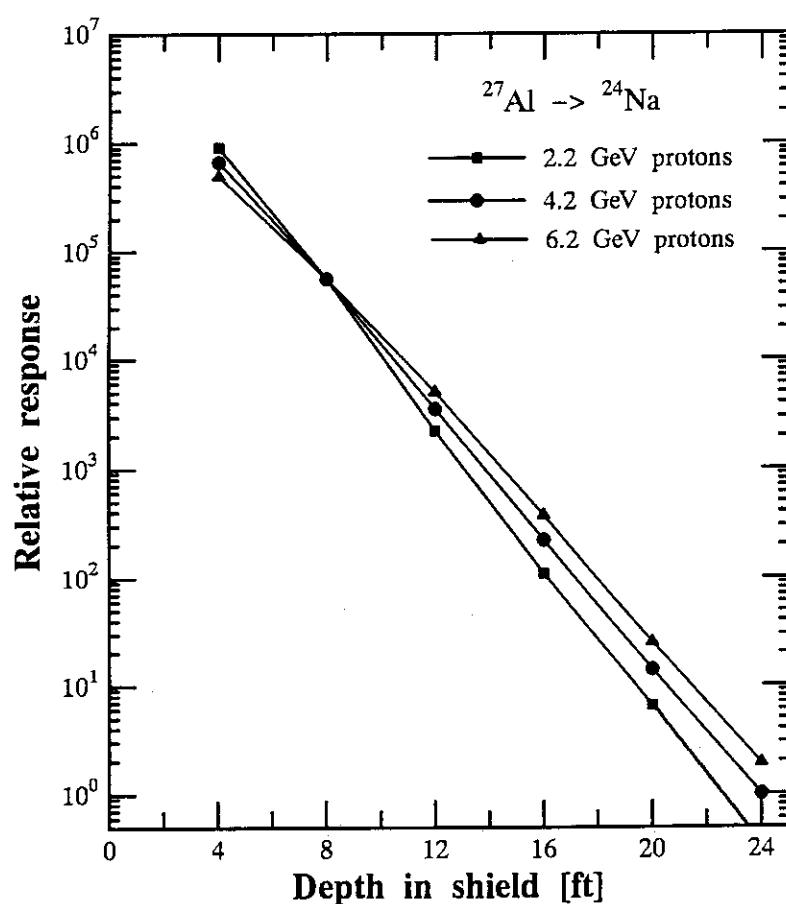


Fig. 3.6 Attenuation profiles along the beam axis measured with  $^{27}\text{Al} \rightarrow ^{24}\text{Na}$  reaction comparing with those for incident protons of 2.2 and 4.2 GeV

Data are normalized at a depth of 8 ft in concrete.

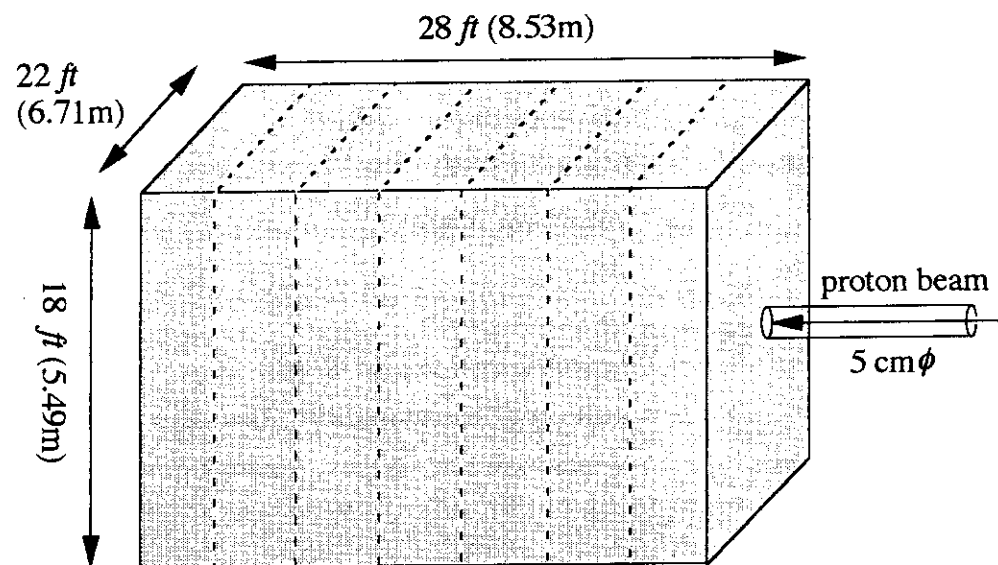


Fig. 3.7 Calculation geometry

Table 3.7 Elemental composition and density of the NBS concrete

Element	Weight fraction
Hydrogen	5.60E-03 *
Oxygen	4.98E-01
Sodium	1.71E-02
Magnesium	2.40E-03
Aluminum	4.56E-02
Silicon	3.16E-01
Sulfur	1.20E-03
Potassium	1.92E-02
Calcium	8.26E-02
Iron	1.22E-02
Sum	1.00E+00
density	2.4 g/cm <sup>3</sup>

\* Read as  $5.60 \times 10^{-3}$

#### 4. Neutron and Hadron Fluxes inside Iron Beam Dump Irradiated by 24 GeV Protons

##### (Summary)

- |                               |  |
|-------------------------------|--|
| 1) Accelerator (Organization) | : Proton Synchrotron (CERN)  |
| 2) Projectile (Energy)        | : Proton (24 GeV)  |
| 3) Target                     | : Iron (Beam Dump)   |
| 4) Shielding material         | : none   |
| 5) Geometry                   | : Rectangular Slabs  |
| 6) Instrument                 | : Activation Detector (In, S, Al),<br>Radiophotoluminescent(RPL) Dosimeter |
| 7) Measured Quantities        | : Neutron and Hadron Flux, Absorbed-Dose                                   |

##### 4.1 Experimental Arrangement

A sketch of a beam dump<sup>1,2)</sup> is given in Fig. 4.1. The beam dump consisted of 20 rectangular iron absorber slabs of 5 cm thickness, separated by 7 mm slots in which thin aluminum plates supporting the activation detectors and dosimeters were placed. The density of the iron absorber slabs was  $7.86 \pm 0.02$  g/cm<sup>3</sup>. The transverse dimensions of the slabs were 30 x 30 cm. Total length of the beam dump is 113.3 cm.

##### 4.2 Methods of Measurement and Instrument

The characteristics of activation detectors and dosimeters for the experiment are summarized in Table 4.1. Composition of RPL dosimeter is given in Table 4.2. The activation detectors and RPL dosimeters were mounted on 0.5-mm-thick and 24 cm x 30 cm cross section aluminum plates with activation detector holding holes which were accurately punched out for every detector size. A sketch of the aluminum plate for holding Al activation detectors is exemplified in Fig. 4.2. In the figure, R and r show, respectively, the exact distance from the center of the aluminum plate and the radius of the activation detectors and RPL dosimeters. An aluminum plate was also placed in front of the first absorber slab in order to measure albedo effects (slot 0th).

##### 4.3 Irradiation Conditions

The 24 GeV proton beam impinged on the beam dump perpendicularly at its center. Three separate irradiations were performed for different durations in order to optimize the production of the various isotopes of different half-lives. Each irradiation conditions are summarized in Table 4.3. Beam intensity of irradiations was measured using a monitor and aluminum activation detectors placed upstream of the beam dump. The values of the beam intensity in this table have an error of 10%. The beam spot size was about 3 mm in diameter. The arrangement of activation detectors and RPL dosimeters for each irradiation is given in Table 4.4.

#### 4.4 Measured Results

The measured fluxes in each slot are shown in Figs.4.3 - 4.6 and are given in Tables 4.5 - 4.8. These fluxes were obtained from measured saturated activity by dividing by  $n \cdot s$ ; ( $n$ : the number of atoms in the detector,  $s$ : effective cross section (see Table 4.1)). The absorbed doses measured by RPL dosimeters are shown in Fig. 4.7 and are given in Table 4.9. In Tables 4.5 - 4.9, all measured data are normalized by a condition of one proton incidence.

#### 4.5 Model for Calculation

##### a. Source Condition

The 24 GeV proton beam of 3 mm in diameter impinges on the beam dump perpendicularly at its center.

##### b. Calculational Geometry

We propose to express the calculation geometry with a three-dimensional (X,Y,Z) model shown in Fig. 4.8. However, it can be expressed with a two-dimensional (R-Z) model.

##### c. Material Descriptions

The density of the iron used for the beam dump is 7.86 g/cm<sup>3</sup>.

#### 4.6 Normalization between Calculation and Measurement

All calculated results are requested to be normalized by a condition of one proton incidence for the comparison with experimental ones.

#### References

1. Fasso A., Stevenson G. R., Bruzzi M., Furetta C., Rancoita P. G., Giubellino P., Steni R. and Russ J. S. : "Measurements of low-energy neutrons in an iron calorimeter structure irradiated by 24 GeV/c protons", CERN/TIS-RP/90-19 (1990).
2. Fasso A., Ferrari A., Ranft J., Sala P. R., Stevenson G. R. and Zazula J. M. : "A comparison of FLUKA simulations with measurements of fluence and dose in calorimeter structures", Nucl. Instrum. Methods Phys. Res., A332(3), 459-468 (1993).

Table 4.1 Summary of activation and dosimetry techniques

Main contributing reaction	Sample size	Measurement technique	Effective cross section	Nominal energy range
$^{115}\text{In}(\text{n},\text{n}')^{115m}\text{In}$	0.3 mm x 10 mm $\phi$	GeLi	120 mb	0.8-15 MeV (neutrons)
$^{32}\text{S}(\text{n},\text{p})^{32}\text{P}$	6 mm x 23 mm $\phi$	GMT	300 mb	3-25 MeV (neutrons)
$^{27}\text{Al}(\text{n},\alpha)^{24}\text{Na}$	0.5 mm x 10-30 mm $\phi$	NaI	85 mb	6-25 MeV (neutrons)
$^{27}\text{Al}(\text{h},\text{x})^{18}\text{F}$	0.5 mm x 10-30 mm $\phi$	NaI	8 mb	>35 MeV (hadrons)
RPL dosimeters	6 mm x 1 mm $\phi$ Schott - Jenner DOS2			

Table 4.2 Composition of RPL dosimeter

Element	Weight fraction
O	53.7 %
P	33.4 %
Al	4.6 %
Ag	3.7 %
Li	3.7 %
B	0.9 %

Table 4.3 Irradiation conditions

Irradiation	Duration [min]	Beam intensity [protons / sec]	Beam spot size (diameter)
1st	180	$10.83 \times 10^9$	3 mm
2nd	112	$5.86 \times 10^9$	3 mm
3rd	22	$11.14 \times 10^9$	3 mm

Table 4.4 Arrangement of activation detectors and RPL dosimeters for each irradiation

Slot	First irradiation	Second irradiation	Third irradiation
0	Al( <sup>24</sup> Na), Sulfur	Indium	Al ( <sup>18</sup> F and <sup>24</sup> Na)
1	Al( <sup>24</sup> Na), RPL	Al( <sup>24</sup> Na)	-
2	Al( <sup>24</sup> Na), Sulfur	Indium	Al ( <sup>18</sup> F and <sup>24</sup> Na)
3	Al( <sup>24</sup> Na), RPL	Al( <sup>24</sup> Na)	-
4	Al( <sup>24</sup> Na)	Indium	Al ( <sup>18</sup> F and <sup>24</sup> Na)
5	Al( <sup>24</sup> Na), Sulfur	-	-
6	Al( <sup>24</sup> Na), RPL	-	-
7	-	Al( <sup>24</sup> Na)	-
8	Al( <sup>24</sup> Na), Sulfur	Indium	Al ( <sup>18</sup> F and <sup>24</sup> Na)
9	-	-	-
10	Al( <sup>24</sup> Na), RPL	-	-
11	Al( <sup>24</sup> Na), Sulfur	-	-
12	-	-	-
13	-	Indium	-
14	-	-	-
15	-	Al( <sup>24</sup> Na)	-
16	Al( <sup>24</sup> Na), RPL	-	-
17	Al( <sup>24</sup> Na)	-	-
18	-	-	-
19	-	-	-
20	Al( <sup>24</sup> Na), RPL	-	Al ( <sup>18</sup> F and <sup>24</sup> Na)

**Table 4.5 Neutron fluxes measured by indium activation detectors using  $^{115}\text{In}(\text{n},\text{n}')^{115m}\text{In}$  reaction**

R [mm]	r [mm]	slot[0]		slot[2]		slot[4]	
		flux	error	flux	error	flux	error
0	5.0	7.21E-02	9.37E-03	1.53E-01	2.30E-03	2.32E-01	1.71E-03
25	5.0	3.26E-02	2.46E-03	1.35E-01	2.20E-03	1.54E-01	3.96E-03
50	5.0	1.82E-02	8.77E-04	7.87E-02	8.70E-04	9.34E-02	5.42E-03
75	5.0	1.21E-02	4.36E-04	5.24E-02	7.30E-04	6.00E-02	1.72E-03
100	5.0	7.69E-03	8.39E-04	3.23E-02	7.40E-04	4.10E-02	1.44E-03
135	5.0	4.69E-03	4.43E-04	1.36E-02	3.30E-04	2.28E-02	6.00E-04

R [mm]	r [mm]	slot[8]		slot[13]	
		flux	error	flux	error
0	5.0	1.51E-01	1.10E-03	5.81E-02	8.10E-04
25	5.0	1.08E-01	1.30E-03	4.58E-02	3.17E-03
50	5.0	6.96E-02	7.60E-04	3.47E-02	6.30E-04
75	5.0	5.26E-02	7.40E-04	2.63E-02	1.11E-03
100	5.0	3.64E-02	6.60E-04	1.91E-02	3.61E-04
135	5.0	2.37E-02	5.50E-04	1.11E-02	2.06E-04

R : detector position, r : detector radius

flux, error : [ n / cm<sup>2</sup> / proton ]

**Table 4.6 Neutron fluxes measured by sulfur activation detectors using  $^{32}\text{S}(\text{n},\text{p})^{32}\text{P}$  reaction**

R [mm]	r [mm]	slot[0]		slot[2]		slot[5]	
		flux	error	flux	error	flux	error
0	11.5	8.77E-03	4.38E-04	4.07E-02	2.04E-03	3.20E-02	1.60E-03
25	11.5	3.69E-03	8.51E-05	1.69E-02	3.72E-04	1.78E-02	5.83E-05
50	11.5	1.94E-03	4.46E-05	8.13E-03	1.59E-04	1.01E-02	5.35E-05
100	11.5	7.78E-04	8.59E-06	2.70E-03	4.46E-05	4.00E-03	2.85E-05
135	11.5	4.37E-04	1.71E-05	1.41E-03	9.26E-06	2.11E-03	3.70E-05

R [mm]	r [mm]	slot[8]		slot[11]	
		flux	error	flux	error
0	11.5	2.00E-02	1.00E-03	1.09E-02	5.46E-04
25	11.5	1.21E-02	3.36E-04	7.54E-03	1.26E-04
50	11.5	7.83E-03	1.78E-04	5.01E-03	1.01E-04
100	11.5	3.38E-03	1.32E-04	2.44E-03	3.95E-05
135	11.5	1.95E-03	6.94E-05	1.42E-03	6.48E-05

R : detector position, r : detector radius

flux, error : [ n / cm<sup>2</sup> / proton ]

**Table 4.7 Neutron fluxes measured by aluminum activation detectors using  $^{27}\text{Al}(\text{n},\alpha)^{24}\text{Na}$  reaction**

R [mm]	r [mm]	slot[0]		slot[1]		slot[2]	
		flux	error	flux	error	flux	error
0	5.0	1.18E-01	2.37E-03	1.75E-01	1.75E-03	1.80E-01	1.80E-03
12	5.0	1.09E-02	8.87E-04	3.65E-02	1.62E-03	4.99E-02	1.54E-03
30	7.5	3.65E-03	1.69E-04	1.17E-02	3.37E-04	1.71E-02	3.08E-04
50	7.5	2.00E-03	6.35E-05	5.42E-03	1.33E-04	8.08E-03	1.61E-04
70	10.0	1.18E-03	3.06E-05	3.07E-03	7.88E-05	4.66E-03	5.32E-05
100	15.0	6.75E-04	1.30E-05	1.53E-03	3.16E-05	2.39E-03	2.54E-05
135	15.0	4.02E-04	1.86E-05	8.92E-04	8.29E-05	1.26E-03	8.54E-06
R [mm]	r [mm]	slot[3]		slot[4]		slot[5]	
		flux	error	flux	error	flux	error
0	5.0	1.41E-01	2.30E-03	1.17E-01	2.95E-02	1.01E-01	1.91E-03
12	5.0	4.81E-02	2.52E-03	5.20E-02	6.23E-03	3.97E-02	4.56E-04
30	7.5	1.88E-02	4.16E-04	2.01E-02	7.45E-04	1.91E-02	5.48E-04
50	7.5	9.77E-03	3.23E-04	1.10E-02	3.81E-04	1.02E-02	9.46E-05
70	10.0	5.65E-03	9.51E-05	6.54E-03	1.98E-04	6.77E-03	7.30E-05
100	15.0	3.05E-03	5.68E-05	3.49E-03	9.48E-05	3.66E-03	3.77E-05
135	15.0	1.66E-03	3.59E-05	1.88E-03	9.27E-05	1.97E-03	3.01E-05
R [mm]	r [mm]	slot[6]		slot[7]		slot[8]	
		Flux	error	Flux	error	flux	error
0	5.0	8.26E-02	1.07E-03	6.96E-02	1.25E-03	4.84E-02	7.19E-04
12	5.0	3.82E-02	1.71E-03	2.94E-02	9.89E-04	2.46E-02	7.92E-04
30	7.5	1.78E-02	7.45E-04	1.52E-02	3.20E-04	1.37E-02	2.79E-04
50	7.5	9.67E-03	4.51E-04	8.92E-03	3.76E-04	8.55E-03	1.82E-04
70	10.0	6.71E-03	1.70E-04	5.81E-03	2.83E-04	5.71E-03	9.21E-05
100	15.0	3.57E-03	5.81E-05	3.48E-03	6.69E-05	3.32E-03	6.53E-05
135	15.0	2.04E-03	3.89E-05	1.98E-03	5.32E-05	2.00E-03	6.10E-05
R [mm]	r [mm]	slot[10]		slot[11]		slot[16]	
		flux	error	flux	error	flux	error
0	5.0	3.02E-02	6.64E-04	2.28E-02	5.70E-04	7.81E-03	3.36E-04
12	5.0	1.81E-02	5.11E-04	1.35E-02	3.97E-04	5.19E-03	3.08E-04
30	7.5	9.73E-03	3.94E-04	8.03E-03	2.47E-04	3.61E-03	1.28E-04
50	7.5	6.13E-03	2.04E-04	5.37E-03	1.72E-04	2.74E-03	9.54E-05
70	10.0	4.35E-03	5.17E-05	3.78E-03	6.96E-05	2.03E-03	3.20E-05
100	15.0	2.70E-03	3.86E-05	2.38E-03	2.97E-05	1.28E-03	5.38E-05
135	15.0	1.67E-03	3.84E-05	1.49E-03	3.58E-05	7.94E-04	2.69E-05
R [mm]	r [mm]	slot[17]		slot[20]			
		flux	error	flux	error		
0	5.0	4.72E-03	2.69E-04	1.77E-03	9.91E-05		
12	5.0	3.80E-03	2.72E-04	1.43E-03	4.58E-05		
30	7.5	2.47E-03	3.94E-05	8.87E-04	2.48E-05		
50	7.5	1.85E-03	5.11E-05	6.58E-04	1.97E-05		
70	10.0	1.36E-03	3.52E-05	5.33E-04	1.44E-05		
100	15.0	9.21E-04	1.84E-05	3.60E-04	9.36E-06		
135	15.0	5.96E-04	2.15E-05	2.67E-04	9.61E-06		

R : detector position, r : detector radius

flux, error : [ n / cm<sup>2</sup> / proton ]

**Table 4.8 Hadron fluxes measured by aluminum activation detectors using  $^{27}\text{Al}(h,x)^{18}\text{F}$  reaction**

R [mm]	r [mm]	slot[0]		slot[2]		slot[4]	
		flux	error	flux	error	flux	error
0	5.0	5.00E-01	2.50E-02	9.34E-01	4.67E-02	6.81E-01	3.41E-02
12	5.0	8.95E-03	1.74E-03	1.38E-01	8.54E-03	1.39E-01	5.76E-03
30	7.5	2.32E-03	1.20E-04	2.75E-02	5.95E-04	3.70E-02	1.06E-03
50	7.5	1.07E-03	1.02E-04	9.54E-03	3.86E-04	1.59E-02	1.46E-04
70	10.0	6.06E-04	4.62E-05	4.29E-03	7.19E-05	7.73E-03	8.36E-05
100	15.0	3.18E-04	1.35E-05	1.67E-03	3.76E-05	3.41E-03	4.78E-05
135	15.0	1.50E-04	1.55E-06	8.15E-04	2.33E-05	1.59E-03	5.18E-06

R [mm]	r [mm]	slot[8]		slot[20]	
		flux	error	flux	error
0	5.0	2.10E-01	1.05E-02	6.43E-03	3.22E-04
12	5.0	6.45E-02	4.60E-03	4.85E-03	3.06E-04
30	7.5	2.58E-02	1.21E-03	2.98E-03	5.93E-04
50	7.5	1.30E-02	2.65E-04	1.95E-03	3.92E-04
70	10.0	7.31E-03	1.55E-04	1.07E-03	1.96E-05
100	15.0	3.70E-03	1.21E-04	6.53E-04	1.80E-05
135	15.0	1.89E-03	5.18E-05	4.10E-04	3.88E-05

R : detector position, r : detector radius

flux, error : [ hadron / cm<sup>2</sup> / proton ]

**Table 4.9 Absorbed dose measured by PRL dosimeters**

R [mm]	r [mm]	slot[1]		slot[3]		slot[6]	
		dose	error	dose	error	dose	error
0	5.0	4.29E-10	2.57E-10	6.80E-10	6.27E-11	3.67E-10	5.39E-11
12	5.0	1.98E-10	5.95E-11	3.07E-10	1.41E-11	1.93E-10	1.42E-11
24	5.0	4.92E-11	4.35E-12	9.69E-11	7.36E-12	7.56E-11	4.21E-12
36	5.0	2.85E-11	2.73E-12	5.24E-11	1.85E-12	4.58E-11	2.64E-12
48	5.0	2.50E-12	9.55E-14	3.32E-11	1.20E-12	2.89E-11	2.08E-12
60	5.0	2.19E-12	1.68E-13	2.30E-11	2.04E-12	2.71E-11	1.26E-12
80	5.0	1.43E-12	6.25E-14	2.93E-12	1.22E-13	5.26E-12	1.52E-12
100	5.0	8.76E-13	4.60E-14	1.99E-12	8.05E-14	2.49E-12	1.27E-13
140	5.0	2.68E-13	1.35E-14	7.80E-13	0.00E+00	1.22E-12	4.51E-14

R [mm]	r [mm]	slot[10]		slot[16]		slot[20]	
		dose	error	dose	error	dose	error
0	5.0	1.17E-10	2.06E-11	5.42E-11	8.78E-12	4.04E-12	4.68E-13
12	5.0	7.73E-11	6.79E-12	3.04E-11	2.46E-12	3.05E-12	1.77E-13
24	5.0	4.78E-11	3.63E-12	2.29E-11	1.37E-12	2.22E-12	1.10E-13
36	5.0	3.80E-11	3.29E-12	3.58E-12	3.32E-13	1.56E-12	9.07E-14
48	5.0	3.12E-11	1.35E-12	2.53E-12	1.85E-13	1.19E-12	4.21E-14
60	5.0	2.86E-12	1.44E-13	2.45E-12	9.69E-14	8.27E-13	5.17E-14
80	5.0	2.57E-12	4.63E-14	1.58E-12	4.64E-14	6.10E-13	2.27E-14
100	5.0	1.87E-12	5.83E-14	1.17E-12	3.62E-14	3.64E-13	2.38E-14
140	5.0	9.46E-13	3.16E-14	5.87E-13	2.02E-14	2.49E-13	2.12E-14

R : detector position, r : detector radius

dose, error : [Gy / proton ]

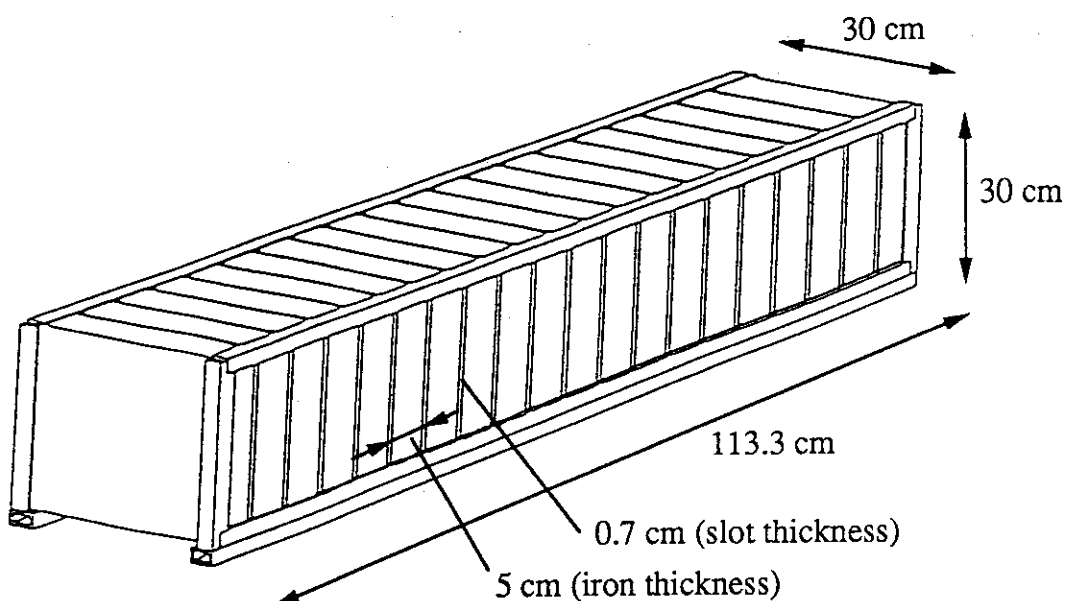


Fig. 4.1 Sketch of the dump assembly

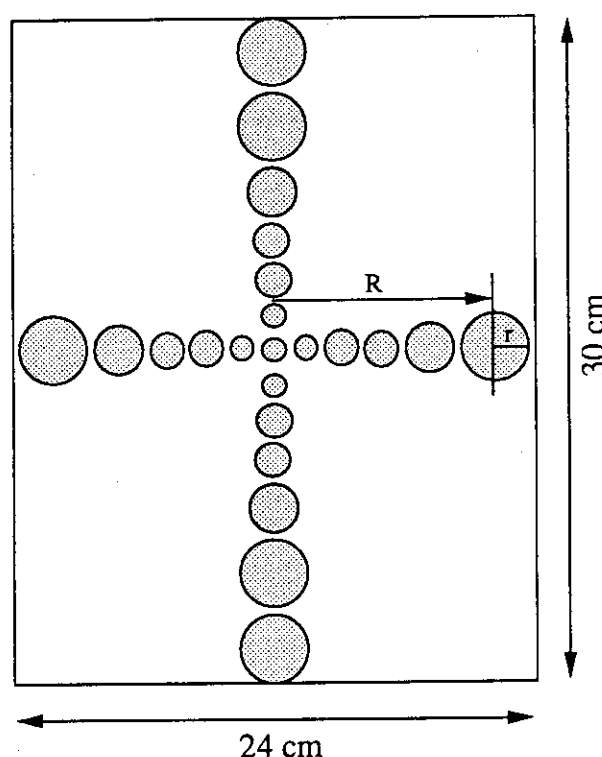


Fig. 4.2 Sketch of a 0.5-mm-thick aluminum plate showing holes for the aluminum detectors

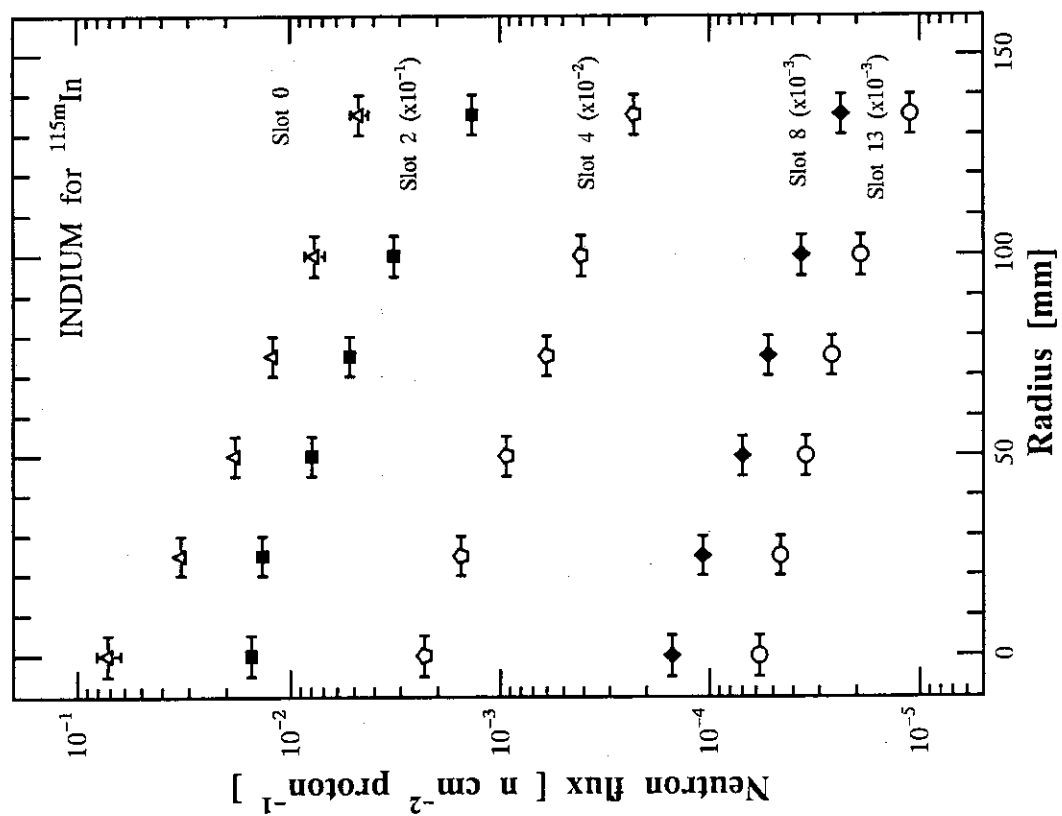
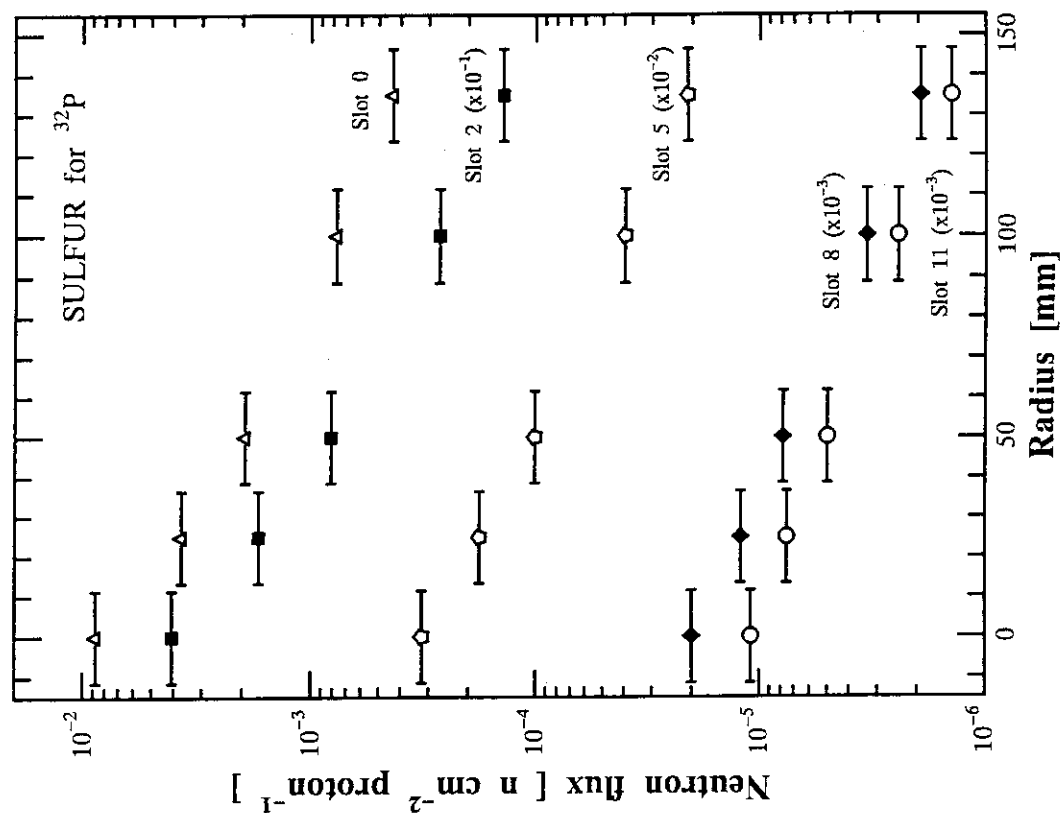


Fig. 4.3 Neutron fluxes measured by indium activation detectors using  $^{115}\text{In}(n,n')^{115\text{m}}\text{In}$  reaction

Fig. 4.4 Neutron fluxes measured by sulfur activation detectors using  $^{32}\text{S}(n,p)^{32}\text{P}$  reaction

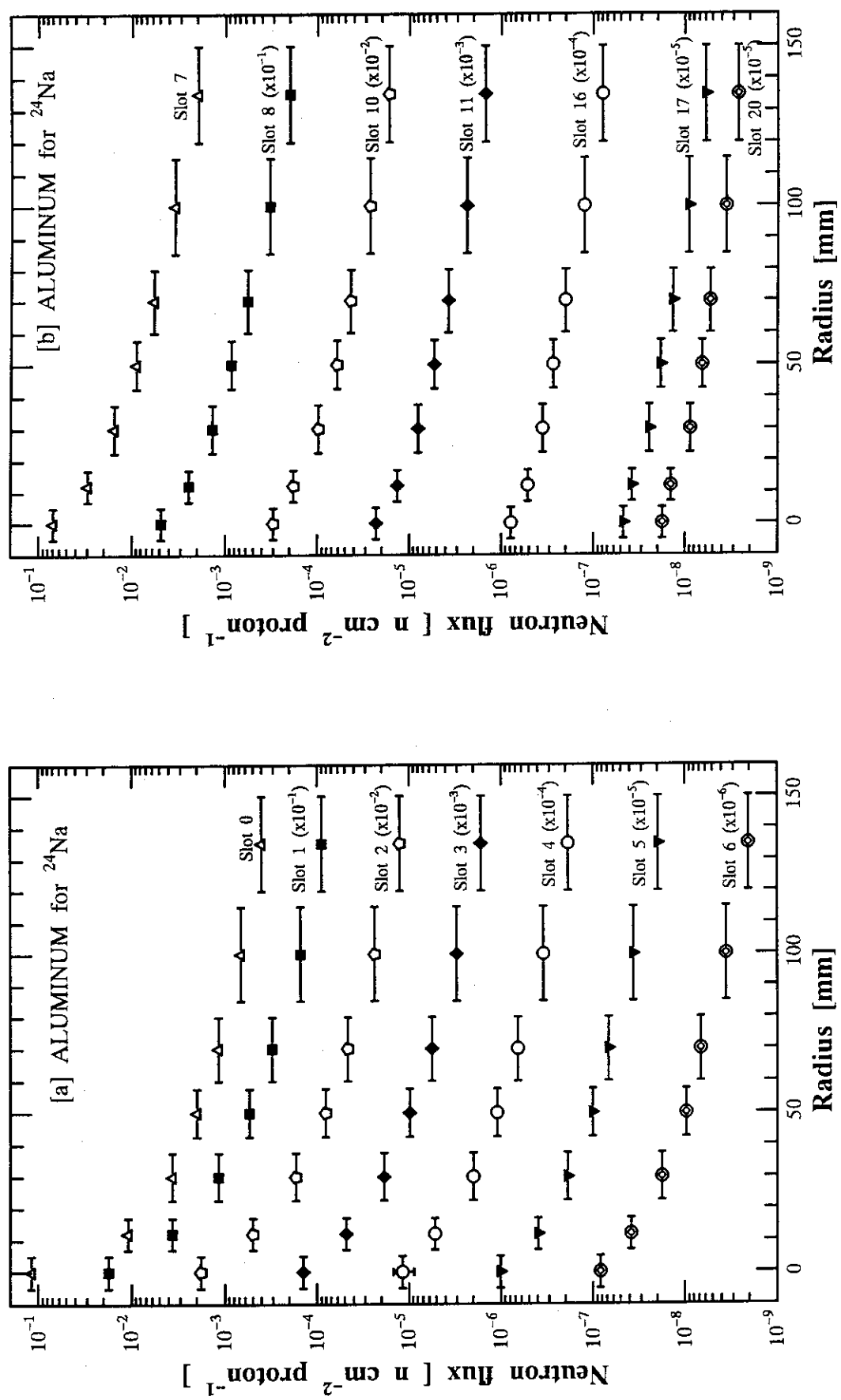


Fig. 4.5 Neutron fluxes measured by aluminum activation detectors using  $^{27}\text{Al}(n,\alpha)^{24}\text{Na}$  reaction  
 [a] for slots 1 to 6 [b] for slots 7 to 20

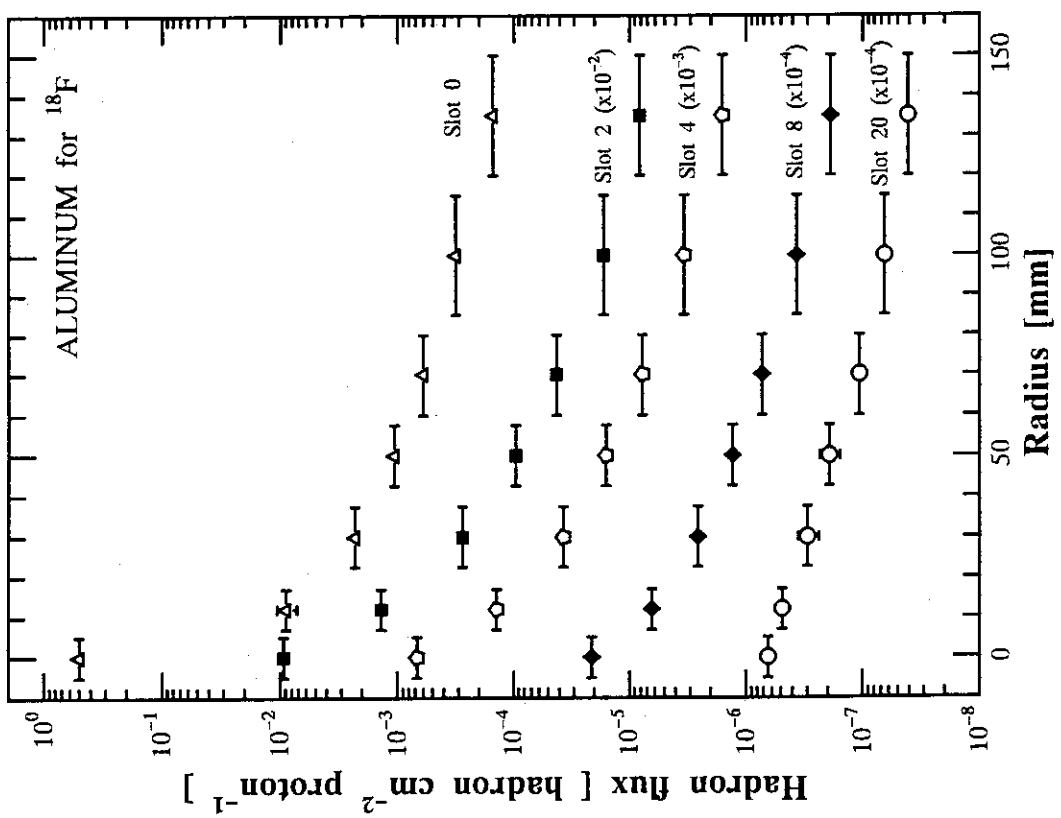
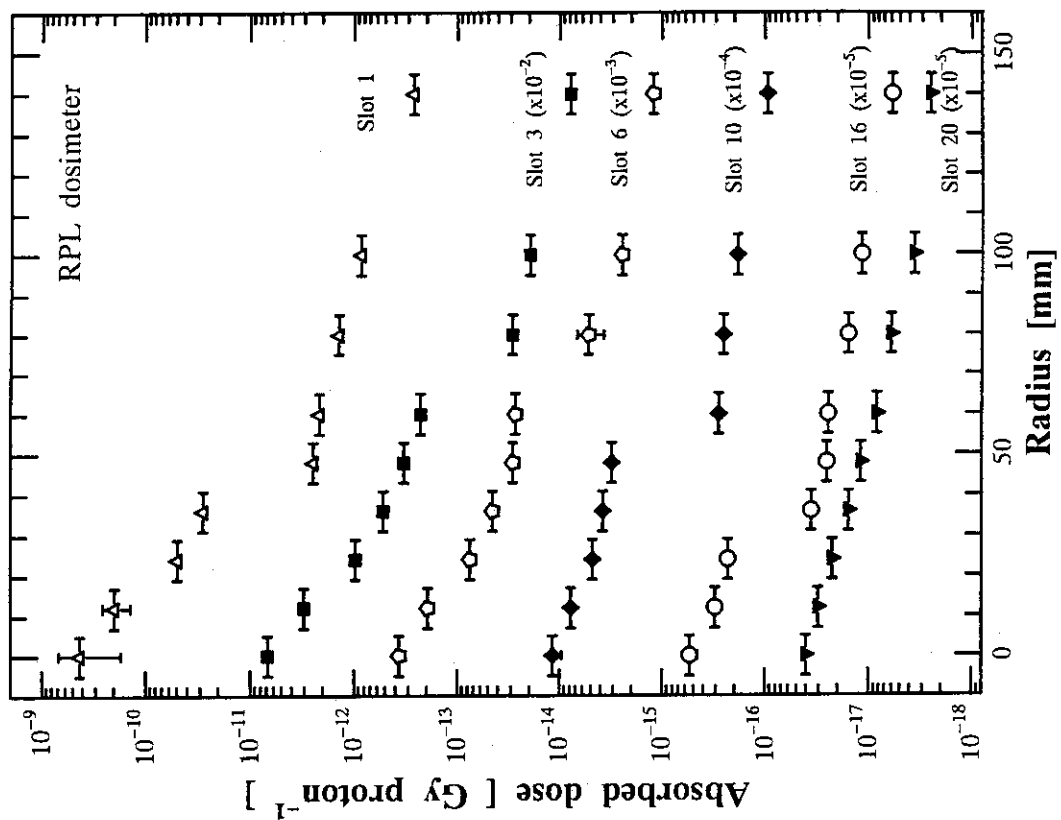


Fig. 4.6 Hadron fluxes measured by aluminum activation detectors using  $^{27}\text{Al}(\text{h},\text{x})^{18}\text{F}$  reaction

Fig. 4.7 Absorbed dose measured by RPL dosimeters

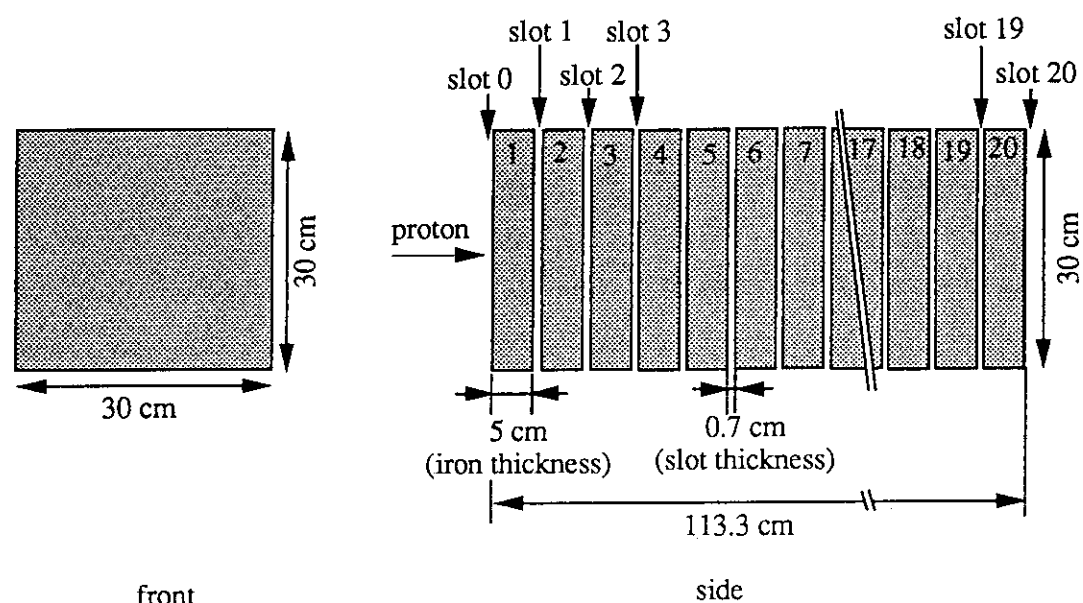


Fig. 4.8 Geometry of iron dump assembly for calculation

## Postscript

The benchmark problems will be mainly distributed to the participants in SATIF-2. They are expected to calculate the problems. The authors will collect and compile the calculation results. A compiled report will be presented and discussed at SATIF-3 which will be held in Tohoku University on 12-13 May, 1997.

## Acknowledgements

The authors would like to express their appreciation to Dr. H. Yasuda for his useful comments.

## Postscript

The benchmark problems will be mainly distributed to the participants in SATIF-2. They are expected to calculate the problems. The authors will collect and compile the calculation results. A compiled report will be presented and discussed at SATIF-3 which will be held in Tohoku University on 12-13 May, 1997.

## Acknowledgements

The authors would like to express their appreciation to Dr. H. Yasuda for his useful comments.